AD_____

Award Number: DAMD17-02-1-0227

TITLE: Molecular Characterization of Androgen Independence to Delay Progression to Hormone Refractory Prostate Cancer

PRINCIPAL INVESTIGATOR: Arie S. Belldegrun, M.D.

CONTRACTING ORGANIZATION: University of California, Los Angeles
Los Angeles, California 90095

REPORT DATE: March 2005

TYPE OF REPORT: Final

PREPARED FOR: U.S. Army Medical Research and Materiel Command
Fort Detrick, Maryland 21702-5012

REPORT DOCUMENTATION PAGE

Form Approved
OMB No. 074-0188

1. AGENCY USE ONLY (Leave blank)	2. REPORT DATE	3. REPORT TYPE AND DATES COVERED
	March 2005	Final (19 Feb 2002 - 18 Feb 2005)

4. TITLE AND SUBTITLE
Molecular Characterization of Androgen Independence to Delay Progression to Hormone Refractory Prostate Cancer

5. FUNDING NUMBERS
DAMD17-02-1-0227

6. AUTHOR(S)
Arie S. Belldegrun, M.D.

7. PERFORMING ORGANIZATION NAME(S) AND ADDRESS(ES)
University of California, Los Angeles
Los Angeles, California 90095

E-Mail: abelldegrun@mednet.ucla.edu

8. PERFORMING ORGANIZATION REPORT NUMBER

9. SPONSORING / MONITORING AGENCY NAME(S) AND ADDRESS(ES)
U.S. Army Medical Research and Materiel Command
Fort Detrick, Maryland 21702-5012

10. SPONSORING / MONITORING AGENCY REPORT NUMBER

11. SUPPLEMENTARY NOTES
Original contains color plates: All DTIC reproductions will be in black and white.

12a. DISTRIBUTION / AVAILABILITY STATEMENT
Approved for Public Release; Distribution Unlimited

12b. DISTRIBUTION CODE

13. ABSTRACT (Maximum 200 Words)
Abstract on page 4.

14. SUBJECT TERMS
prostate

15. NUMBER OF PAGES
98

16. PRICE CODE

17. SECURITY CLASSIFICATION OF REPORT	18. SECURITY CLASSIFICATION OF THIS PAGE	19. SECURITY CLASSIFICATION OF ABSTRACT	20. LIMITATION OF ABSTRACT
Unclassified	Unclassified	Unclassified	Unlimited

Table of Contents

Cover..... 1

SF 298..... 2

Table of Contents..... 3

Introduction..... 4

Body..... 6

Key Research Accomplishments..... 21

Reportable Outcomes..... 22

Conclusions..... 23

References..... 24

Appendices..... 25

a. Revised Summary of Statement of Work (SOW)
b. Manuscript: Liu, A. Y., Brubaker, K. D., Goo, Y. A., Quinn, J. E., Kral, S., Sorensen, C. M., Vessella, R. L., Belldegrun, A. S., Hood, L. E. "Lineage relationship between LNCaP and LNCaP-derived prostate cancer cell lines" (2004) Prostate 60(2): 98-108.
c. Manuscript: John S. Lam, Hong Yu, Ai Li, Mervi Eeva, John T. Leppert, Oleg Shvarts, Allan J. Pantuck, Steve Horvath, David B. Seligson, and Arie S. Belldegrun "Flap Endonuclease 1 is Overexpressed and Associated with High Gleason Score in Prostate Cancer." Submitted.
d. Manuscript: An, J. Sun, Y. P., Adams, J., Fisher, M., Belldegrun, A., Rettig, M. B. "Drug interactions between the proteasome inhibitor bortezomib and cytotoxic chemotherapy, tumor necrosis factor (TNF) alpha, and TNF-related apoptosis-inducing ligand in prostate cancer" Clinical Cancer Research 9(12): 4537-45 (2003).
e. Manuscript: Singh, S., Sadacharan, S., Su, S., Belldegrun, A., Persad, S., Singh, G. "Overexpression of vimentin: role in the invasive phenotype in an androgen-independent model of prostate cancer" Cancer Res. 63(9): 2306-11 (2003).
f. Manuscript: Stephen J. Freedland, Allan J. Pantuck, Sun H. Paik, Amnon Zisman, Thomas G. Graeber, David Eisenberg, William H. McBride, David Nguyen, Cho-Lea Tso, and Arie S. Belldegrun "Heterogeneity of Molecular Targets on Clonal Cancer Lines Derived From a Novel Hormone-Refractory Prostate Cancer Tumor System" The Prostate 55:299-307 (2003).
g. Manuscript: Stephen J. Freedland, David B. Seligson, Alvin Y. Liu, Allan J. Pantuck, Sun H. Paik, Steve Horvath, Jeffrey A. Wieder, Amnon Zisman, David Nguyen, Cho-Lea Tso, Aarno V. Palotie, and Arie S. Belldegrun "Loss of CD10 (Neutral Endopeptidase) Is a Frequent and Early Event in Human Prostate Cancer" The Prostate 55:71-80 (2003).
h. Flap Endonuclease 1 (FEN-1_ is Overexpressed in Prostate Cancer and Associated with High Gleason Score. Society of Urologic Oncology 2004 - Abstract
i. Population Heterogeneity of LNCaP: Possible lineage relationship between CD26+ LNCaP and C4-2 cells: Liu A, Brubaker K, Vessala R, Belldegrun A, Hood L: AUA Annual Meeting -Chicago, 2003. Abstract # 223
j. CL1-GFP: A Novel Hormone Refractory Metastatic Prostate Cancer Tumor Model Tagged with Green Flourescence. A. Zisman, A. Pantuck, B. Patel, C-L Tso, A. Belldegrun. 2000 Western Section American Urological Association. Palm Desert, CA. Abstract # 455
k. In Vivo modeling of prostate Cancer Progression Using a Novel Flourescent-Labeled, Clonal Tumor System. S Freedland, A Liu, A Pantuck, A Zisman, D Nguyen, C-L Tso, S Paik, A Belldegrun. 2002 AUA Annual Meeting, Orlando, FL, Abstract 574.

Abstract:

Progression to hormone-refractory prostate cancer (HRPC) remains a major obstacle to effective control of metastatic disease. The overall goal of this project is to define cellular and molecular markers for the progression of androgen dependent (AD) to androgen independent (AI) and to develop more effective androgen deprivation-based treatment schedules capable of delaying prostate cancer (CaP) tumor progression from locally advanced to widely metastatic disease.

In the past year, primary efforts were focused on the following tasks: 1) Establishment of an in vitro assay to demonstrate the cross-talk between androgen dependent LNCaP and the androgen independent CL1 progeny; The cross-talk between AD LNCaP and AI CL1 was also investigated in vivo in SCID mice; 2) Validation of the Flap structure-specific endonuclease (FEN-1), one of the molecular markers identified through the LNCaP/CL1 model, as a CaP prognosis marker on large-scale human CaP tissue microarrays. 3) Delineation of the lineage relationship between LNCaP and CL1 based on characterization of cell surface CD markers.

In summary of all the results obtained in the funding period, the current DOD grant has allowed us to understand the molecular and cellular changes during progression from AD to AI cancer, which provides clinically useful biomarkers for CaP prognosis. Studies of intermittent androgen depletion and chemotherapy agents that induce apoptosis to AI cancer open doors for novel therapies targeting AI CaP.

Introduction:

Progression to hormone-refractory prostate cancer (HRPC) remains a major obstacle to effective control of metastatic disease. The treatment of choice for palliation of patients with advanced prostate cancer (CaP) is withdrawal of androgen by continuous androgen blockade. However, androgen ablation fails to eliminate the entire malignant cell population and, as such, does not prolong time to HRPC progression or offer definite survival benefit (1, 2). Androgen-independent (AI) variants acquire alternative growth mechanisms that allow CaP survival and proliferation during androgen deprivation therapy. Understanding the molecular mechanisms and alternative growth pathways induced by androgen deprivation treatment is crucial before a more rational strategy for the management of CaP can be developed and AI cell growth can be prevented. Androgen deprivation based treatments must be optimized and cooperative therapy targeting both androgen dependent (AD) and independent growth signaling pathways may be necessary to adequately treat patients with CaP.

Previously, we have established a metastatic AI CL1 tumor model derived from AD LNCaP in order to characterize clinical properties of HRPC (3). In contrast to the slow growing, AD, and poorly tumorigenic phenotype of parental LNCaP cells, the AI CL1 subline selected by androgen deprivation treatment, is fast-growing, and has significant resistance to radiation and anti-cancer cytotoxic agents. CL1 is highly tumorigenic, exhibiting invasive and metastatic characteristics in intact and castrated mice, even in the absence of other growth supplements (e.g. Matrigel). The pathologic development and molecular properties of the CL1-GFP mouse model closely resembles the clinical characteristics of HRPC (4). The metastatic sites of CL1-GFP can be visualized by fluorescence microscopy, thus offering a unique and reproducible animal model to evaluate the efficacy of various therapeutic modalities (4).

Individual clones from CL1 subline were also derived and compared in *in vitro* and *in vivo* studies. All clones demonstrated similar resistance to traditional therapeutic efforts *in vitro*, including chemotherapy and radiation therapy, but differential sensitivity to cell-mediated cytotoxicity. The clones demonstrated differential gene expression relative to each other and to the parental CL1 and LNCaP cell lines. Following orthotopic implantation into mice, three distinct growth patterns were observed: fast growth with widespread metastasis; slower grower with widespread metastasis; and no tumor formation (5).

These well-characterized cell lines provide an attractive model for understanding the cellular and molecular changes associated with the development of AI in CaP, which is critical in developing novel treatment for HRPC. Our overall objective is to define cellular and molecular markers for the progression of AD to AI and to develop more effective androgen deprivation-based treatment schedules capable of delaying CaP tumor progression from locally advanced to widely metastatic disease.

Molecular markers for the progression from AD to AI CaP: In our previous progress report, we described the loss of CD10 expression that occurs with the development of AI CaP. Neutral endopeptidase (NEP/CD10) is a cell surface enzyme, which cleaves and inactivates neuropeptides implicated in the growth of AI CaP that is highly expressed by benign prostatic epithelial cells and by the AD CaP line LNCaP, which is lost in CL1 cells. NEP expression and activity is centrally involved with the metabolic inactivation of several pathogenic peptides thought to be involved in alternative growth-promoting pathways in the progression to AI CaP, including bombesin, endothelin 1, and neurotensin. Loss of NEP function disrupts normal cellular hemostasis and contributes to the progression to AI CaP by allowing uncleaved neuropeptides to act as alternative sources to androgen to stimulate cell proliferation. Restoration of NEP, as the enzyme responsible for the inactivation of all of these AI associated peptides, is one possible therapeutic strategy to target in combination with hormonal manipulation to delay progression in prostate cancer.

New androgen deprivation-based therapy targeting AI CaP: Intermittent androgen deprivation therapy has been proposed as an alternative to continuous androgen deprivation, with on-going clinical trials evaluating its effects on time to tumor progression and quality of life. However, currently there is no data available on the optimal time schedule, kinetics, cycle length, or target PSA nadir for IAD. Ongoing studies in this project hope to address this gap in our knowledge. Thus far, our data suggests that androgen deprivation induces selective outgrowth of unique clonal populations over time. Furthermore, these clones possess unique molecular/gene expression profiles that are responsible for disease progression and metastasis that can be identified and targeted for the treatment of metastatic HRPC. We have been making use of this unique set of single-cell derived AI and metastatic CaP clones to study their differential cellular and molecular expression relating to hormone regulation, growth factor signaling, and gene expression during the progression to an AI, metastatic state. Data from our lab and others suggest that the molecular mechanisms underlying the progression of CaP during hormonal therapy involve numerous adaptive mechanisms involving cell growth, apoptosis, and the development of alternative, non-androgen based growth-signaling pathways, and that AI propagation of CaP cells arises as a consequence of the development or up-regulation of these alternative autocrine/paracrine growth signal transduction pathways. It has been demonstrated that a number of growth factors, including EGF, are capable of directly activating the androgen receptor in the absence of the androgen ligand, bypassing the normal activation of the hormone-signaling pathway. These changes in the pattern of expression of growth factors and their ligands

as CaP progresses from localized AD to metastatic AI suggest that inhibition of these autocrine growth factors may be of therapeutic importance for the treatment of HRPC.

We believe that intermittent androgen deprivation alone or in combination with chemotherapy inducing differential apoptosis of AI cell death may offer an advantage in delaying tumor progression over continued androgen deprivation therapy. We also identified differential sensitivities to chemotherapy drugs between AI and AD CaP populations as additional aims during the funding period of this project.

Body:

Task 1: To identify new molecular and cellular markers for the conversion from AD to AI CaP using a novel LNCaP/CL1-GFP tumor model.

Aim 1.1. Screening of single-cell derived CL1-GFP subclones for their metastatic potential.

In summary, following orthotopic implantation of tumor cells into SCID mice, three distinct patterns of in vivo growth were identified: CL1.1 was characterized as a fast growing clone (FGC) with tumor formation and development of distant metastases within five weeks; CL1.4, CL1.5, CL1.10, and CL1.28 were characterized as slow growing clones (SGC) with tumor formation and development of distant metastases by 7 to 12 weeks; and CL1.31 was characterized as a non-growing clone (NGC), with no demonstrable tumor development in any of 10 mice injected (five castrated, five intact). CL1.4 and CL1.10 from the SGC group demonstrated tumor development only in intact mice.

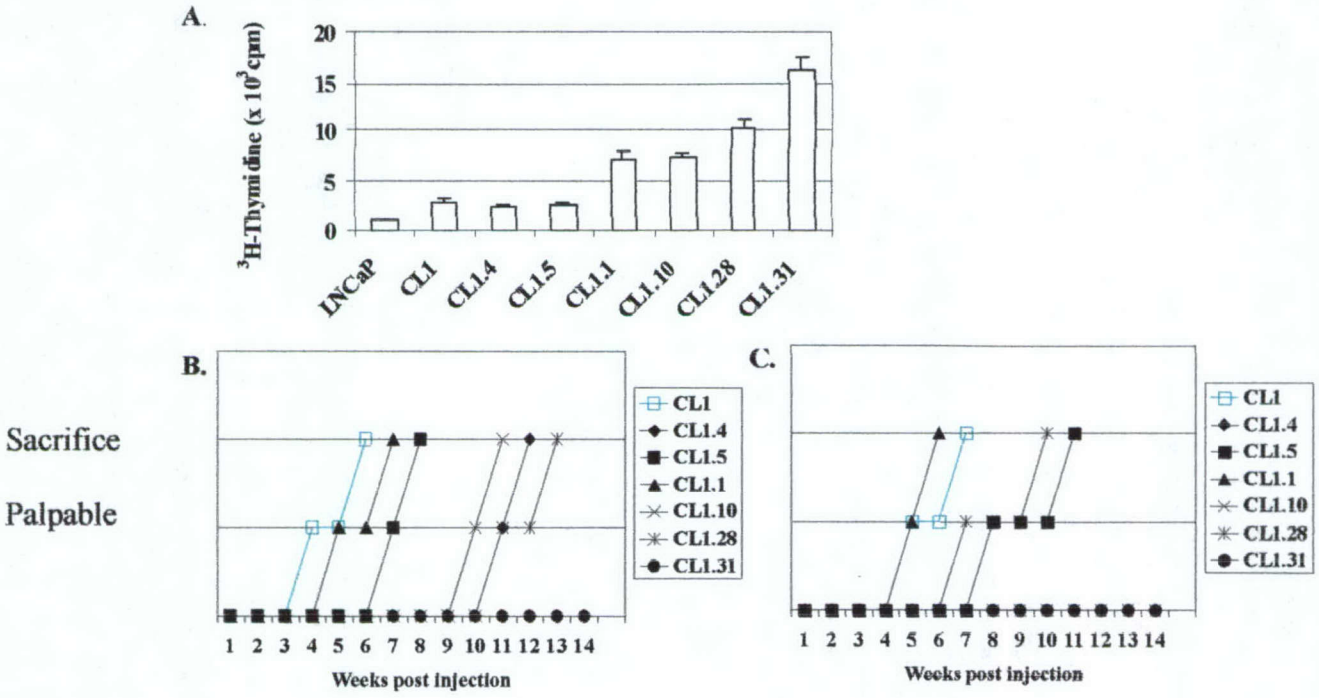

Fig. 1. Growth activity of CL1 clones. *A*, In vitro ^{3}H-thymidine incorporation assay for LNCaP, CL1 and CL1 clones. Error bars are the standard deviation. Proliferation activity of the clones ranged from 0.8 to six-fold that of CL1, with CL1 having a two-fold increase relative to LNCaP. *B* and *C*, In

vivo growth curve of CL1 and the clones following orthotopic injection into intact (B) and castrated (C) SCID mice. Note three patterns of growth: fast growing clones (CL1.1); slow growing clones (CL1.4, CL1.5, CL1.10, and CL1.28), and non-growing clones (CL1.31).

Aim 1.2-1.3. Gene expression analysis using commercially available cDNA microarrays and analysis of expression array data.

In summary, total RNA was extracted from LNCaP, CL1, and CL1 clones by acid guanidine isothiocyanate-phenol-chloroform and purified by column isolation. RNA was transcribed into cDNA, labeled with biotin and hybridized separately to oligonucleotide microarrays (human U95A chip, Affymetrix, Santa Clara, CA). Samples were run in duplicates with gene expression determined by the average expression across the two samples. Conversion of raw data into numeric values of expression was done using software provided by Affymetrix. The difference in expression measurements of the same gene in the duplicate samples was used to determine the parameters of a Poisson statistics-based error model. Genes with higher levels of expression had greater reproducibility in the results and therefore had lower percent uncertainty. Once the parameters of the error model were fit, the probability that a gene's expression differed by a minimum of five-fold between the two samples was determined. Gene expression measurements from oligonucleotide microarrays were used to identify genes that were differentially expressed between the most aggressive clone, CL1.1, and the nontumorigenic clone, CL1.31. Using a statistical error model, we were able to determine which genes had a five-fold or greater difference in expression level between any two samples ($p<0.01$). Using these criteria, we identified 148 genes that were significantly differentially expressed between AD LNCaP and AI CL1 (of which 50 are listed in Table 1), and 41 genes that were differentially expressed between the non-tumorigenic clone, CL1.31, and the fast growing clone, CL1.1 (Table 2). The human U95A chip contains multiple probe sets for each gene/oligonucleotide on the microarray. Table 1 summarizes for each of these differentially expressed genes the number of probe sets that differ at different levels of statistical significance ($p=0$; $p=0.0001$; $p=0.01$) Expanded spread-sheets containing the complete list of differentially expressed genes and probe sets is included as an Appendix. In Table 1, many initial differences noted by RT-PCR were confirmed by gene array analysis, including expressin of PSA, PSMA, Androgen Receptor (AR), and e-cadherin. Other differentially expressed genes of potential interest to our group include STEAP and Insulin Growth Factor Binding Protein 2.

Table 1: Significant Gene Expression Differences Between AD LnCAP and AI CL1:

Gene	p=0, n=37*	p=0.0001, n=103	p=0.01, n=175	Total # of probe sets showing differential expression
PSA	7#			7
MAO-A	2	1		3
PSMA	2	1		3
cytochrome b5	2			2
GAGE-3	2			2
hK2	2			2
alpha catenin	1	3	1	5
AR	1			1
capthesin H	1			1
claudin 7	1			1

dopa decarboxylase	1			1
GAGE-2	1			1
GAGE-4	1			1
GAGE-5	1			1
GAGE-6	1			1
GAGE-7	1			1
hepsin	1			1
ladinin 1	1			1
phosphatidic acid phosphatase type 2A	1			1
PRKACB	1			1
Ribosomal protein S4	1			1
STEAP	1			1
TM7SF2	1			1
GATA binding protein 2		2	1	3
IGFBP-2		2		2
LPS-induced_TNF-alpha_factor		2		2
acid_ceramidase		1		1
aldehyde_dehydrogenase_2		1		1
caldesmon 1		1	1	2
Chorionic_Somatomammotropin_Hormone_Cs-5		1		1
chymotrypsin-like		1		1
claudin 3		1		1
COMT		1		1
creatine_kinase		1		1
DEAD/H_box_polypeptide		1		1
degenerative_spermatocyte		1		1
DHFR		1		1
DKFZp434A091		1		1
DKFZP586A0522		1		1
DKFZP586O1624		1		1
E-cadherin		1		1
endobrevin		1		1
EST, Hs.125170		1		1
even-skipped_homeo_box_1		1		1
FabG_(beta-ketoacyl-[acyl-carrier-protein]_reductase,_E_coli)_like		1		1
fibronectin_1		1		1
FLJ12587		1		1
FLJ20811		1		1
glycine_C-acetyltransferase_(2-amino-3-ketobutyrate_coenzyme_A_ligase)		1		1

*The total number of genes on the array (from approximately 12,000 total known genes) showing a five-fold or greater differential expression. #The total number of oligonucleotide probe sets for each indicated gene (such as PSA) at the indicated level of statistical significance (p value) used in the array.

From Table 2, the most differentially expressed gene between the fast growing and the non-tumorigenic clones was 8-oxoguanine DNA glycosylase, which was over-expressed in the

CL1.1 ($p<0.001$). 8-oxoguanine DNA glycosylase is an enzyme involved in DNA repair that removes 8-oxoguanine, a highly mutagenic oxidative DNA adduct. This enzyme has been shown to undergo mutation during cancer progression. Therefore, the reduced expression of this gene in the fast growing clone, CL1.31 may allow further genetic alterations to accumulate, thus helping to contribute to cancer progression.

Table 2: Significant Gene Expression Differences Between Fast Growing (CL1.1) and Non-Tumorigenic CL1 Clones (CL1.31).

Gene	p=0.05, n=41*	p=0.1, n=78	Total # of probe sets showing differential expression
8-oxoguanine_DNA_glycosylase	1#		1
a_disintegrin_and_metalloproteinase_domain_10	1		1
activin_A_receptor_type_II-like_1	1		1
calponin_3,_acidic	1		1
CCR4-NOT_transcription_complex,_subunit_8	1		1
chymotrypsinogen_B1	1		1
DEAD/H_(Asp-Glu-Ala-Asp/His)_box_polypeptide_21	1		1
DnaJ-like_heat_shock_protein_40	1		1
ectonucleoside_triphosphate_diphosphohydrolase_1	1		1
filamin_C,_gamma_(actin-binding_protein-280)	1		1
FLJ22699	1		1
glutamate_receptor,_ionotropic,_kainate_2	1		1
glutathione_S-transferase_M4	1		1
Guanine_Nucleotide_Exchange_Factor_1	1		1
heterogeneous_nuclear_ribonucleoprotein_D-like	1		1
Hs.145020	1		1
Huntingtin_interacting_protein_B	1		1
HUS1_(S._pombe)_checkpoint_homolog	1		1
keratin_6A	1		1
KIAA0176	1		1
KIAA0657	1		1
KIAA0690	1		1
latent_transforming_growth_factor_beta_binding_protein_2	1		1
lethal_giant_larvae_(Drosophila)_homolog_1	1		1
long_fatty_acyl-CoA_synthetase_2_gene	1		1
ovalbumin	1		1
paralemmin	1		1
piccolo_(presynaptic_cytomatrix_protein)	1		1
protein_tyrosine_phosphatase,_non-receptor_type_14	1		1
ring_finger_protein_9	1		1
skin-specific_protein	1		1
sodium_channel,_voltage-gated,_type_II,_beta_polypeptide	1		1
target_of_myb1_(chicken)_homolog	1		1
transketolase-like_1	1		1
transthyretin_(prealbumin,_amyloidosis_type_I)	1		1
UDP_glycosyltransferase_2_family,_polypeptide_B	1		1

UDP-glucose_ceramide_glucosyltransferase	1		1
urocortin	1		1
v-erb B2 homolog 2	1		1
sialyltransferase_4A		1	1

*The total number of genes on the array (from approximately 12,000 total known genes) showing a five-fold or greater differential expression. #The total number of oligonucleotide probe sets for each indicated gene (such as PSA) at the indicated level of statistical significance (p value) used in the array.

Many of the genes matched our initial findings using semi-quantitative RT-PCR approaches (Fig. 2). In addition, A parallel research avenue pursued by our team in collaboration with Dr. Alvin Liu, Research Asociate Pofessor in the Department of Urology at the University of Washington, and Dr. Biaoyang Lin from Dr. Leroy Hood's Institute for Systems Biology utilized a separate approach called massively parallel signature sequencing (MPSS) on microbead arrays to analyze differential gene expression between CL1 and LNCaP. This sequencing approach combines non-gel-based signature sequencing with in vitro cloning of millions of templates on separate 5 μm diameter microbeads. After constructing a microbead library of DNA templates by in vitro cloning, a planar array of a million template-containing microbeads is assembled in a flow cell at a density greater than 3×10^6 microbeads/cm^2. Sequences of the free ends of the cloned templates on each microbead are then simultaneously analyzed using a fluorescence-based signature sequencing method that does not require DNA fragment separation. Signature sequences of 16–20 bases are obtained by repeated cycles of enzymatic cleavage with a type IIs restriction endonuclease, adaptor ligation, and sequence interrogation by encoded hybridization probes. The approach provides an unprecedented depth of analysis permitting application of powerful statistical techniques for discovery of functional relationships among genes, whether known or unknown beforehand, or whether expressed at high or very low levels.

MPSS analyses were performed on the androgen-dependent LNCaP cell line and its androgen-independent variant CL1 cell line. Using MPSS technology, we sequenced 2.22 and 2.96 millions respectively for the androgen-dependent LNCaP cell line and its androgen-independent variant CL1 cell line. The frequency of each MPSS signature was calculated for each sample and represented in tpm (transcripts per million). We identified a total of 21, 644 unique transcript signatures. The signatures were classified into three major categories: 1165 signatures matched to repeat sequences, 16469 signatures matches to a cDNA or EST and 4010 signatures have no matches to any cDNA or EST matches (but match to genomic sequences). A preliminary comparison of differential gene expression using Affymetrix oligonucleotide microarrays and MPSS demonstrates significant overlapping gene profiles, including PSA, HK2, STEAP, PRKACB, and CED-6.

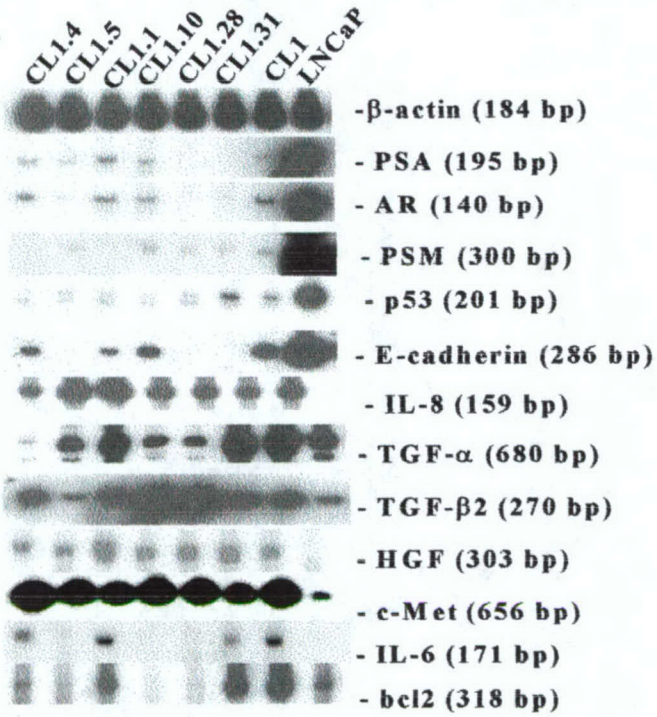

Figure 2. Gene expression of LNCaP, CL1, and CL1 clones. There is marked down-regulation of PSA, AR, PSMA, E-cadherin and p53; and up-regulation of IL-8, HGF, c-met, and IL-6 as estimated from the band intensities. Additional gene expression differences revealed by DNA microarrays are reported in the appendix.

Aim 1.4. Differential expression of cell surface molecules (CD) in AD and AI CaP cells.

In summary, 8 CD markers (Fig. 3) were found to be associated with the progression from AD to AI cancer (6, 7). Of the 8 differentially expressed surface markers, only 5 had commercially available antibodies for formalin-fixed paraffin embedded tissue. Therefore, the expression of these 5 surface markers (CD10, CD13, CD44, CD54, and CD104) was determined using IHC staining of a custom-made cell line microarray constructed of formalin fixed, paraffin embedded cells derived from cell culture that contained the prostate cancer lines LAPC-4, LNCaP, DU145, PC-3, CL1, and CL2, and CL1 clones (see Figure 4). Subsequently, the CD10 and FEN-1 markers were analyzed in large-scale tissue arrays using clinical samples of CaP (see Aim 4).

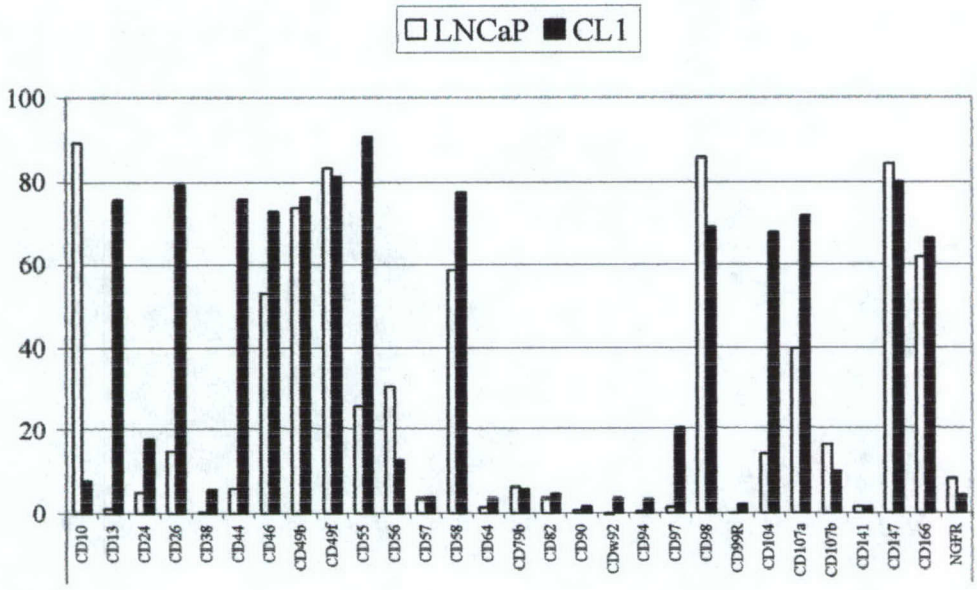

Figure. 3. CD profiles of LNCaP and CL1 cells. The percentages of positive events scored by flow cytometry are indicated on the *Y* axis, and the specificities tested are listed on the *X* axis.

In addition to the characterization of CD surface marker changes associated with transition from AD to AI tumors, we are in the process of characterizing the differential CD surface markers between non-tumorigenic CL1.31 and tumorigenic CL1.1. We are hopeful that this study will provide further information associated with the tumorigenicity of prostate cancers. A full result of this study is expected in the coming year.

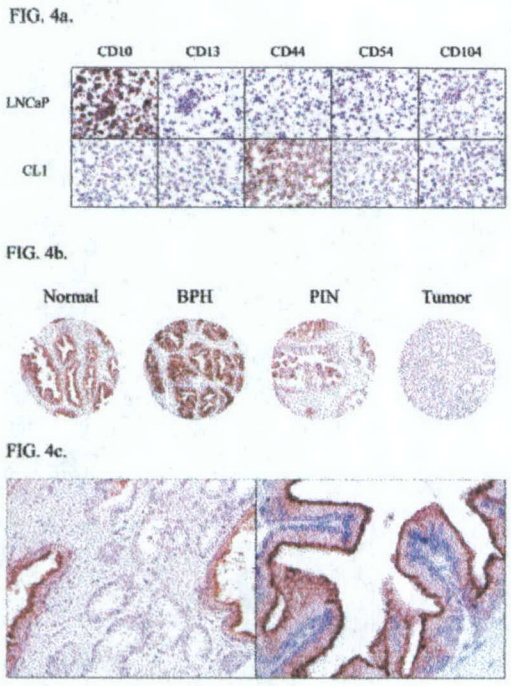

Figure 4. (a) IHC staining with antibodies against five surface markers (CD10, CD13, CD44, CD54, and CD104) on a custom-made cell line microarray constructed of formalin fixed, paraffin embedded cells derived from cell culture that contained the prostate cancer lines LAPC-4, LNCaP, DU145, PC-3, CL1, and CL2, and CL1 clones. (b) IHC staining of CD10 in various stages of CaP tissue arrays. (c) CD10 staining in PIN specimens showing low expression in normal tissues and high expression in tumor tissues. (d) and (e) are summary of CD10 staining results from the prostate tissue microarray. In d, the percent of spots that stained negative to weak (0-1 on a 3 point scale) or moderate to strong (2-3 on a 3 point scale) for CD10 are segregated by histological type. In e, box plots of the percent of spots that stained positive at any intensity multiplied by the maximum intensity of staining on a 0 to 3 scale. For box plots, the black box represents the 75th and 25th percentiles. The thin white box represents the median. The single black line with brackets containing the dots represents the 5th and 95th percentiles. The single black lines represent outliers beyond the 5th or 95th percentiles.

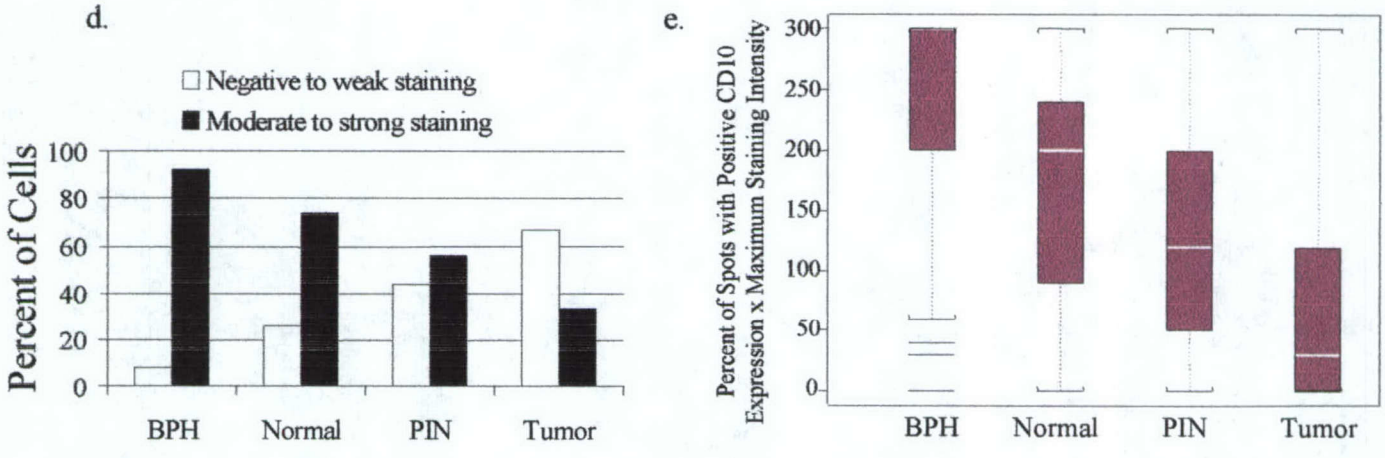

Task 2. To develop an improved therapeutic schedule of intermittent androgen deprivation therapy capable of delaying progression to the AI stage using the molecular and cellular markers identified in specific aim 1 as experimental endpoints.

Aim 2.1. Intratumoral cellular interactions and growth regulation of AI and AD populations exposed to androgen deprivation therapy.

Based on our preliminary data, we believe that AI growth control is mediated, in part, by the proliferative activity of the AD population. To further test the effect of continued androgen deprivation therapy on the "cross-talk" between AD and AI population, experiments have been performed *in vitro* by monitoring the relative growth of LNCaP cells mixed with CL1-GFP cells. We have now adopted a strategy using a constant total number of cells and varying the ratio of CL1-GFP/LNCaP from 1:10,000 to 1:1 including a culture with CL1-GFP alone. We have shortened the time for monitoring differential growth between the AI and AD populations to 3 times at day 3, day 5 and day 7 in a 1-week period of time (Fig. 5). The number of doubling for CL1 and LNCaP in a co-culture system was determined by using flow cytometry (Fig. 6). Based on these experimental conditions, we determined the number of doublings at each ratio of CL1-GFP/LNCaP co-cultures at each time points during the co-culture (Fig. 7). The number of doubling is calculated based on the formula as follows. An irrelevant human kidney cancer cell line 293 was used as a control to assess whether the effect on CL1-GFP is specifically due to cross-talk with its parental line LNCaP. LNCaP was capable suppressing the growth of CL1 at ratios of 10,000:1 to 100:1. The suppressive influence of LNCaP is lost as the ratio becomes even and there appears to be an overall mitogenic effect, such that the growth of CL1, as well as LNCaP, is over stimulated compared to the growth rate of the individual cell line alone.

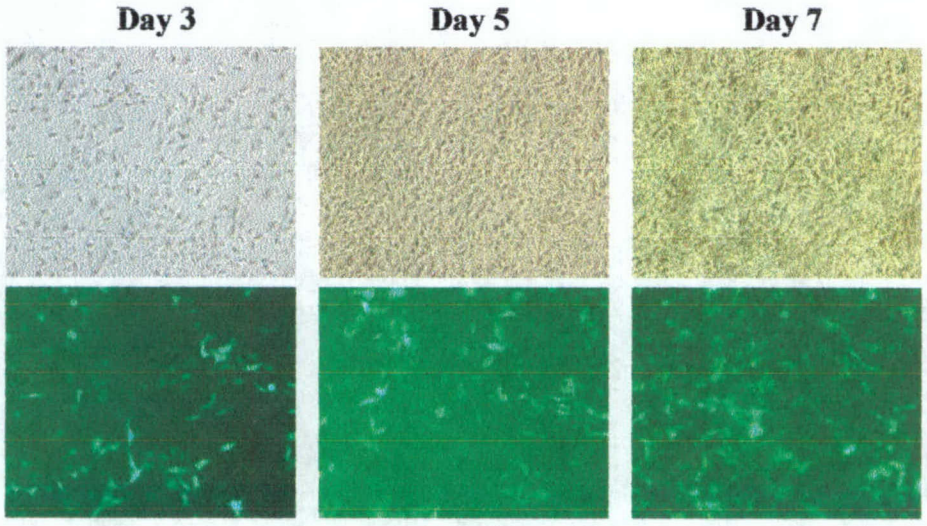

Figure 5. Tissue culture of AI CL1-GFP and AD LNCaP co-cultured in regular serum at 1:1 ratio. Phase-contrast microscopy is shown on the top row with the corresponding green-florescence microscopy shown on the bottom row.

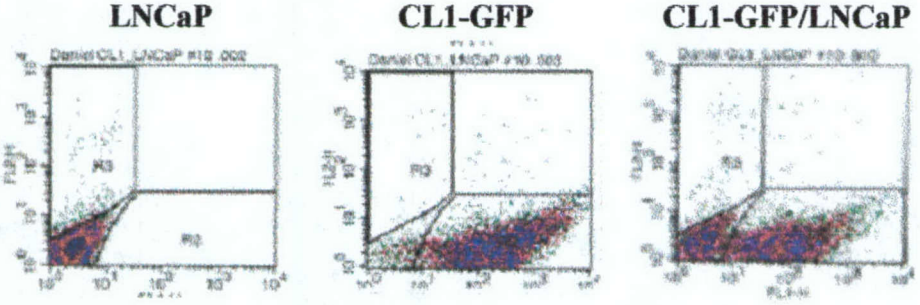

Figure 6. Flow cytometry of AI CL1-GFP, AD LNCaP, and co-cultured of CL1-GFP/LNCaP at 1:1 ratio.

Number of CL1 at a given time (Nt) = Initial number of CL1 cells (Ni) x 2^n
$n = \log (Nt/Ni) / \log 2$

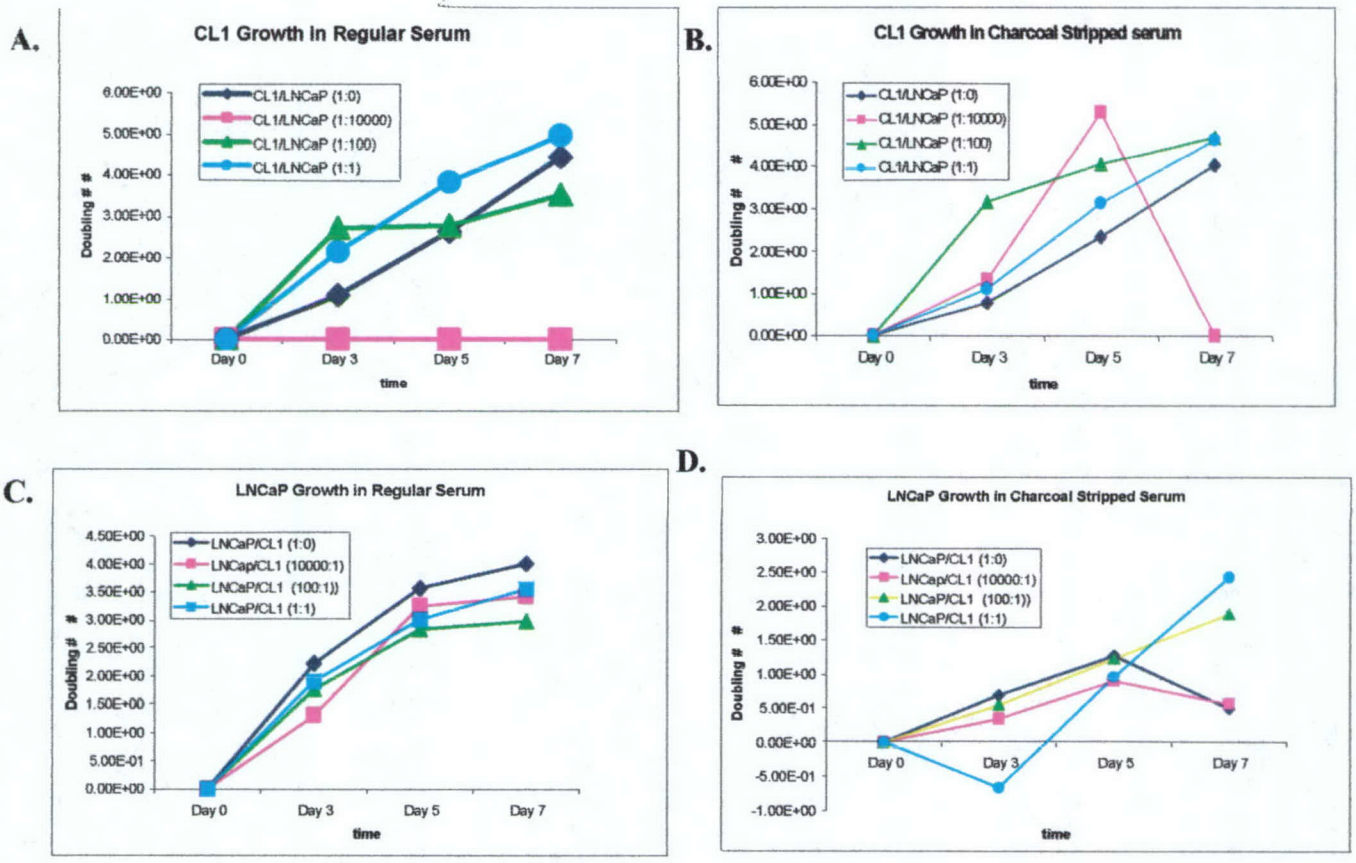

Figure 7. Growth rates of AI CL1 and AD LNCaP in CL1/LNCaP co-cultures. The number of doubling for CL1 (A and B) and LNCaP (C and D) on day 3, 5, and 7 in a co-culture system was determined by using flow cytometry. Cell proliferation rate under regular serum (A and C) and charcoal-stripped serum (B and D) was determined separately. These experiments have been repeated 4 times with similar results obtained.

A pilot study has also been performed to find the optimal growth inhibitory concentrations of LNCaP cells to CL1 *in vivo*. Concentrations of 1 x 10^7, 1 x 10^6, 1 x 10^5, and 0 LNCaP cells are being mixed with a constant number of CL-1/GFP (1 x 10^4 cells) and injected intraprostatically with 5 µl Matrigel (a stimulator of LNCaP growth) into castrated and non-castrated SCID mice (20 mice/group, total 160 mice). The kinetic profile of tumor volume, PSA production, tumor progression-associated gene expression, and CL1-GFP invasion and metastasis over time are being determined, analyzed, and compared. Preliminary results are shown in Fig. 8. Thus, it appears that a similar observation occurs *in vivo* as in the *in vitro* experiments. Ongoing experiments are being conducted to validate these preliminary findings.

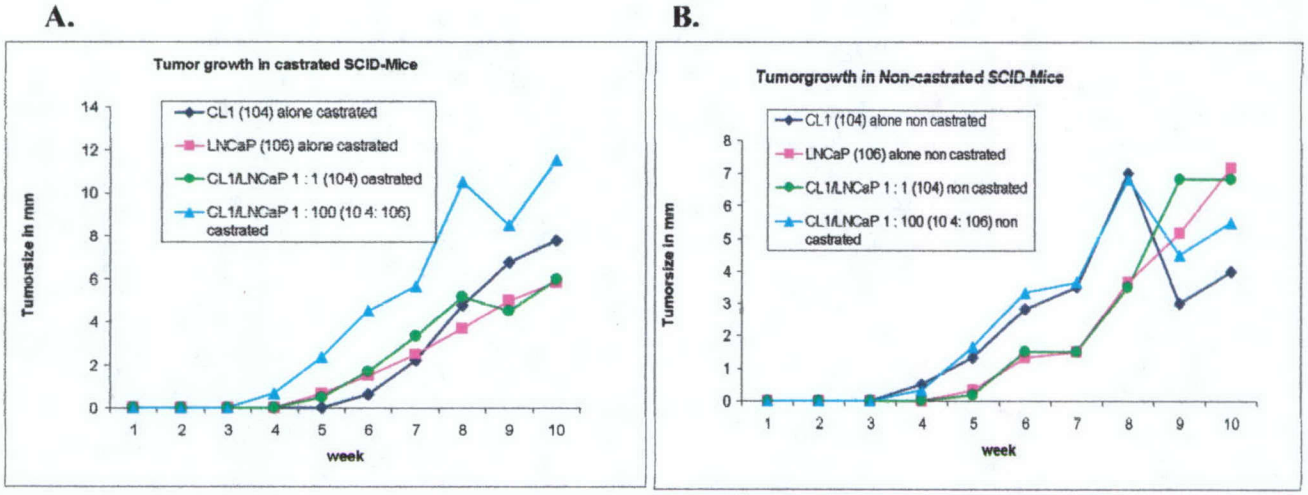

Figure. 8. Tumor growth in vivo in SCID mice under castrated (A) and non-castrated conditions (B). Cells were mixed in the indicated ratios, supplemented with equal volumes of matrigel and injected subcutaneously into male SCID mice of 6-8 weeks of age. Tumor growth was monitored twice a week. The in vivo results have been repeated.

In summary, we found that *in vitro* the AD LNCaP line was able to suppress the growth of CL1 as long as there was a clear numeric superiority of LNCaP (ratios from 10,000:1 to 100:1). As the cell ratio of CL1 and LNCaP becomes more even, this suppressive influence is lost and turns into a mutually mitogenic effect, such that the growth of CL1 as well as LNCaP is over stimulated compared to the growth rate of the individual cell line alone. These experiments have been repeated in quadruplicate and similar results were observed each time. *In vivo* experiments support the *in vitro* observations, but more vigorous studies are still needed to confirm this effect in vivo. We therefore conclude that there is clearly a cross-talk between CL1 and its parental line LNCaP. At LNCaP/CL1 ratios that are close to pre-androgen ablation conditions, LNCaP suppresses the growth of AI populations and thus overgrowth of AD tumor is the dominant event. However, AI and AD populations appear to promote growth between each other when this balance is offset. For example, during androgen ablative therapy, the LNCaP/CL1 ratio becomes lower than 1:1 reflecting the outcome of this therapy. Therefore, the cross-talk is clinically relevant to the outcome of androgen ablation therapy.

The interaction between LNCaP and CL1 was further investigated by understanding the lineage relationships of the two cell lines based on expression of CD markers. Analyses were performed to determine whether CL1 cells were selected from pre-existent subpopulations in LNCaP. Prostate cancer cells were characterized by CD phenotyping. Specific cell populations were sorted by flow cytometry. DNA array analysis was used to probe differential gene expression. CD phenotyping demonstrated that CL1 was dissimilar to LNCaP. One common difference between LNCaP and its derivatives was CD26, in which virtually all CL1 and other AI cells were CD26(+), whereas only approximately 10% of LNCaP cells were CD26(+). The CD26(+) subpopulation of LNCaP was isolated and cultured in vitro. Following culture, a high percentage of the cells (descended from the sorted cells) were CD26(+), in contrast to those sorted by CD13 or CD44. The cultured CD13 and CD44 populations did not show a high percentage of CD13(+) and CD44(+) cells, respectively. CD13 and CD44 are markers, in addition to CD26, for CL1. Therefore, this suggests that CL1 may arise de novo (8).

Aim 2.2. Kinetics of tumor progression and metastatic potential of the LNCaP/CL1-GFP model treated with various pulsed androgen deprivation (PAD) therapies.

This aim is still under investigation.

Aim 3 (new). To investigate strategies to simultaneously target both hormonal and other growth factor and apoptotic signaling pathways to synergistically delay the development of AI and metastatic CaP.

In addition to the proposed intermittent androgen deprivation therapy, we also investigated whether chemotherapy could induce differential sensitivity to apoptosis between AI and AD cells. We believe that combining intermittent androgen depletion with chemotherapy may achieve better efficacy to treat HRPC. Two avenues of investigation were carried out: 1) use of proteasome inhibitor, bortezomib in combination with TRAIL for induction of differential apoptosis in AD lines (LNCaP) and AI lines (CL1) (9). 2) use of DETANONOate (NO donor) for induction of TRAIL and FasL-mediated apoptosis specifically in AI CL1 line.

A.

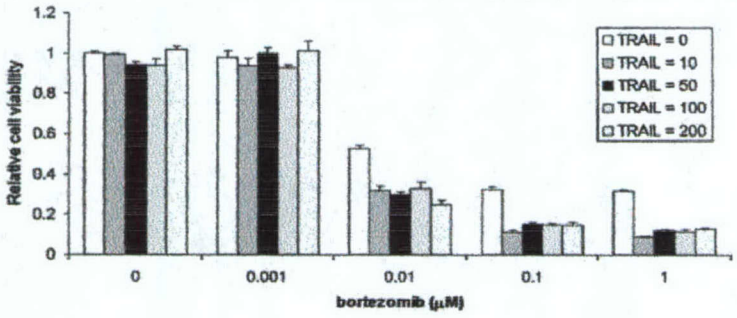

B.

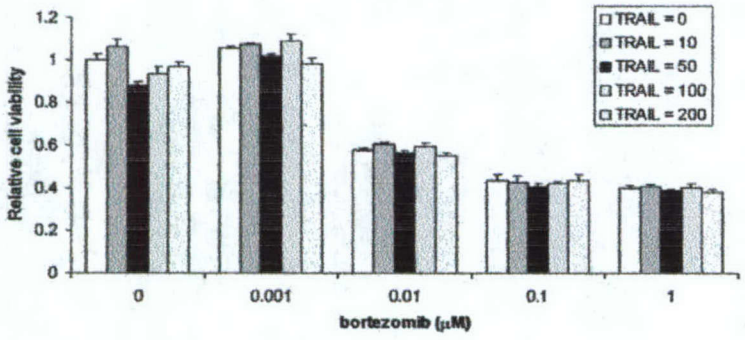

C.

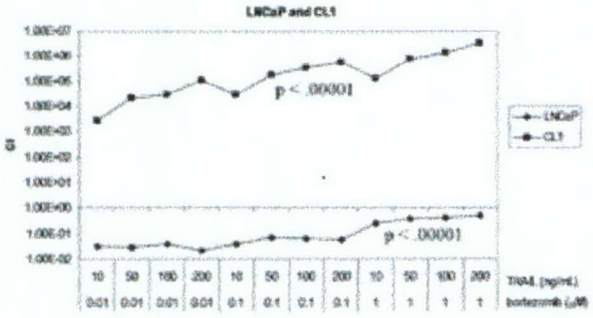

Figure. 9. Cytotoxicity of combinations of TRAIL or TNF and bortezomib in AD and AI prostate cancer cells (**A:** LNCaP, **B:** CL1). Prostate cancer cells were plated in the 96-well format and incubated overnight. TRAIL or TNF alone or in combination with bortezomib or appropriate vehicle controls were added at the indicated concentrations for 48 h, and cell viability was measured by the MTT assay. For drug combinations, bortezomib was added 90 min before TRAIL. Experiments were performed in quadruplicate and are reported as means +/- SD. **C:** The effect of drug combinations on cytotoxicity was performed by the median effect method using Calcusyn software, version 1.1.1 (Biosoft, Ferguson, MO; Ref. 24). CI values were calculated using the most conservative assumption of mutually nonexclusive drug interactions. CI values were calculated from median results of the cytotoxicity (MTT) assays, which were performed in quadruplicate. CI values significantly greater than 1 indicate drug antagonism, CI values significantly less than 1 are indicative of synergy, and CI values not significantly different than 1 indicate an additive drug effect. Linear regression correlation coefficients of the median effects plots were required to be >0.90 to demonstrate that the effects of the drugs follow the law of mass action, which is required for a median effect analysis.

As shown in Fig. 9, when bortezomib and TRAIL were used in combination, median effect analysis demonstrated synergistic interactions across all concentrations of both bortezomib and TRAIL in AD (LNCaP and LAPC4, not shown in this report) and AI (DU145, not shown in this report) cell lines but not the AI CL1 cell line (antagonistic effect). Up to 90% cell death was observed at concentrations well below those that induced death by either agent alone in both AD and AI cells. Bortezomib and TRAIL were antagonistic in CL1 cells. In addition, we also demonstrated that NO sensitizes CL1 for TRAIL and Fas-mediated apoptosis (Fig. 10).

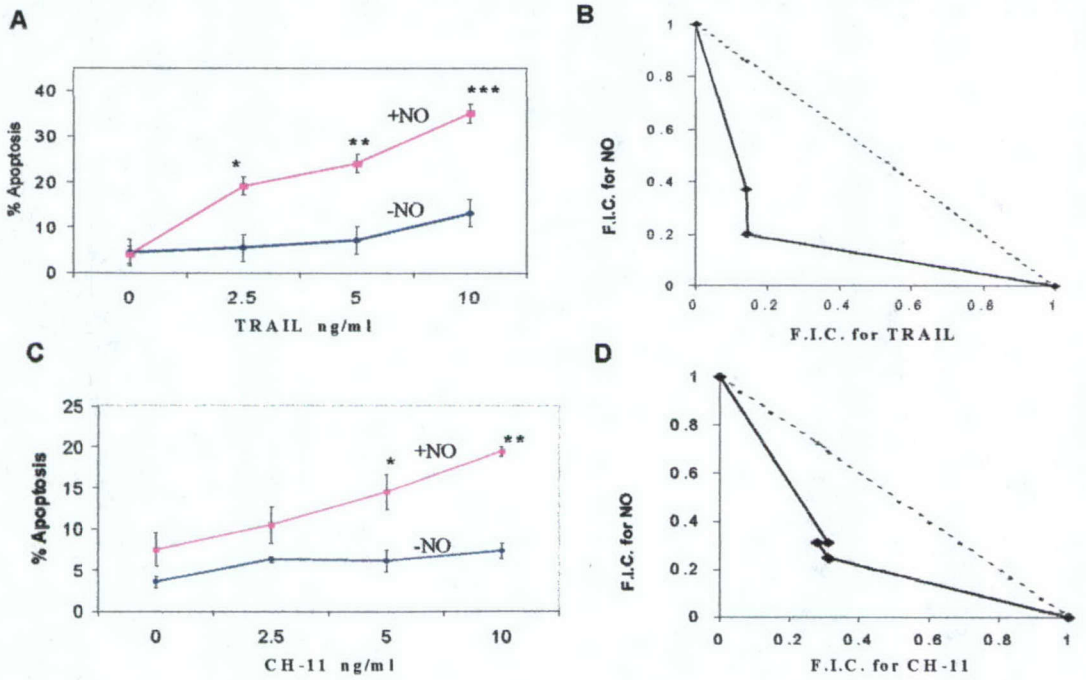

Figure. 10. A) The CaP cell line CL-1 was grown in serum-free medium and the cells were treated with different concentrations of TRAIL (0, 2.5, 5 and 10 ng/ml), and treated or left untreated with DETANONOate (1000 μM) (nitric oxide (NO) donor) for 18 h at 37°C in a 5% CO2 incubator. Fixed and permeabilized cells were stained with anti-active-caspase-3-FITC (for apoptosis) antibody and analyzed by flow cytometry. Significant potentiation of apoptosis was observed (wTRAIL; nTRAIL and NO). **B)** Synergy was achieved by combination of NO and TRAIL as determined by isobologram analysis. The

data are the mean of three independent experiments. * $p<0.05$, **$p<0.02$,*** $p<0.004$. **C)** The CaP cell line CL-1 was grown in serum-free medium and the cells were treated with different concentrations of CH-11 (0, 2.5, 5 and 10 ng/ml) (anti-Fas agonist mAb), and treated or left untreated with DETANONOate (1000 μM) for 18 h at 37°C in 5% CO2 incubator. Fixed and permeabilized cells were stained with anti-active-caspase-3-FITC antibody and analyzed by flow cytometry. Significant potentiation of Apoptosis was observed. **D)** Synergy was achieved by combination of NO and CH-11 as determined by isobologram analysis (wCH-11 alone; nCH-11 and NO). The data are the mean of three independent experiments. * $p<0.05$, **$p<0.02$

Aim 3. (now Aim 4) Validation of tumor-specific gene expression in fresh human CaP tumors and other AD, AI, and metastatic CaP cell lines by tissue array.

Following Internal Review Board approval, formalin-fixed paraffin-embedded tissue from primary radical prostatectomy specimens between 1984 and 1995 were selected. To provide adequate sampling at least 3 replicate tumor (mean 3.4) and one matching normal tissue samples were taken in a widely representative fashion. When available, tumor samples were accompanied by matching benign (morphologically normal and hyperplastic) and PIN lesions. Ultimately, tissue from 246 prostatectomy specimens was arrayed into 3 blocks encompassing a total of 1364 individual spots (6). Currently, the following markers have been validated.

Tissue microarray expression of CD10. Once it was identified that decreased CD10 expression correlated with hormone refractory phenotype in our limited cell line sampling, we sought to determine the expression of CD10 among clinical prostate samples to examine the prevalence of loss of CD10 expression among hormone naïve patients with early stage prostate cancer. To accomplish this, a tissue microarray containing tissue spots from surgical specimens of 219 hormone naïve patients that underwent radical prostatectomy was examined for CD10 expression. CD10 expression was scored for the maximal intensity of staining (0 to 3) and the percent of cells that stained positive at any intensity (0 to 100%). Prostate cancer spots demonstrated significantly reduced intensity of CD10 expression relative to matched morphologically normal ($p<0.0001$) and BPH samples ($p<0.0001$). PIN specimens showed CD10 staining that was intermediate between the high expression of normal ($p=0.033$) and the low expression of prostate cancer ($p=0.0001$) (Fig. 4C). The median number of CD10 positive cells was 100% for BPH, 90% for normal prostate tissue and PIN, but only 30% for prostate cancer cases. Moreover, 34% of prostate cancer spots showed no CD10 expression relative to only 3% of normal or hyperplastic prostatic tissue, and 5% of PIN spots. In order to combine the information obtained from the maximum staining intensity and percent of cells staining positive, these two variables were multiplied to generate a new variable. This new variable was scored from 0 (0% cells staining at an intensity of 0) to 300 (100% of cells staining at an intensity of 3). A trend was found with BPH having the highest median score (300) followed by normal prostate tissue (200), with decreased expression found in PIN (120) and prostate cancer (30). Among prostate cancer samples, 86% showed CD10 expression below the median expression of normal prostatic tissue and 68% showed expression below the 25% percentile of normal prostate tissue. While several clinical and pathological variables (Gleason sum, organ confinement, node status, seminal vesicle involvement, capsular invasion and margin status) were significant predictors of biochemical recurrence and time to recurrence, no relationship was identified between any of the CD10 expression measures and pathological Gleason score, pathological stage, or biochemical recurrence in either univariate or multivariate analysis ($p>0.1$ for all comparisons).

Tissue microarray analysis of FEN-1: Immunohistochemical analysis using a FEN-1 monoclonal antibody was performed on tissue microarrays constructed from paraffin embedded specimens from 246 patients who underwent radical retropubic prostatectomy (Fig. 11). FEN-1 staining was correlated with established prognostic factors (Gleason score, PSA, and pathologic stage) and biochemical recurrence-free survival was analyzed. Data were compared using standard statistical methods. There were a total of 1083 informative tissue spots, which included 651 cancer, 264 normal, 120 benign prostatic hyperplasia (BPH), and 48 prostatic intraepithelial neoplasia (PIN). Mean expression of FEN-1 was significantly higher in cancer (36.7%) compared to normal (13.2%), BPH (4.5%), and PIN (15.4%) specimens ($p < 0.0001$) (Fig. 12A). FEN-1 expression was significantly correlated with Gleason score ($\sigma = 0.24$, $p = 0.0008$) (Fig. 12B). Preoperative PSA ($p = 0.0052$), Gleason score ≥ 7 ($p < 0.0001$), seminal vesicle invasion ($p < 0.0001$), extraprostatic extension ($p = 0.0013$) were associated with recurrence-free survival, whereas FEN-1 expression was not (Table 4). On multivariate analysis, only Gleason score ≥ 7 ($p = 0.0007$), seminal vesicle invasion ($p = 0.004$), and extraprostatic extension ($p = 0.0084$) were retained as independent prognostic indictors for PSA recurrence. In conclusion, FEN-1 is overexpressed in prostate cancer with a Gleason score of 7 and higher. These results suggest that FEN-1 may be a potential tumor marker for the selection of patients at high risk and a target for prostate cancer diagnosis and therapy.

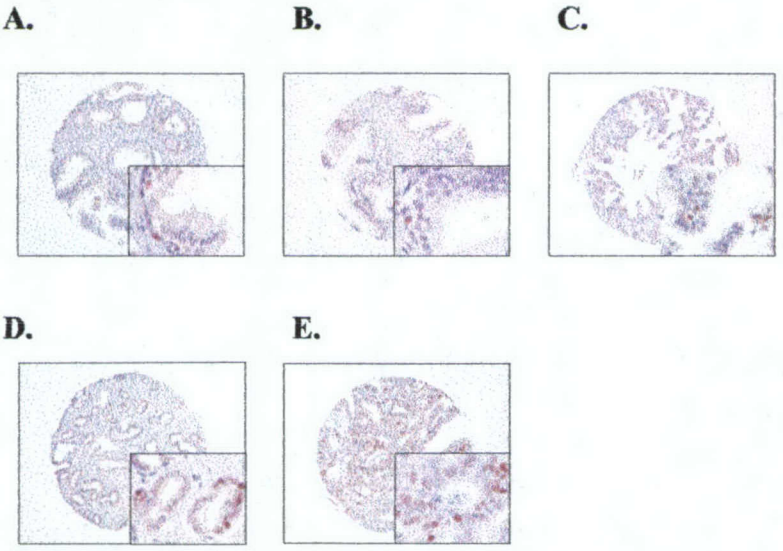

Figure. 11. Immunohistochemical analysis of a prostate tissue microarray using anti-FEN-1 antibody. A. normal, B. benign prostatic hyperplasia (BPH), C. prostatic intraepithelial neoplasia (PIN), D. low grade prostate cancer, E. high grade prostate cancer. Reduced from x10 (A to E) and x40 (inserts).

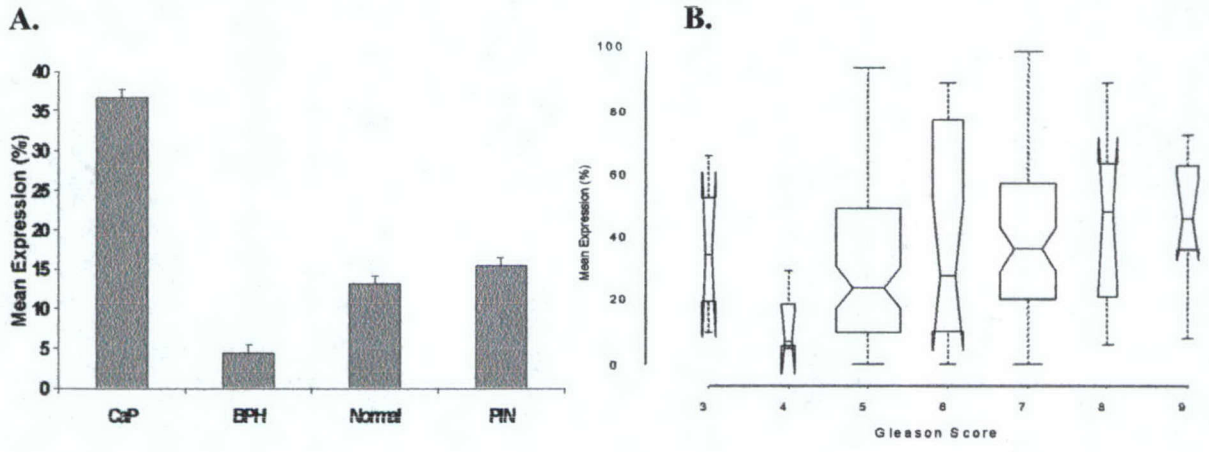

Figure 12. (A) Mean percentage of cells with positive staining for FEN-1 in prostate cancer (CaP), benign prostatic hyperplasia (BPH), normal prostate, and prostatic intraepithelial neoplasia (PIN). Total of 1,083 spots were available. Error bars represent 1 standard error. (B) Mean percent positive expression of FEN-1 according to Gleason score shown in a box plot graph. The middle line represents the median; the upper and lower hinges of the box show the medians of the upper and lower halves of the data. The width of the boxes represents the number of tumor spots. The ends of the line segments attached to the box extend to the smallest data value and the largest data value. All data values are shown.

Table 3. Mean FEN-1 expression of paired primary and metastatic prostate cancers.

	Mean expression FEN-1 (%)
Matched pair 1	
Primary prostate cancer	12
Metastatic lesion	10
Matched pair 2	
Primary prostate cancer	53
Metastatic lesion	40
Matched pair 3	
Primary prostate cancer	8
Metastatic lesion	0

Table 4. Mean FEN-1 expression and clinical prognostic factors.

	Mean expression FEN-1 (%) ± SE	p value*
Gleason score		0.004
6 or less	32.2 ± 26.7	
7 or greater	41.7 ± 24.5	
Seminal vesicle invasion		0.36
No	35.6 ± 26.4	
Yes	39.3 ± 25.0	
Organ confined		0.6
Yes	35.7 ± 26.3	
No	37.2 ± 25.3	
Capsular involvement		0.77
None	36.0 ± 24.8	
Capsular invasion	35.4 ± 26.3	
Extraprostatic extension	38.7 ± 27.4	

PSA (ng/ml)		0.9
Less than 10	36.9 ± 26.8	
10 or greater	37.0 ± 25.8	
Nodal involvement		0.72
No	36.4 ± 26.1	
Yes	33.2 ± 23.8	

* p value from a Kruskal-Wallis test.

Key Research Accomplishments During the DOD Funding (1-3 are achievements in the past year alone):

1) Cross-talk between AD LNCaP and AI CL1 was investigated: Depending on the ratio of the two lines, LNCaP is able to suppress the growth of CL1 when there is a numeric superiority of the former (ratio 10000:1). The more the cell numbers of CL1 and LNCaP get equal this suppressive influence gets lost and turns into a stimulating effect, so that the growth of CL1 as well as the growth of LNCaP is over stimulated compared to the growth rate of the individual cell line alone.
2) The lineage relationship between AD LNCaP and AI CL1 was investigated: CD phenotyping showed that CL1 and LNCaP were very dissimilar. One common difference between LNCaP and its derivatives was CD26, in which virtually all CL1 cells were CD26(+) but only approximately 10% of LNCaP cells were CD26(+). The CD26(+) subpopulation of LNCaP was isolated and cultured in vitro. After culture, a high percentage of the cells (descended from the sorted cells) were CD26(+), in contrast to those sorted by CD13 or CD44. The cultured CD13 and CD44 populations did not show a high percentage of CD13(+) and CD44(+) cells, respectively. CD13 and CD44 are markers, in addition to CD26, for CL1. Therefore, CL1 arose de novo.
3) Validations of previously identified cellular and molecular markers associated with the development from AD to AI prostate cancers are carried out: FEN-1 expression was significantly correlated with Gleason score ($\sigma = 0.24$, $p = 0.0008$). Preoperative PSA ($p = 0.0052$), Gleason score ≥ 7 ($p < 0.0001$), seminal vesicle invasion ($p < 0.0001$), extraprostatic extension ($p = 0.0013$) were associated with recurrence-free survival, whereas FEN-1 expression was not. On multivariate analysis, only Gleason score ≥ 7 ($p = 0.0007$), seminal vesicle invasion ($p = 0.004$), and extraprostatic extension ($p = 0.0084$) were retained as independent prognostic indictors for PSA recurrence. Therefore, FEN-1 is overexpressed in prostate cancer with a Gleason score of 7 and higher, suggesting that FEN-1 may be a potential tumor marker for the selection of patients at high risk and a useful target for prostate cancer diagnosis and therapy.
4) We investigated chemotherapy agents with the potential of inducing differential sensitivity to apoptosis between AI and AD cells. Proteasome inhibitor, bortezomib, was shown to synergize with TRAIL and TNF-α and induced cell death of AD LnCaP but not AI Cl1. In addition, DETANONOate (NO donor) was shown to synergize with TRAIL and FasL to induce apoptosis of the AI CL1 lines. Chemotherapy agents that induce differential sensitivity to apoptosis between AI and AD cells may synergize with intermittent androgen deprivation for treatment of hormone refractory cancer, a hypothesis we hope to further explore in year 3.

5) We identified global gene changes between CL1 and its parental line LnCaP by using human cancer-specific cDNA microarray, MPSS, PCR, and flow cytometry.
6) One of the genes differentially expressed between LNCaP and CL1 was vimentin. It was demonstrated using an *in vitro* invasion assay that decreased vimentin expression in the constitutively vimentin-expressing CL1 cells led to a significant decrease in their invasiveness, which implied that vimentin represented an attractive target for therapy against AI CaP.
7) Construction of a custom-made cell line microarray consisted of formalin fixed, paraffin embedded cells derived from cell cultures containing AD and AI prostate cancer lines, including LAPC-4, LNCaP, DU145, PC-3, CL1, and CL2, and CL1 clones has been completed and pilot studies performed. CD10 has been confirmed as a biomarker, the loss of its expression is associated with progression from AD to AI disease.

Reportable outcomes of the DOD funding period (1-3 are manuscripts of the past year):

1. Manuscript: Liu, A. Y., Brubaker, K. D., Goo, Y. A., Quinn, J. E., Kral, S., Sorensen, C. M., Vessella, R. L., Belldegrun, A. S., Hood, L. E. "Lineage relationship between LNCaP and LNCaP-derived prostate cancer cell lines" (2004) Prostate 60(2):98-108.
2. Manuscript: John S. Lam, Hong Yu, Ai Li, Mervi Eeva, John T. Leppert, Oleg Shvarts, Allan J. Pantuck, Steve Horvath, David B. Seligson, and Arie S. Belldegrun "Flap Endonuclease 1 is Overexpressed and Associated with High Gleason Score in Prostate Cancer." Submitted.
3. Manuscript: Daniel Seiler, Randy Caliliw, John Leppert, Allan Pantuck, Allen Y. Wang, John S. Lam, Arie S. Belldegrun, Gang Zeng "Cross-talk between the androgen-dependent cell-line LNCaP and the androgen-independent cell-line CL1 in an in vitro model." In preparation.
4. Manuscript: An, J. Sun, Y. P., Adams, J., Fisher, M., Belldegrun, A., Rettig, M. B. "Drug interactions between the proteasome inhibitor bortezomib and cytotoxic chemotherapy, tumor necrosis factor (TNF) alpha, and TNF-related apoptosis-inducing ligand in prostate cancer" *Clinical Cancer Research* 9(12): 4537-45 (2003).
5. Manuscript: Singh, S., Sadacharan, S., Su, S., Belldegrun, A., Persad, S., Singh, G. "Overexpression of vimentin: role in the invasive phenotype in an androgen-independent model of prostate cancer" Cancer Res. 63(9): 2306-11 (2003).
6. Manuscript: Stephen J. Freedland, Allan J. Pantuck, Sun H. Paik, Amnon Zisman, Thomas G. Graeber, David Eisenberg, William H. McBride, David Nguyen, Cho-Lea Tso, and Arie S. Belldegrun "Heterogeneity of Molecular Targets on Clonal Cancer Lines Derived From a Novel Hormone-Refractory Prostate Cancer Tumor System" *The Prostate* 55:299-307 (2003).
7. Manuscript: Stephen J. Freedland, David B. Seligson, Alvin Y. Liu, Allan J. Pantuck, Sun H. Paik, Steve Horvath, Jeffrey A. Wieder, Amnon Zisman, David Nguyen, Cho-Lea Tso, Aarno V. Palotie, and Arie S. Belldegrun "Loss of CD10 (Neutral Endopeptidase)Is a Frequent and Early Event in Human Prostate Cancer" *The Prostate* 55:71-80 (2003).
8. More than 6 abstracts were presented in national and international conferences, including annual meetings of the AUA and AACR.

Conclusions:

The overall goal of this project is to understand the cellular and molecular changes associated with the development of AI in CaP to develop novel treatment for HRPC. During the last year of our grant support from DOD, we continued our efforts of identifying global gene changes between CL1 and its parental line LNCaP with a focus on lineage relationship between these two lines. We also studied the cross-talk between the androgen-dependent cell-line LNCaP and the androgen-independent cell-line CL1 using an in vitro tissue culturing system and an in vivo tumor growth model.

Overall, we have identified cellular and molecular markers for the progression of androgen dependent (AD) to androgen independent (AI). Many of these markers have been confirmed in large-scale tissue array analysis, which may be valuable biomarkers for the prognosis of CaP. Our study also provided biological mechanisms of developing more effective androgen deprivation-based treatment schedules capable of delaying prostate cancer tumor progression from locally advanced to widely metastatic disease.

References

1. Eisenberger, M. A., B. A. Blumenstein, E. D. Crawford, G. Miller, D. G. McLeod, P. J. Loehrer, G. Wilding, K. Sears, D. J. Culkin, I. M. Thompson, Jr., A. J. Bueschen, and B. A. Lowe. 1998. Bilateral orchiectomy with or without flutamide for metastatic prostate cancer. *N Engl J Med 339:1036.*
2. de Voogt, H. J., U. Studer, F. H. Schroder, J. G. Klijn, M. de Pauw, and R. Sylvester. 1998. Maximum androgen blockade using LHRH agonist buserelin in combination with short-term (two weeks) or long-term (continuous) cyproterone acetate is not superior to standard androgen deprivation in the treatment of advanced prostate cancer. Final analysis of EORTC GU Group Trial 30843. European Organization for Research and Treatment of Cancer (EROTC) Genito-Urinary Tract Cancer Cooperative Group. *Eur Urol 33:152.*
3. Pantuck, A. J., F. Berger, A. Zisman, D. Nguyen, C. L. Tso, J. Matherly, S. S. Gambhir, and A. S. Belldegrun. 2002. CL1-SR39: A noninvasive molecular imaging model of prostate cancer suicide gene therapy using positron emission tomography. *J Urol 168:1193.*
4. Patel, B. J., A. J. Pantuck, A. Zisman, K. H. Tsui, S. H. Paik, R. Caliliw, S. Sheriff, L. Wu, J. B. deKernion, C. L. Tso, and A. S. Belldegrun. 2000. CL1-GFP: an androgen independent metastatic tumor model for prostate cancer. *J Urol 164:1420.*
5. Freedland, S. J., A. J. Pantuck, S. H. Paik, A. Zisman, T. G. Graeber, D. Eisenberg, W. H. McBride, D. Nguyen, C. L. Tso, and A. S. Belldegrun. 2003. Heterogeneity of molecular targets on clonal cancer lines derived from a novel hormone-refractory prostate cancer tumor system. *Prostate 55:299.*
6. Freedland, S. J., D. B. Seligson, A. Y. Liu, A. J. Pantuck, S. H. Paik, S. Horvath, J. A. Wieder, A. Zisman, D. Nguyen, C. L. Tso, A. V. Palotie, and A. S. Belldegrun. 2003. Loss of CD10 (neutral endopeptidase) is a frequent and early event in human prostate cancer. *Prostate 55:71.*
7. Liu, A. Y., M. P. Roudier, and L. D. True. 2004. Heterogeneity in primary and metastatic prostate cancer as defined by cell surface CD profile. *Am J Pathol 165:1543.*
8. Liu, A. Y., K. D. Brubaker, Y. A. Goo, J. E. Quinn, S. Kral, C. M. Sorensen, R. L. Vessella, A. S. Belldegrun, and L. E. Hood. 2004. Lineage relationship between LNCaP and LNCaP-derived prostate cancer cell lines. *Prostate 60:98.*
9. An, J., Y. P. Sun, J. Adams, M. Fisher, A. Belldegrun, and M. B. Rettig. 2003. Drug interactions between the proteasome inhibitor bortezomib and cytotoxic chemotherapy, tumor necrosis factor (TNF) alpha, and TNF-related apoptosis-inducing ligand in prostate cancer. *Clin Cancer Res 9:4537.*

Revised Summary of Statement of Work (SOW)

The ultimate goal of this grant is to identify markers for the development of androgen-independent (AI) prostate cancer (CaP) in order to design the most effective regimen of hormone therapy that can then be translated to a meaningful Phase I clinical trial.

Specific aim 1: To identify new molecular and cellular markers for the conversion from AD to AI CaP using a novel LNCaP/CL1-GFP tumor model (months 1-18).

All of the following tasks are completed.

Task 1. Screening of single–cell derived CL1-GFP subclones for their metastatic potential (175 mice will be used in this specific task) (months 1-6).

Task 2. Gene expression analysis using commercially available cDNA expression arrays (months 6-12).

Task 3. Analysis of expression array data (months 12-18).

Task 4. Differential expression of CD cell surface markers in androgen-dependent (AD) and AI CaP cells (months 6-12).

Task 5: Identification of AD cell-derived growth inhibitory factors (months 6-18).

Specific aim 2: To develop an improved therapeutic schedule of intermittent androgen deprivation therapy that is capable of delaying progression to the AI stage using the molecular and cellular markers identified (Specific aim 1) as experimental endpoints (months 18-36).

In vitro experiments have been completed; In vivo experiments are partially completed (task 2 still on-going).

Task 1: Intratumoral cellular interactions and growth regulation of AI and AD populations exposed to androgen deprivation therapy (months 18-30)

Task 2: Kinetics of tumor progression and metastatic potential of the LNCaP/CL1-GFP model treated with various PAD therapy (100 mice will be used in this specific task) (months 24-36).

Task 3: Tumor progression, regression, and animal survival (months 24-36)

Task 4: Feasibility study in other AD tumor models (months 30-36).

Specific Aim # 3: To investigate strategies to simultaneously target both hormonal and other growth factor and apoptotic signaling pathways to synergistically delay the development of AI and metastatic CaP (months 12-36)

Both tasks are completed.

Task 1: To explore the proteasome inhibitor bortezomib in combination with TRAIL for induction of differential apoptosis in AD lines (LNCaP) and AI lines (CL1) (months 12-36)

Task 2: To explore the use of DETANONOate (NO donor) for induction of TRAIL and FasL-mediated apoptosis specifically in the AI CL1 line (months 12-36)

Specific Aim #4: To validate the applicability of our new molecular and cellular markers for AI CaP using tissue arrays of clinical prostate cancer specimens (months 28-36).

Tasks completed.

The Prostate 60:98 – 108 (2004)

Lineage Relationship Between LNCaP and LNCaP-Derived Prostate Cancer Cell Lines

Alvin Y. Liu,[1,2]* Kristen D. Brubaker,[1] Young Ah Goo,[2] Janna E. Quinn,[1] Sabine Kral,[1] Carrie M. Sorensen,[2] Robert L. Vessella,[1] Arie S. Belldegrun,[3] and Leroy E. Hood[2]

[1]*Department of Urology, University of Washington, Seattle, Washington*
[2]*Institute for Systems Biology (ISB), Seattle, Washington*
[3]*Department of Urology, University of California, Los Angeles, California*

BACKGROUND. LNCaP and its derivative cell lines, which include C4-2 (and the related C4-2B) and CL1, are used as models of prostate cancer. Unlike LNCaP, the other cell lines show features of progressed disease such as metastatic capability and hormone independence. Analyses were done to determine if C4-2 or CL1 cells were selected from pre-existent subpopulations in LNCaP.

METHODS. Prostate cancer cells were characterized by cluster designation (CD) phenotyping. Specific cell populations were sorted by flow cytometry. DNA array analysis was used to probe differential gene expression.

RESULTS. CD phenotyping showed that CL1 and C4-2 (and C4-2B) were very dissimilar, and C4-2 was more similar to LNCaP. One common difference between LNCaP and its derivatives was CD26, in which virtually all C4-2 or CL1 cells were $CD26^+$ but only ~10% of LNCaP cells were $CD26^+$. The $CD26^+$ subpopulation of LNCaP was isolated and cultured in vitro. After culture, a high percentage of the cells (descended from the sorted cells) were $CD26^+$, in contrast to those sorted by CD13 or CD44. The cultured CD13 and CD44 populations did not show a high percentage of $CD13^+$ and $CD44^+$ cells, respectively. CD13 and CD44 are markers, in addition to CD26, for CL1 but not for C4-2.

CONCLUSIONS. C4-2 arose probably from $CD26^+$ LNCaP cells, while CL1 arose de novo. *Prostate 60: 98–108, 2004.* © 2004 Wiley-Liss, Inc.

KEY WORDS: **C4-2; CL1; LNCaP subpopulations; CD26**

INTRODUCTION

LNCaP is a prostate-specific antigen (PSA)-secreting, androgen receptor (AR)-positive cancer cell line established from a lymph node metastasis [1]. Its transcriptome has been extensively characterized (http://www.pedb.org), especially for the gene subset under androgen regulation [2]. Since LNCaP cells retain the response to androgen, they can be experimentally treated by hormone manipulation either in vivo (by growth in castrated animal hosts) or in vitro (by growth in androgen-depleted media) to generate variants with stable genotypic and phenotypic alterations. The variant cells show not only gain of androgen independence but also metastatic capability [3].

Abbreviations: BPH, benign prostatic hyperplasia; EST, expressed sequence tag; MMP-9, matrix metalloproteinase; PBS, phosphate buffered saline solution; RT-PCR, reverse transcriptase polymerase chain reaction.

Grant sponsor: National Institutes of Health; Grant numbers: CA85859, CA98699, DK63630; Grant sponsor: CaP CURE Foundation.

*Correspondence to: Alvin Y. Liu, Department of Urology, Box 356510, University of Washington, Seattle, WA 98195; or Institute for Systems Biology, 1441 N 34th Street, Seattle, WA 98103.
E-mail: aliu@u.washington.edu.

Received 14 October 2003; Accepted 20 November 2003
DOI 10.1002/pros.20031
Published online 28 January 2004 in Wiley InterScience (www.interscience.wiley.com).

C4-2 and C4-2B are two LNCaP derivatives that resulted from "selection" or "induction" by certain cells (stromal cells of human bone but not lung, kidney, or NIH3T3 cells) in concert with perhaps host epigenetic factors when LNCaP and inducer cells were co-implanted in animals. Specifically, 10^6 LNCaP and 10^6 stromal cells were inoculated into male athymic mice. After 4 weeks in a castrated host, C4 was obtained. Further co-implantation of C4 and stromal cells in castrated hosts led to the C4-2 line. C4-2 exhibits androgen independent growth associated with skeletal metastasis, produces metastases when injected either subcutaneously or orthotopically in intact or castrated mice, and shows tropism for the skeletal environment to produce bone metastasis. It shares common marker chromosomes with the parental LNCaP [4,5]. A selected derivative of C4-2 from bone metastasis, C4-2B, demonstrates a faster growth rate and is osteoblastic. The osteotropism of C4-2 or C4-2B presumably results from the interaction between cancer cells and bone stromal cells. It is thought that cancer cells perturb normal bone remodeling via secretion of factors that stimulate bone resorption and bone production [6,7].

CL1, a fast growing, highly tumorigenic, and androgen independent derivative, was obtained from LNCaP cells grown in culture under androgen-free conditions [8]. CL1 shows aggressive growth, with metastasis to bone and other organs when implanted orthotopically in mice. It is characterized by increased expression of growth and pro-angiogenic factors, and decreased expression of PSA, AR, and tumor suppressor genes, and it retains marker chromosomes of LNCaP [9].

For cell-type analysis, we previously showed that expression of cluster designation (CD) cell surface molecules could be used to differentiate LNCaP and other prostate cancer cell lines [10], and to identify the component cell types of the prostate parenchyma [11]. This was accomplished by flow analysis and immunohistochemistry using a set of more than 150 commercially available, well-characterized CD antibodies. When used collectively, the multiple CD antibodies can differentiate not only prostate cancer cells from normal cells, but also several types of cancer cells that are postulated to be the basis of heterogeneity in tumor behavior (ref. [11], unpublished data). The differential CD expression between normal and cancer cells is not unexpected since CD expression is linked to physiological conditions. More relevant to our present study, CD profiles are unique for individual prostate cancer cell lines [10,12]. Furthermore, CD expression can be utilized as a means to isolate specific cell populations [13]. In this study, we attempted to uncover the lineage relationship between LNCaP and its derivative cell lines.

MATERIALS AND METHODS

Prostate Cancer Cell Lines and Xenografts

LNCaP, C4-2, and C4-2B were grown in serum-supplemented RPMI1640 media with 10^{-8} M dihydrotestosterone. CL1 was grown in charcoal stripped media. Growth of CL1 in serum-supplemented media did not alter significantly its (CD) expression profile [12]. LuCaP xenografts were implanted and passaged in immune-compromised mice as previously described [14]. Like LNCaP, LuCaP 35 was established from a lymph node metastasis while LuCaP 41 was from a primary tumor. To obtain androgen independent growth, the host animals were castrated. For LuCaP 35-AD (androgen dependent), a tumor was harvested 5 weeks after subcutaneous implantation (passage 50); for LuCaP 35-AI (androgen independent), the host animal was castrated 4 weeks after implantation, and the tumor harvested 4½ months later (passage 49). For LuCaP 41-AD, a tumor was harvested after nearly 4 months (passage 12), and for LuCaP 41-AI, a tumor was harvested after 8 weeks post-castration (passage 12). Another LuCaP 35-AD was included in the LuCaP 41 analysis for comparison.

CD Phenotyping of Cells

For CD antibody labeling, cultured cells were trypsinized and resuspended in 50-µl aliquots of 0.1% bovine serum albumin–Hanks' balanced salt solution (BSA–HBSS). Fluorescent dye [principally R-phycoerythrin (PE)]-conjugated CD antibodies (0.1 µg) were added for 15 min at room temperature. All monoclonal CD antibodies were obtained from BD-PharMingen (San Diego, CA). After labeling, the cells were resuspended in 0.35 ml 2% formalin–HBSS for flow analysis. Omission of the primary antibody, or use of an irrelevant isotype-specific fluorochromated antibody, was employed as a negative control to delineate the autofluorescent cell population. Events outside this population were scored as positive. For each antibody specificity, 5,000 events (cells) on average were recorded, and the percentage of fluorescent (i.e., labeled) cells was calculated and presented in a histogram format. In the case of unconjugated primary antibodies, a second 15-min incubation with PE-conjugated goat anti-mouse light chain (Vector Labs, Burlingame, CA) was performed. To corroborate CD expression detected by flow analysis, cytospins of the cells were prepared and stained with CD antibodies at a concentration of 8 ng/µl. Immunocytochemistry was also done on cells cultured in chambered slides to ensure that cell trypsinization did not affect the expression of CD molecules. In either method, the cells were fixed in cold acetone for 10 min. An indirect avidin-biotin-peroxidase method was used

for immunostaining. The secondary antibody used for chromogen detection was a biotinylated anti-mouse IgG (BA-2000, Vector Labs). The slides were developed in a solution of diaminobenzidine and counterstained with hematoxylin. For the analysis of xenografts, the harvested tumors were cut and digested with collagenase at 37°C overnight in RPMI1640 media supplemented with 5% serum [13]. The cell suspension was filtered and aspirated through a 23-gauge needle, and then labeled with antibodies. No attempt was made to remove any mouse cells as the antibodies used were specific for human antigens. In this study, the reactivities to CD10, CD13, CD26, and CD44 were sufficient to distinguish the different cell lines. CD10 (neutral endopeptidase), CD13 (aminopeptidase N), and CD26 (dipeptidylpeptidase IV) are cell surface enzymes that process bioactive peptide molecules; CD44 is a receptor for hyaluronan in the extracellular matrix. In the normal prostate, CD10, CD13, and CD26 are expressed by luminal secretory cells whereas CD44 is expressed by basal cells. In primary tumors, CD26 is expressed by a majority of the cancer cells whereas CD10 and CD13 are expressed by a minority of the cancer cells; and CD44, being a basal cell marker, is usually absent [11].

Cell Sorting by Flow Cytometry

After trypsinization, LNCaP cells were resuspended in 100–200 μl of 0.1% BSA–HBSS, and the appropriate antibody conjugate (CD10-PE, CD13-PE, CD26-PE, or CD44-PE) was added to a concentration of ≤ 8 ng/μl for $\sim 1.5 \times 10^6$ cells. Cells were incubated without antibody as a negative control. After a 15-min incubation at room temperature, 1 ml of 0.1% BSA–HBSS was added. The suspension was centrifuged and resuspended in 0.5 ml 0.1% BSA–HBSS for sorting by FACStar^{Plus} (Becton Dickinson, Mountain View, CA) into individual wells of a 24-well plate, each containing 1 ml media. Negative cells were "sorted" from the autofluorescent population. The $CD10^+$, $CD10^-$, $CD13^+$, $CD13^-$, $CD26^+$, $CD26^-$, $CD44^+$, and $CD44^-$ populations were then cultured under the same conditions. Once the cell number reached $0.5–1.0 \times 10^6$, the populations were reanalyzed by flow.

Gene Expression Analysis by DNA Microarrays

A 40,000-gene chip was used to probe gene expression of the cell lines. With the number of expressed human genes estimated at below 35,000 [15], there is a high probability that most of the human transcriptome is represented on this chip. For example, these CD molecules were among those detected in C4-2 cells: CD9, CD10, CD26, CD63, CD71, CD81, CD151, which were shown by flow analysis or immunocytochemistry to be present. Other genes detected include the prostate cancer-associated hepsin and α-methylacyl-CoA racemase, and those related to bone biology such as osteoglycin, osteoclast stimulating factor, bone morphogenetic protein 2, and MMP-9. The technology of DNA microarray analysis entailed generation of spottable material, chip printing, fluorescent labeling of probes, hybridization of probes to the array, scanning of the result, quantification, and data analysis. For this human array, 40,032 cDNA clones were obtained from the IMAGE Consortium (Invitrogen/Research Genetics, Carlsbad, CA) representing 35,013 UniGENE clusters (5,019 were redundant), and all were successfully amplified for spotting. Clones were spotted on polylysine-coated slides with a robotic spotter (GeneMachines, Omnigrid, San Carlos, CA). Fluorescent probes were generated by reverse transcriptase and fluorescent dye (Cy3 or Cy5)-tagged dUTP. RNA was prepared by cell lysis in STAT60 solution (Tel-Test "B", Friendswood, TX). Approximately 30–50 μg total RNA was used per experiment. Hybridization and washing were performed in an automatic slide processor. After washing in 0.1× SSC, the slides were scanned with a confocal laser scanner (Axon, Union City, CA). The experiments were done in quadruplicate (including switching of fluorochromes). Expression ratios for each spotted cDNA were calculated from the intensity difference. Data analysis in scoring spot intensity and background was done by two spot-finding/extraction applications: Dapple (ISB) and GenePix (Axon). Intensity data was integrated and recorded, and a script (VERA and SAM) had been added that allowed robust statistical error estimation [16]. For each gene, the likelihood that it was differentially expressed was evaluated by a statistical measure, λ. A set of control experiments, in which two samples of the same were labeled with different dyes, was used to determine a suitable λ threshold based on an acceptable false-positive rate. Values ≥ 25 are considered to be indicative of differential expression.

RESULTS

Differential CD26 Expression Between LNCaP and Its Aggressive Derivatives

CD phenotyping was carried out on C4-2 and C4-2B, and the result was compared to the published one of LNCaP. Figure 1 shows the histogram display for C4-2 (that of C4-2B was similar). The major difference between it and LNCaP was that nearly all C4-2 cells in a population were positive for CD26 compared to only ~10% of LNCaP. Many other CD markers used showed a similar pattern between C4-2 and LNCaP (low percentages for CD6, CD13, CD24, CD33, CD38, CD57, CD90, CD97; intermediate to high percentages

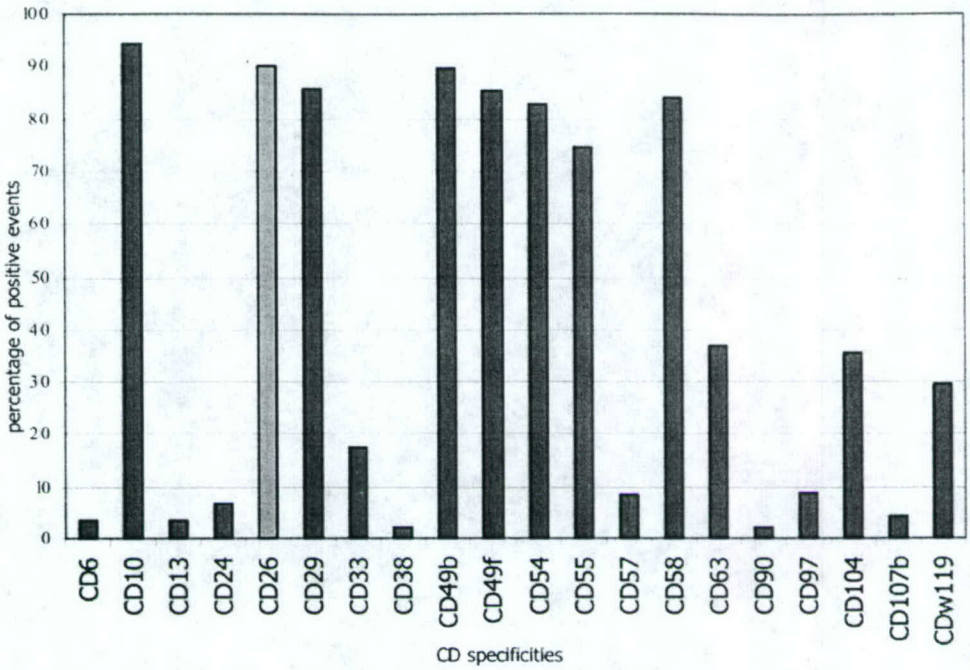

Fig. 1. Cluster designation (CD) expression of C4-2. The histogram displays the profile of C4-2 cells with regard to the expression of selected CD molecules identified on the X-axis. The percentage of positive cells is indicated on the Y-axis. In particular, the bulk of the population is positive for CD26 (fifth bar). C4-2 is also positive for CD10 (second bar). In this experiment, CD44 was not used, and a second experiment showed that C4-2 was not positive for CD44 (data not shown). The complete CD profile of LNCaP was previously published (ref. [10]). [Color figure can be viewed in the online issue, which is available at www.interscience.wiley.com.]

for CD49b, CD49f, CD63, CD104, CDw119). The CD107b percentage was lower in C4-2; a small increase in CD44 positivity (not shown) and increases in CD54, CD55 were seen. That both C4-2 and LNCaP were typed positive for CD10 was noteworthy because the expression of CD10 was reported to be under androgen regulation [17], and would, therefore, be expected to be down-regulated in C4-2. Previously, CD phenotyping between LNCaP and CL1 showed the latter to be also positive for CD26 [12]. CL1, however, showed many more different CD reactivities such as presence of CD13 and CD44, and absence of CD10 as indicated by the comparative flow analysis of LNCaP versus CL1 in Figure 2. The dominant cell type in LNCaP was characterized by the CD phenotype of $CD10^{+}/CD13^{-}/CD26^{-}/CD44^{-}$, whereas that in CL1 was characterized

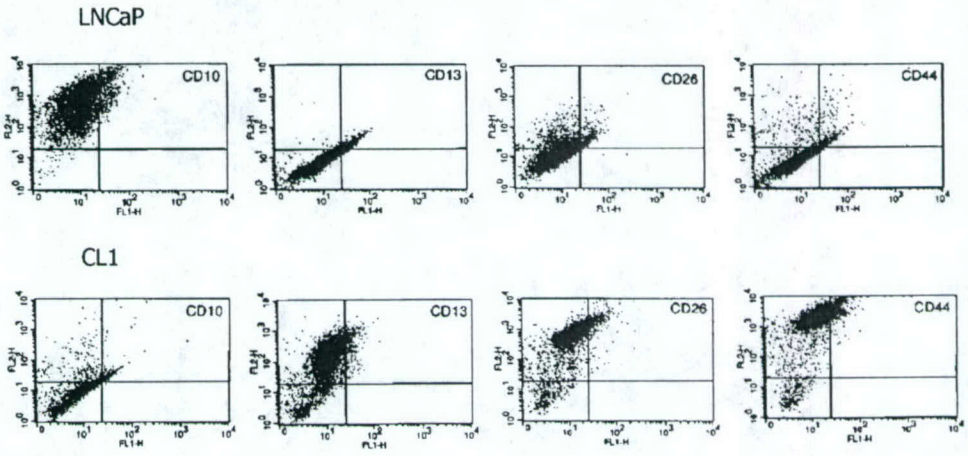

Fig. 2. Flow analysis of LNCaP and CL1. The first set of cytograms shows the reactivity of LNCaP cells and the second set shows the reactivity of CL1 cells. PE-conjugated antibodies to CD10, CD13, CD26, and CD44 were used for labeling. PE fluorescence is measured on the Y-axis (FITC fluorescence would be measured on the X-axis if a FITC-conjugated antibody were used). Percentages of positive cells were scored from 5,000 events collected. Not shown are the results of the no-antibody controls.

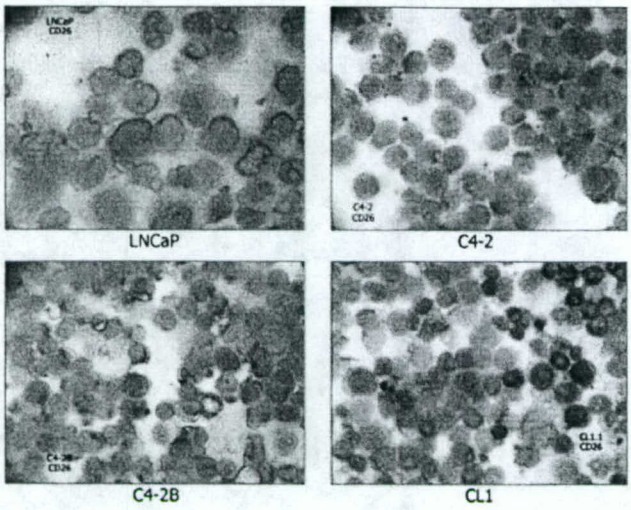

Fig. 3. CD26 expression in LNCaP and its derivatives. Cytospins were prepared for the different cell lines, and processed for CD26 immunocytochemistry. Shown are the results for LNCaP, C4-2, C4-2B, and CLI.1 (a selected clone of CLI). Except for LNCaP, virtually all the cells in C4-2, C4-2B, and CLI are positive for CD26, as indicated by the brown stain.

by $CD10^-/CD13^+/CD26^+/CD44^+$. Note that the CD profile of CL1 closely resembles that of the PC3 prostate cancer cell line (cf. refs. [10,12]), but the morphological appearance of CL1 on culture dish is similar to that of LNCaP and readily distinguishable from that of PC3. The flow cytometry result of CD26 was evaluated by immunocytochemistry. Figure 3 shows cytospin preparations (in which cells were centrifuged onto slides) of LNCaP, C4-2, C4-2B, and CL1 stained by CD26. Nearly every cell in C4-2, C4-2B, and CL1 was positive for CD26 in contrast to LNCaP (virtually none of the cells in this field were stained).

Transcriptome Profiling for Differentially Expressed Genes

To determine whether genes other than *CD26* were differentially expressed between the two similarly CD-phenotyped LNCaP and C4-2/C4-2B cell lines, gene expression profiling using a 40,000-gene array was carried out. Total cellular RNA was prepared from the cell lines for labeling and hybridization. In agreement with the cell typing result, the expression of CD26 was found to be 11-fold higher in C4-2B compared to LNCaP as listed in Table I. Included in the table are 25 up-regulated genes in C4-2B with higher λ values (hence, statistically significant) than that of CD26. No other CD genes were detected to be significantly different to such a degree between the two cell lines. Nine genes showed a higher fold of change than that of CD26. The gene with the highest fold difference was a transcription factor, Krüppel-like factor 7 (*KLF7*), which could be involved in the alteration of gene expression in the derivation of C4-2. The top three genes overexpressed in LNCaP (not shown) were Y chromosome ubiquitin specific protease 9 (*USP9Y*), transcription factor ETS variant gene 1 (*ETV1*), and protein kinase inhibitor (*PKIB*). The expression of these genes might be relevant in prostate cancer progression.

LNCaP Subpopulations

Since the variant cell lines were derived from LNCaP, the question was whether these cells (C4-2- or CL1-like) were pre-existent in the LNCaP population. CD flow analysis of LNCaP population showed minor subpopulations that scored as $CD10^-$ (CL1-like), $CD13^+$ (CL1-like), $CD26^+$ (C4-2- and CL1-like), or $CD44^+$ (CL1-like). Cell binding to an array of several CD antibodies spotted on plastic also indicated that a given population of LNCaP cells contained cells not homogeneously labeled by various CD antibodies [10]. Accordingly, $CD10^-$, $CD13^+$, $CD26^+$, and $CD44^+$ cells were sorted individually from LNCaP (Fig. 4), and the sorted cells were allowed to expand in numbers by culture. For comparison, $CD10^+$, $CD13^-$, $CD26^-$, and $CD44^-$ LNCaP cells were also individually sorted and cultured. The following were sorted: 50,000 $CD10^+$ and 80 $CD10^-$ cells; 960 $CD13^+$ and 50,000 $CD13^-$ cells; 5,000 $CD26^+$ and 50,000 $CD26^-$ cells; 4,500 $CD44^+$ and 50,000 $CD44^-$ cells. The $CD10^-$ well containing the fewest number of cells did not produce an outgrowth and hence was lost to the analysis (small numbers of LNCaP typically do not thrive). After 2 weeks, the $CD10^+$, $CD13^-$, $CD26^-$, and $CD44^-$ populations reached a sufficient level of cells for flow analysis. The cells were trypsinized and resuspended for labeling by CD10, CD13, CD26, and CD44 as was done for the unsorted LNCaP cells. Because of lower cell numbers to begin with, the other sorted populations took longer to expand. After 3 weeks, the $CD26^+$ and $CD44^+$ populations were ready for analysis; and after 5 weeks, the $CD13^+$ population was ready. Except for the $CD26^+$ sorted population, all other CD-sorted populations displayed a CD profile of these four CD specificities not remarkably different from that of non-sorted LNCaP (Fig. 5A,B). Remarkable was the high percentage (~80%) of $CD26^+$ cells seen only in the CD26 population versus ~10% in all other populations. The culture of sorted $CD26^+$ cells was also serially passaged three-times, and the high percentage of $CD26^+$ cells was maintained in these passages (Fig. 5B,C). These results suggested that the $CD26^+$ LNCaP cells could represent a pre-existent or precursor population of C4-2 cells as both were typed $CD10^+/CD13^-/CD26^+/CD44^-$. However, other than CD26, this population

TABLE I. Differentially Expressed Genes Between LNCaP and C4-2B*

Gene name	Gene symbol	λ value	Ratio	Fold increase
Krüppel-like factor 7	KLF7	45.9	1.3071	20.28
Chromosome 1 open reading frame 24†	C1orf24	43.2	1.3755	23.74
Zinc α-2-glycoprotein 1†	AZGP1	42.9	1.1685	14.74
Acetyl-coenzyme A synthetase 2	ACAS2L	39.5	1.3371	21.73
Chromosome 1 open reading frame 24†	C1orf24	39.4	1.0103	10.24
Hypothetical protein DKFZp434F0318		36.9	0.922	8.36
Homo sapiens cDNA FLJ33790 fis		36.1	0.8232	6.66
Peptidylprolyl isomerase C	PPIC	34.5	0.6961	4.97
Cathepsin Z	CTSZ	34	1.1504	14.14
Hypothetical protein FLJ10462		33.6	0.7793	6.02
Chromosome condensation 1	CHC1	32.6	0.8078	6.42
Nicotinamide nucleotide transhydrogenase	NNT	32.4	1.2271	16.87
ESTs†		32.4	1.193	15.6
Zinc α-2-glycoprotein 1†	AZGP1	32.3	0.8111	6.47
KIAA1001 protein		32.3	0.8304	6.77
Hypothetical protein MGC39325		32.2	0.8683	7.38
Hypothetical protein FLJ32915		32.1	0.8993	7.93
BCL2-associated athanogene 2	BAG2	31.9	0.5972	3.96
EST		31.6	0.6727	4.71
ESTs†		31.6	1.3473	22.25
Collagen, type IX, α3	COL9A3	31.5	0.8894	7.75
GS3955 protein	GS3955	31.1	1.2856	19.3
S100 calcium binding protein P	S100P	31.1	0.5553	3.59
Up-regulated by BCG-CWS	LOC64116	31.1	0.5142	3.27
Epithelial protein up-regulated in carcinoma	DD96	31	0.9287	8.49
γ-Glutamyltransferase 1	GGT1	30.7	0.7773	5.99
Solute carrier family 2	SLC2A5	30.4	1.1116	12.93
Potassium channel, subfamily K, member 1	KCNK1	30	0.6239	4.21
Dipeptidylpeptidase IV (CD26)	DPP4	29.9	1.0365	10.88

*Genes whose λ values are larger than that of CD26 (indicated in **bold**) are listed. The ratio is the log intensity difference between Cy3 and Cy5 labeling of the individual array spots, and can be converted into x-fold difference in expression level. Three entries (marked by †) are repeated in this cohort: C1orf24, AZGP1, and one EST.

was unlike CL1 with regard to CD10, CD13, and CD44 ($CD10^+/CD13^-/CD44^-$ vs. $CD10^-/CD13^+/CD44^+$), and hence it could not represent a pre-existent population of CL1 cells.

CD Phenotypes of Xenografts

Since C4-2 and C4-2B were derived from interaction between LNCaP and stromal cells in vivo under androgen-free conditions while CL1 was not, we decided to analyze if androgen-free conditions (in castrated mice) without stromal cell interaction could select for altered clones with features (as defined by CD expression) of CL1. For this, we used LuCaP 35 and LuCaP 41, two xenografts developed in our laboratory. LuCaP 35 was like LNCaP in the CD pattern whereas LuCaP 41 was not. For comparison, the xenografts were grown and harvested from intact mice. LuCaP 35-AD (harvested from intact mice) showed a similar pattern of $CD10^+/CD13^-/CD26^-/CD44^-$ to that of LNCaP (data not shown). LuCaP 35-AI (harvested from castrated mice) showed increases in the percentages of CD13, CD26, and CD44 cells (Fig. 6, left), and these $CD13^+$, $CD26^+$, or $CD44^+$ cells could represent emerging CL1-like cancer cells. At the time of analysis, these cells did not appear to constitute the predominant population. Whether they will take over the population over time remains to be determined (which may not be possible as the animals are sacrificed within a prescribed period for humane reasons). Unfortunately, the LuCaP cells could not be cultured in vitro so that we could not sort the $CD13^+$, $CD26^+$, or $CD44^+$ LuCaP 35-AI cells to expand by cell culture as was done for LNCaP cells. The percentage of $CD10^+$ tumor cells (lower percentages of positive cells scored from xenograft tumors were due to "contaminating" mouse cells and particulate debris), however, did not differ between LuCaP 35-AD and LuCaP 35-AI (because CL1

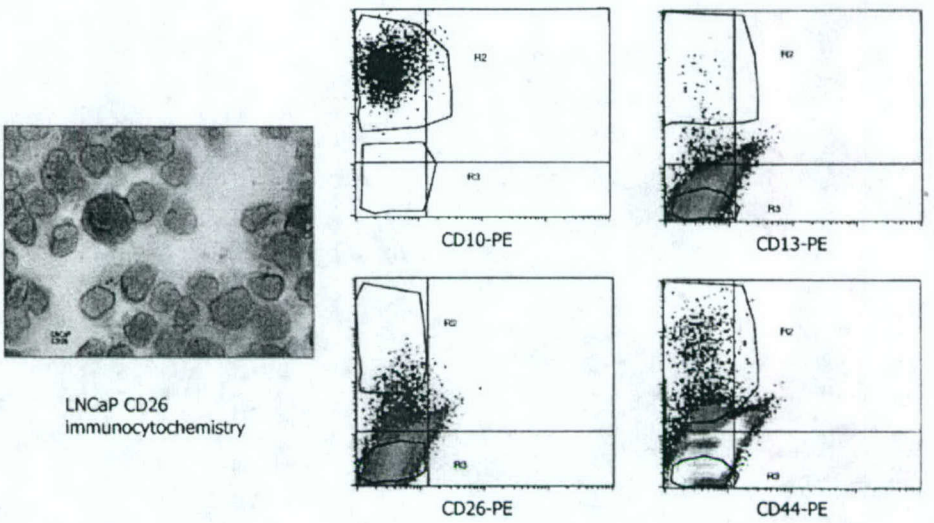

Fig. 4. LNCaP subpopulations. LNCaP cells were sorted into populations of $CDI0^+$, $CDI0^-$, $CDI3^+$, $CDI3^-$, $CD26^+$, $CD26^-$, $CD44^+$, and $CD44^-$ cells. The positive cells were sorted from the region outlined as R2, and the negative cells were sorted from the region outlined as R3 in the individual cytograms. The photomicrograph shows a cytospin of LNCaP cells stained with anti-CD26. A positive cell among many negative cells in this field is seen.

is $CD10^-$). Unlike LuCaP 35, LuCaP 41 contained a higher proportion of $CD26^+$ and a much smaller proportion of $CD10^+$ cells; and this was corroborated by RT-PCR analysis for CD10, CD13, CD26, and CD44 transcripts in the two tumors (Fig. 6, right and bottom). There were essentially no changes in the percentages of CD10, CD13, CD26, and CD44 cells between LuCaP 41-AD and LuCaP 41-AI. Androgen alone (vs. concurrent interaction with stromal cells) apparently did not affect dramatically the expression of these particular CD molecules in the xenograft population in vivo. None of the subcutaneously implanted xenografts showed detectable metastatic spread.

DISCUSSION

Gain of androgen independence and that of metastatic capability are both characteristics of progression in prostate cancer. Probably different sets of genes are responsible for the two cancer phenotypes. Some of these genes are likely those that encode CD molecules, perhaps more so with metastasis as that process entails cell–cell interaction mediated by cell surface molecules. One candidate in prostate cancer metastasis could be CD26. The C4-2 and CL1 cell lines are both metastatic and can proliferate without androgen yet their gene expression is very dissimilar. This is evident in their transcriptomes (ref. [12], unpublished gene expression data) and CD phenotypes. A common CD between CL1 and C4-2 is CD26. The differential expression of CD26 between the marginally tumorigenic, non-metastatic LNCaP (even though it was originally established from a metastasis) and its metastatic variants C4-2, C4-2B, and CL1 suggests that CD26 might be (one of several molecules) involved in cancer metastasis. CD26 is normally found in the luminal membrane of prostate epithelial cells [11,18]. CD26 activity is reported to be elevated in urological diseases, e.g., BPH [19] and prostate cancer [11,20]. There is quite a large amount of literature on the biological function of CD26. Of relevance is the role of CD26 in mediating cell migration and being responsible in part for the tissue-invasion phenotype. For example, CD26 expression appears in cells migrating

Fig. 5. CD analysis of sorted subpopulations. **A**: After in vitro culture, the resultant cells were re-analyzed for CDI0, CDI3, CD26, and CD44. The histogram displays the results for the $CDI0^+$, $CDI3^-$, $CD26^-$, $CD44^-$, $CDI3^+$, $CD26^+$, and $CD44^+$ populations (represented in different hues of the bars as indicated in the box inset). The notable result is the high percentage of $CD26^+$ cells in the sorted $CD26^+$ population (sixth bar in the CD26 specificity). A small increase in the percentage of $CD26^+$ cells is also seen in the sorted $CDI3^+$ and $CD44^+$ populations (fifth and seventh bar, respectively). **B**: Shown are the cytogram displays for the flow analysis of the sorted CD26 and CD44 populations. The increased percentage of $CD26^+$ cells is clearly evident in the CD26 LNCaP population. For each cytogram, the Y-axis is log PE fluorescence and the X-axis is log FITC fluorescence. **C**: The high percentage of $CD26^+$ cells in the CD26 LNCaP population is shown to be maintained in three serial passages (CD26 LNCaP-1, -2, and -3), compared to the sorted $CD26^-$ and unsorted LNCaP populations. [Color figure can be viewed in the online issue, which is available at www.interscience.wiley.com.]

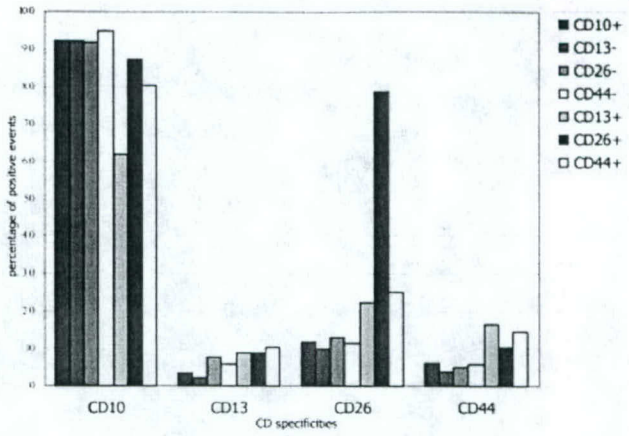
CD10+
CD13-
CD26-
CD44-
CD13+
CD26+
CD44+
percentage of positive events
CD10
CD13
CD26
CD44
CD specificities

B

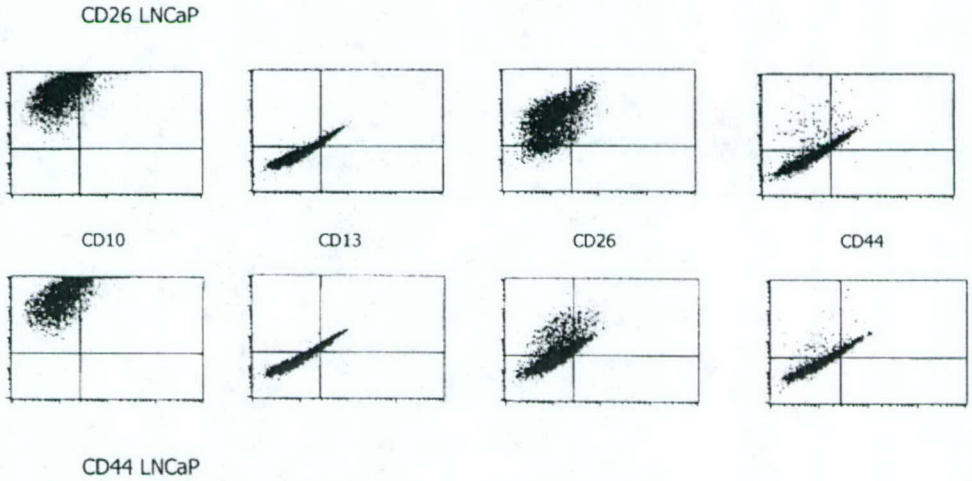
CD26 LNCaP
CD10
CD13
CD26
CD44
CD44 LNCaP

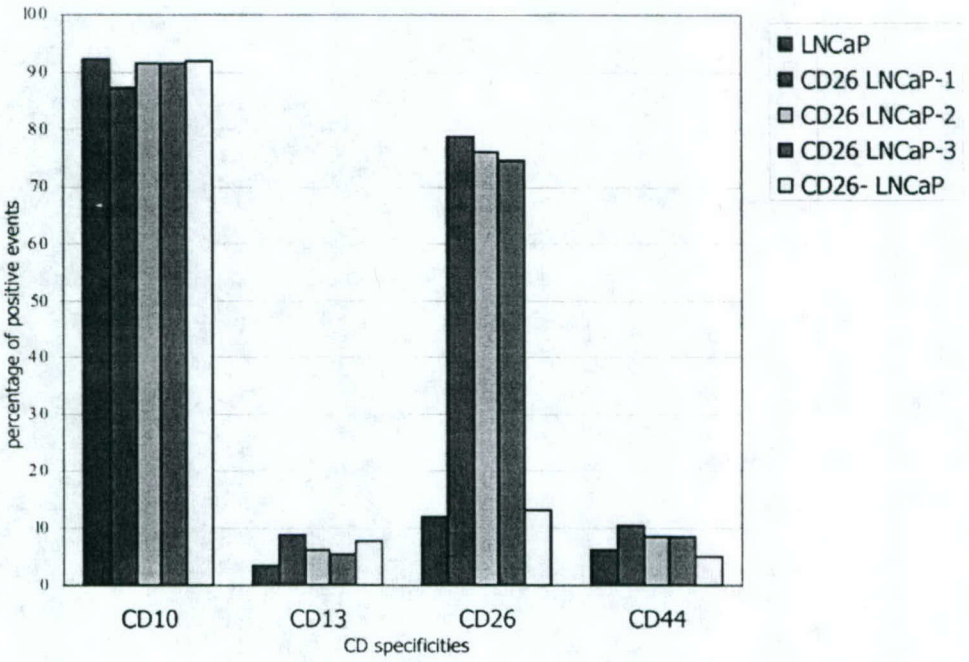
LNCaP
CD26 LNCaP-1
CD26 LNCaP-2
CD26 LNCaP-3
CD26- LNCaP
percentage of positive events
CD10
CD13
CD26
CD44
CD specificities

Fig. 5.

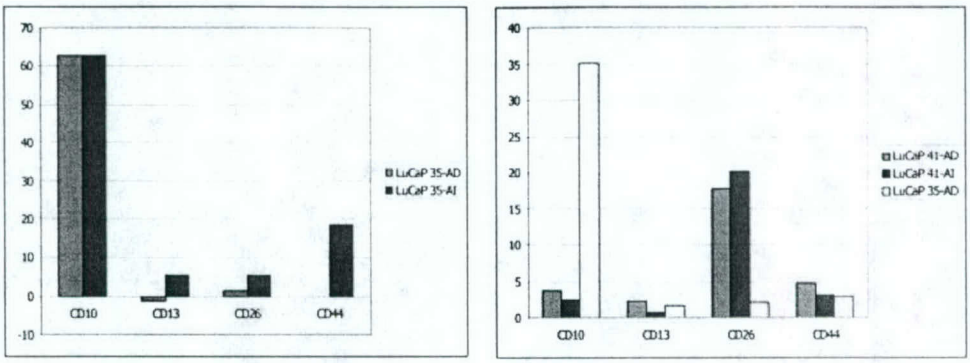

	CD10	CD13	CD26	CD44
LuCaP 35	++++++	–	+	+
LuCaP 41	+	+	++++	++

Fig. 6. CD expression of xenografts. The panel on the left contrasts the expression of CD10, CD13, CD26, and CD44 for an LNCaP-like xenograft, LuCaP 35, harvested from intact (AD) versus castrated (AI) hosts. The right panel contrasts the expression for LuCaP 41, which contained $CD26^+$ cells. Another sample of LuCaP 35-AD was analyzed in this experiment. Single cells were prepared from the tumors by collagenase digestion and CD expression was analyzed by flow cytometry. The xenograft RT-PCR results are included below the CD panels with the level of expression of markers tested indicated by the number of plus signs. [Color figure can be viewed in the online issue, which is available at www.interscience.wiley.com.]

through connective tissue during wound closure. Specifically, an enzyme complex of CD26/separase is constituted at invadopodia of migratory fibroblasts [21]. CD26-expressing endothelial cells of the lung vasculature permit binding of tumor cells, whereas non-expressing endothelial cells in the vasculature of leg muscle, a nonmetastasized organ, do not [22]. This binding may be between CD26 and fibronectin/collagen. A published report showed that a CD26 fragment containing the fibronectin binding site could inhibit up to 80% lung colony formation by breast cancer cells [23]. CD26 also serves to bind plasminogen 2ε to initiate a Ca^{2+}-mediated signaling response that leads to an increase in the expression of MMP-9 [24]. MMP-9 enzymatic activity on the extracellular matrix is known to promote cancer cell migration. Many tumors, especially those of high-grade, are positive for MMP-9 expression, and so are lymph node metastases [25]. CD26 was shown to be useful in the rediagnosis of follicular thyroid carcinoma with distant metastasis. About 70% of the rediagnosed cases were positive for CD26, but only a very small percentage of adenoma and nodular hyperplasia were positive [26].

With regards to the genesis of the LNCaP derivatives, our results suggest that a possible lineage relationship between C4-2 cells, which are $CD26^+$, and $CD26^+$ LNCaP cells. Interaction between LNCaP and stromal cells may involve the selection of $CD26^+$ cells in the LNCaP population. Cell sorting showed that sorted $CD26^+$ LNCaP cells maintained their CD26 expression. Whether the $CD26^+$ LNCaP cells are metastasis capable or not remains to be tested. Xenograft LuCaP 35 cells prepared from tumors that resulted from subcutaneous injection had <10% CD26-staining cells as shown here, and no metastasis was observed [27]. More recently, metastatic LuCaP 35 variants were observed after orthotopic implantation [14,28], and these can be tested for CD26 expression. Our hypothesis is that the metastatic variant was selected through appropriate interaction with the mouse prostatic stromal cells (as provided via the orthotopic route) akin to the derivation of C4-2 from LNCaP and human bone stromal cells, and that the resultant variants would be positive for CD26 expression. Highly malignant LNCaP can also be promoted via the orthotopic route [29] (i.e., interaction with mouse prostate stromal cells leads to selection of the $CD26^+$ LNCaP cells within the tumor inoculum). Without stromal cell interaction, LNCaP cells may have to undergo many more genetic changes to become androgen independent and/or metastasis capable as represented in the derivation of CL1. Furthermore, adaptation to growth under androgen-free conditions alone may not be sufficient for the gain of metastatic capability, as demonstrated by the subcutaneously implanted LuCaP 35-AD/-AI xenografts, in which no metastasis was observed. For metastasis to occur, interaction with the appropriate stromal cells is required. Our results also suggest that CD expression has perhaps less to do with gain of hormone independence than with gain of metastasis.

The CD phenotype of LuCaP 41 ($CD10^-/CD26^+$, same as that of cancer cells in primary tumors) indicates that CD26 could not alone confer metastasis, since LuCaP 41 is not metastatic despite containing a sizeable proportion of $CD26^+$ cells. A metastasis co-promoting function may be contributed by other CD molecules

such as CD10 and CD13. Both, like CD26, are cell surface peptidases. Although cancer cells in both primary tumors and metastases are $CD26^+$, a majority of primary prostate tumors are negative for CD10 expression, whereas lymph node metastases almost invariably contain $CD10^+$ cancer cells (LNCaP and LuCaP 35 are both $CD10^+$). Indeed, CD10 expression correlates with liver metastasis of colorectal adenocarcinoma [30], and CD10 is upregulated in melanoma metastasis [31]. CD13, which is present in CL1 (negative for CD10), has been reported to confer an invasive phenotype on expressing cells [32]. Non-small cell lung cancer containing $CD13^+$ cells has a worse prognosis than that without [33]. Thus, these peptidases as a group could play a central role in prostate cancer metastasis. As these CD molecules are localized on the cell surface, they are prime therapeutic targets. We have generated an anti-CD26 (clone A6H) scFv in our previous studies [34,35], and a cytotoxic immunoconjugate can in principle be generated to target $CD26^+$ cancer cells in our mouse model.

ACKNOWLEDGMENTS

We thank Susan Saiget of BD-PharMingen for her help in making this study possible, and Michèl Schummer for comments.

REFERENCES

1. Horoszewicz JS, Leong SS, Kawinski E, Karr J, Rosenthal H, Chu TM, Mirand EA, Murphy GP. LNCaP model of a human prostatic carcinoma. Cancer Res 1983;43:1809–1818.
2. Nelson PS, Clegg N, Arnold H, Ferguson C, Bonham M, White J, Hood L, Lin B. The program of androgen-responsive genes in neoplastic prostate epithelium. Proc Natl Acad Sci USA 2002; 99:11890–11895.
3. Zhau HE, Chung LWK. Establishment of human prostate carcinoma skeletal metastasis models. Cancer 2000;88:2995–3001.
4. Wu H, Hsieh J, Gleave ME, Brown NM, Pathak S, Chung LWK. Derivation of androgen-independent human LNCaP prostatic cancer cell sublines: Role of bone stromal cells. Int J Cancer 1994;57:406–412.
5. Thalmann GN, Sikes RA, Wu TT, Degeorges A, Chang S, Ozen M, Pathak S, Chung LWK. LNCaP progression model of human prostate cancer: Androgen-independence and osseous metastasis. Prostate 2000;44:91–103.
6. Koeneman KS, Yeung F, Chung LWK. Osteomimetic properties of prostate cancer cells: A hypothesis supporting the predilection of prostate cancer metastasis and growth in the bone environment. Prostate 1999;39:246–261.
7. Lin D, Tarnowski CP, Zhang J, Dai J, Rohn E, Patel AH, Morris MD, Keller ET. Bone metastatic LNCaP-derivative C4-2B prostate cancer cell line mineralizes in vitro. Prostate 2001;47: 212–221.
8. Tso C, McBride WH, Sun J, Patel B, Tsui KH, Paik SH, Gitlitz B, Caliliw R, van Ophoven A, Wu L, deKernion J, Belldegrun A. Androgen deprivation induces selective outgrowth of aggressive hormone-refractory prostate cancer clones expressing distinct cellular and molecular properties not present in parental androgen-dependent cancer cells. Cancer J Sci Am 2000;6:220–233.
9. Patel BJ, Pantuck AJ, Zisman A, Tsui KH, Paik SH, Caliliw R, Sheriff S, Wu L, deKernion JB, Tso C, Belldegrun AS. CL1-GFP: An androgen independent metastatic tumor model for prostate cancer. J Urol 2000;164:1420–1425.
10. Liu AY. Differential expression of cell surface molecules in prostate cancer cells. Cancer Res 2000;60:3429–3434.
11. Liu AY, True LD. Characterization of prostate cell types by CD cell surface molecules. Am J Pathol 2002;160:37–43.
12. Freedland SJ, Seligson DB, Liu AY, Pantuck AJ, Paik SH, Horvath S, Wieder JA, Zisman A, Nguyen D, Tso C, Palotie AV, Belldegrun AS. Loss of CD10 (neutral endopeptidase) is a frequent and early event in human prostate cancer. Prostate 2003;55:71–80.
13. Liu AY, True LD, LaTray L, Nelson PS, Ellis WJ, Vessella RL, Lange PH, Hood L, van den Engh G. Cell–cell interaction in prostate gene regulation and cytodifferentiation. Proc Natl Acad Sci USA 1997;94:10705–10710.
14. Corey E, Quinn JE, Buhler KR, Nelson PS, Macoska JA, True LD, Vessella RL. LuCaP 35: A new model of prostate cancer progression to androgen independence. Prostate 2003;55:239–246.
15. Ewing B, Green P. Analysis of expressed sequence tags indicates 35,000 human genes. Nat Genet 2000;25:232–234.
16. Ideker TE, Thorsson V, Siegel AP, Hood LE. Testing for differentially expressed genes by maximum-likelihood analysis of microarray data. J Comput Biol 2000;7:805–817.
17. Papandreou CN, Usmani B, Geng Y, Bogenrieder T, Freeman R, Wilk S, Finstad CL, Reuter VE, Powell CT, Scheinberg D, Magill C, Scher HI, Albino AP, Nanus DM. Neutral endopeptidase 24.11 loss in metastatic human prostate cancer contributes to androgen-independent progression. Nat Med 1998;4:50–57.
18. Dinjens WN, ten Kate J, van der Linden EP, Wijnen JT, Meera Khan P, Bosman FT. Distribution of adenosine deaminase complexing protein (ADCP) in human tissues. J Histochem Cytochem 1989;37:1869–1875.
19. Dinjens WN, ten Kate J, Kirch JA, Tanke HJ, van der Linden EP, van den Ingh HF, van Steenbrugge GJ, Meera Khan P, Bosman FT. Adenosine deaminase complexing protein (ADCP) expression and metastatic potential in prostatic adenocarcinomas. J Pathol 1990;160:195–201.
20. Vanhoof G, DeMeester I, van Sande M, Scharpe S, Yaron A. Distribution of proline-specific aminopeptidase in human tissues and body fluids. Eur J Clin Chem Clin Biochem 1992;30:333–338.
21. Ghersi G, Dong H, Goldstein LA, Yeh Y, Hakkinen L, Larjava HS, Chen WT. Regulation of fibroblast migration on collagenous matrix by a cell surface peptidase complex. J Biol Chem 2002; 277:29231–29241.
22. Johnson RC, Zhu D, Augustin-Voss HG, Pauli BU. Lung endothelial dipeptidyl peptidase IV is an adhesion molecule for lung metastatic rat breast and prostate carcinoma cells. J Cell Biol 1993;121:1423–1432.
23. Abdel-Ghany M, Cheng H, Levine RA, Pauli BU. Truncated dipeptidyl peptidase IV is a potent anti-adhesion and anti-metastasis peptide for rat breast cancer cells. Invasion Metastasis 1998;18:35–43.
24. Gonzalez-Gronow M, Grenett HE, Weber MR, Gawdi G, Pizzo SV. Interaction of plasminogen with dipeptidyl peptidase IV initiates a signal transduction mechanism which regulates

expression of matrix metalloproteinase-9 by prostate cancer cells. Biochem J 2001;355:397–407.

25. Ishimaru H, Kageyama Y, Hayashi T, Nemoto T, Eishi Y, Kihara K. Expression of matrix metalloproteinase-9 and bombesin/gastrin-releasing peptide in human prostate cancers and their lymph node metastases. Acta Oncologia 2002;41: 289–296.
26. Hirai K, Kotani T, Aratake Y, Ohtaki S, Kuma K. Dipeptidyl peptidase IV (DPPIV/CD26) staining predicts distant metastasis of 'benign' thyroid tumor. Pathol Int 1999;49:264–265.
27. Corey E, Quinn JE, Bladou F, Brown LG, Roudier MP, Brown JM, Buhler KR, Vessella RL. Establishment and characterization of osseous prostate cancer models: Intra-tibial injection of human prostate cancer cells. Prostate 2002;52:20–33.
28. Corey E, Quinn JE, Vessella RL. A novel method of generating prostate cancer metastases from orthotopic implants. Prostate 2003;56:110–114.
29. Wang X, An Z, Geller J, Hoffman RM. High-malignancy orthotopic nude mouse model of human prostate cancer LNCaP. Prostate 1999;39:182–186.
30. Yao T, Takata M, Tustsumi S, Nishiyama K, Taguchi K, Nagai E, Tsuneyoshi M. Phenotypic expression of gastrointestinal differentiation markers in colorectal adenocarcinomas with liver metastasis. Pathology 2002;34:556–560.
31. Kanitakis J, Narvaez D, Claudy A. Differential expression of the CD10 antigen (neutral endopeptidase) in primary versus metastatic malignant melanomas of the skin. Melanoma Res 2002;12:241–244.
32. Saiki I, Fujii H, Yoneda J, Abe F, Nakajima M, Tsuruo T, Azuma I. Role of aminopeptidase N (CD13) in tumor-cell invasion and extracellular matrix degradation. Int J Cancer 1993;54:137–143.
33. Tokuhara T, Adachi M, Hashida H, Ishida H, Taki T, Higashiyama M, Kodama K, Tachibana S, Sasaki S, Miyake M. Neutral endopeptidase/CD10 and aminopeptidase N/CD13 gene expression as a prognostic factor in non-small cell lung cancer. Jpn J Thorac Cardiovasc Surg 2001;49:489–496.
34. Hass GM, Meyer JL, Newitt RA, Labuda T, Brown L, Aebersold R, Vessella RL. Identification of the target of monoclonal antibody A6H as dipeptidyl peptidase IV/CD26 by LC MS\MS Hybridoma 2001;20:231–236.
35. Tan PH, Chu V, Stray JE, Hamlin DK, Pettit D, Wilbur DS, Vessella RL, Stayton PS. Engineering the isoelectric point of a renal cell carcinoma targeting antibody greatly enhances scFv solubility. Immunotechnology 1998;4:107–114.

Flap Endonuclease 1 is Overexpressed and Associated with High Gleason Score in Prostate Cancer

John S. Lam,[1] Hong Yu,[2] Ai Li,[3] Mervi Eeva,[2] John T. Leppert,[1] Oleg Shvarts,[1] Allan J. Pantuck,[1] Steve Horvath,[3,4] David B. Seligson,[2] and Arie S. Belldegrun[1]

[1] Department of Urology
[2] Department of Pathology and Laboratory Medicine
[3] Department of Biostatistics
[4] Department of Human Genetics
David Geffen School of Medicine at UCLA
10833 Le Conte Avenue
66-128 CHS, Box 951738
Los Angeles, California 90095-1738

Heading: FEN-1 expression in prostate cancer

Key Words: cancer; Flap endonuclease 1; Gleason grade; prostate; tumor markers

Word Count: 2,353

Corresponding author:
Arie S. Belldegrun, MD
Department of Urology
David Geffen School of Medicine at UCLA
10833 Le Conte Avenue
66-118 CHS, Box 951738
Los Angeles, California 90095-1738
(310) 206-1434 (phone)
(310) 206-5343 (fax)
abelldegrun@mednet.ucla.edu (email)

ABSTRACT

Purpose: Few successful therapeutic options exist for men who present with metastatic prostate cancer or for the 30% that recur following definitive treatment. The development and characterization of molecular markers are vital to the development of prognostic and therapeutic modalities in prostate cancer. We recently developed a new hormone refractory prostate cancer cell line, CL1, derived from LNCaP via in vitro androgen deprivation and generated a pure clonal tumor system based upon single-cell derived clones of CL1. Using oligonucleotide microarrays, structure-specific flap endonuclease 1 (FEN-1) was identified to be overexpressed the most aggressive clone, CL1.1. In this study, we investigated the expression and potential clinical usefulness of FEN-1 in prostate cancer using tissue microarray technology.

Materials and Methods: Immunohistochemical analysis using a FEN-1 monoclonal antibody was performed on tissue microarrays constructed from paraffin embedded specimens from 246 patients who underwent radical retropubic prostatectomy. FEN-1 staining was correlated with established prognostic factors (Gleason score, PSA, and pathologic stage) and biochemical recurrence-free survival was analyzed. Data were compared using standard statistical methods.

Results: There were a total of 1083 informative tissue spots, which included 651 cancer, 264 normal, 120 benign prostatic hyperplasia (BPH), and 48 prostatic intraepithelial neoplasia (PIN). Mean expression of FEN-1 was significantly higher in cancer (36.7%) compared to normal (13.2%), BPH (4.5%), and PIN (15.4%) specimens ($p < 0.0001$). FEN-1 expression was strongly correlated with Gleason score ≥ 7 ($\sigma = 0.24$, $p = 0.0008$). Preoperative PSA ($p = 0.0052$), Gleason score ≥ 7 ($p < 0.0001$), seminal vesicle invasion ($p < 0.0001$), capsular invasion ($p = 0.0013$) were associated with recurrence-free survival, whereas FEN-1 expression was not. On multivariate analysis, only Gleason score ≥ 7 ($p = 0.0007$), seminal vesicle invasion ($p = 0.004$),

and extraprostatic extension ($p = 0.0084$) were retained as independent prognostic indictors for PSA recurrence.

Conclusions: FEN-1 is overexpressed in prostate cancer with a Gleason score of 7 and higher. These results suggest that FEN-1 may be a potential tumor marker for the selection of patients at high risk and a useful target for prostate cancer diagnosis and therapy.

INTRODUCTION

An estimated 230,110 American men were diagnosed with prostate cancer and 29,900 deaths were estimated to have resulted from this disease in 2004, making it the most commonly diagnosed cancer and the second leading cause of cancer deaths among American men.[1] The widespread use of prostate-specific antigen (PSA) as a screening test for prostate cancer has led to an impressive stage migration with more patients presenting with organ-confined disease. Although current clinical and pathological features, such as Gleason score, stage, and PSA, provide useful information allowing clinicians to stratify patients into different risk categories and dictate treatment, differences remain in terms of accurately predicting outcome for any particular patient.[2] More patients are also presenting within a very narrow range of these parameters in the PSA era, limiting the predictive value of staging and prognosis. Furthermore, there are currently no means to assess which tumors are clinically significant. Therefore, additional prognostic biomarkers are urgently needed. The exponential growth of techniques in molecular biology and the progressive elucidation of the biological pathways of prostate cancer offer hope that this demand will soon be met.

In order to study progression from androgen sensitive to hormone refractory prostate cancer, we recently developed a new hormone refractory prostate cancer cell line, CL1, derived from LNCaP, a well described androgen-sensitive human prostate cancer cell line, via in vitro androgen deprivation.[3, 4] A pure clonal tumor system based upon single-cell derived clones of CL1 stably transfected with the green fluorescence protein (GFP) gene was generated to study gene expression during prostate cancer progression and to identify molecular targets for therapy.[5] Using oligonucleotide microarrays, structure-specific flap endonuclease 1 (FEN-1) was identified to be overexpressed the most aggressive clone, CL1.1. Based on these findings, we evaluated the

expression of FEN-1 protein in normal prostate, benign prostatic hyperplasia (BPH), prostatic intraepithelial neoplasia (PIN), and prostate cancer. In order to investigate the importance and clinical significance of FEN-1 expression, we used tissue microarrays for high-throughput molecular profiling of prostate cancer tumor specimens based on their FEN-1 expression.

MATERIALS AND METHODS

Patients

The study cohort consisted of 246 patients who underwent radical retropubic prostatectomy between 1984 and 1995. A total of 20 patients who received neoadjuvant hormones were excluded, 10 had tumors that were not informative for FEN-1 due to the lack of tumor representation and another 14 had incomplete clinical data for outcomes analysis, leaving 202 available for evaluation. Tissue spots from 245 cases were included in the spot distribution of FEN-1 staining and 88% of all tissue spots were informative. One case did not have any informative spots. A retrospective analysis for outcome assessment was based on chart review of clinical, laboratory and pathological data. Mean patient age was 63.6 years (range 46 to 76) and median follow-up was 50 months (maximum 62). Prostate specific antigen (PSA) recurrence was defined as any PSA level greater than 0.2 ng/ml and increasing.

Tissue array construction

Archival tumor specimens were obtained from the Department of Pathology under IRB approval. Prostatectomy specimens were originally processed using transverse sections per UCLA protocol (5 slices). Three slices were submitted, and the seminal vesicles (SVs), vas deferens, bladder neck and apical margins were submitted separately. Cases were selected randomly between 1985 and 2000. Case material was reviewed for tissue array construction by a pathologist (DBS). All prostate tumors were staged according to the 1997 American Joint Committee on Cancer staging system[6] and histologically graded using the Gleason scoring system.[7] At least 3 core tissue biopsies (each 0.6 mm in diameter) were taken from select, morphologically representative regions of each paraffin embedded prostate tumor and precisely

arrayed using a custom built instrument, as previously described.[8] An additional core biopsy was taken from a morphologically benign-appearing region of the same prostate. Benign tissue included normal glands and glands consistent with a histological diagnosis of BPH. Sections (4 μm) of each tissue array block were then transferred to glass slides using the paraffin sectioning aid system with adhesive coated slides PSA-CS 4×, adhesive tape and an ultraviolet lamp (Instrumedics Inc., Hackensack, New Jersey) to support cohesion of the 0.6 mm array elements. Quality control was assessed by cross-checking the expected histology and grade at each spot on each FEN-1 stained slide.

Immunohistochemistry.

Immunohistochemical staining was performed with anti-FEN-1 antibody (1:50 dilution) using a peroxidase technique with antigen retrieval using heat treatment.[9] Semiquantitative assessment of staining was performed by 2 pathologists (HY and DBS) blinded to patient clinical outcomes. Two measures of FEN-1 nuclear expression were scored, intensity on a 0-3 scale (0=negative, 1=weakly positive, 2=moderately positive, 3=strongly positive), and percentage of positive target cells at each intensity (range 0-100% positive). We found that the cellular intensity and the percentage positive were highly correlated (Spearman correlation, $\sigma = 0.86$, $p < 0.0001$), so we chose only one measure for all analyses, the total percentage of positive cells. To represent expression within cases, the mean pooled percent positive of the tumor spots was used. There was an average of 2.5 informative invasive tumor spots per patient.

Statistical analysis

The Kruskal-Wallis test was used to determine the significance of FEN-1 protein expression differences between the histologic specimen categories and between clinical prognostic factors: Gleason score ≥ 7, seminal vesicle involvement, organ confinement, capsular penetration, preoperative PSA ≥ 10 ng/ml, and nodal involvement. The Spearman correlation coefficient and its corresponding p-value was used to determine the correlation between FEN-1 protein expression and Gleason score. Univariate and multivariate Cox regression models were used to relate the censored clinical outcome (time to PSA recurrence) with patient characteristics. The proportional hazards assumption was verified using Schoenfeld residuals.[10] Kaplan-Meier plots were used to visualize the distributions of recurrence-free time and the log rank test was used to test for differences across groups. All p values were 2-sided and $p \leq 0.05$ was considered significant. All statistical analyses were performed using the freely available statistical software R (http://www.r-project.org/).

RESULTS

FEN-1 protein expression was consistently seen by immunohistochemistry in cellular nuclei, with occasional cytoplasmic staining also seen. FEN-1 staining was analyzed on spots that contained tumor, prostatic intraepithelial neoplasia (PIN) or benign tissue (morphologically normal and benign prostatic hyperplasia (BPH) tissue) and scoring was limited to the nuclear compartment. There were a total of 1083 informative tissue spots: 651 cancer, 264 normal, 120 BPH, and 48 PIN. Mean expression of FEN-1 was significantly higher in cancer (36.7%) compared to normal (13.2%), BPH (4.5%), and PIN (15.4%) specimens ($p < 0.0001$) (FIG. 1). FEN-1 expression was higher in PIN compared to normal tissue ($p = 0.027$), whereas FEN-1 expression was less in BPH compared to normal tissue ($p = 0.0004$). FEN-1 staining patterns in a variety of prostate tissues are shown in Figure 2. In addition, 3 cases of matched primary and metastatic prostate cancers were stained. Of the metastatic lesions, 2 (66.7%) of 3 were positive for FEN-1 expression (Table 1). Expression of FEN-1 appears to be similar between the matched primary and metastatic prostate cancer pairs.

The results of cross-tabulating mean FEN-1 expression with established prognostic factors in prostate cancer is shown in Table 2. FEN-1 expression in Gleason 7 and higher cancers was greater than tumors that were Gleason 6 or lower ($41.7\% \pm 24.5$ vs. $32.2\% \pm 26.7$, $p = 0.004$). There was no significant difference in FEN-1 expression in tumors with SV invasion compared to tumor without SV involvement ($39.3\% \pm 25.0$ vs. $35.6\% \pm 26.4$, $p = 0.36$). Organ confined tumors (T2 or less and N0M0) had similar levels of FEN-1 expression compared to tumors with extraprostatic involvement (T3a–T4b or nodal disease, ($35.7\% \pm 26.3$ vs. $37.2\% \pm 25.3$, $p = 0.6$). Finally, $38.7\% \pm 27.4$ of tumors with extraprostatic extension, $35.4\% \pm 26.3$ of tumors with capsular invasion, and $36\% \pm 24.8$ of tumors with no capsular involvement stained for FEN-1 (p

= 0.77). FEN-1 staining did not statistically correlate with PSA values using a cutoff of 10 ng/ml ($p = 0.9$) or with tumors that had associated nodal involvement ($p = 0.72$). FEN-1 expression was significantly correlated with Gleason score ($\sigma = 0.24$, $p = 0.0008$) (FIG. 3).

The results of univariate analysis performed for established prognostic factors for time to PSA recurrence is shown in Table 3. Preoperative PSA ($p = 0.005$), Gleason score ≥ 7 ($p < 0.0001$), SV invasion ($p < 0.0001$), and extraprostatic extension ($p = 0.001$) were associated with decreased PSA recurrence-free survival, whereas FEN-1 expression ($p = 0.99$) was not. On multivariate analysis, only Gleason score ≥ 7 (HR: 3.00; CI: 1.59–5.67; $p < 0.0001$), SV invasion (HR: 2.43; CI: 1.33–4.45; $p = 0.004$), and extraprostatic extension (HR: 1.85; CI: 1.17–2.93; $p = 0.008$) were retained as independent prognostic indictors for PSA recurrence.

DISCUSSION

Our study demonstrates that FEN-1 is expressed in a large panel of prostate cancer specimens. Tissue microarray analysis demonstrated that FEN-1 expression in primary prostate cancer was significantly increased compared to matched normal prostate tissue controls and FEN-1 expression was significantly correlated with Gleason score. In addition, FEN-1 expression was present at similar levels in prostate cancer metastases. This confirms prior gene expression microarray data linking FEN-1 expression to prostate cancer.[5] Furthermore, FEN-1 gene expression was overexpressed in an aggressive hormone refractory cell line based on *in vivo* animal studies.[5]

In our study, Gleason score ≥ 7 was associated with and shown to be an independent predictor of poor PSA recurrence-free survival, whereas FEN-1 expression was not. Although mean expression of FEN-1 was significantly correlated with Gleason score, the correlation coefficient was only 0.24. This is the likely explanation as to why FEN-1 expression was not associated with a poorer PSA recurrence-free survival. Nevertheless, a significant positive correlation was found between FEN-1 expression and Gleason score and thus expression of FEN-1 may be a tumor marker for the selection of patients at high risk for progression and a potentially useful target for prostate cancer.

Structure-specific FEN-1,[11] which was initially detected and called DNase IV,[12] is a key enzyme for maintaining genetic stability. FEN-1 plays a critical role in RNA and DNA primer removal during lagging-strand DNA synthesis and in DNA repair by cleaving RNA and DNA substrates in a sequence-independent manner.[13-15] The flap 5'-end DNA structures resulting from strand displacement of the downstream primer by DNA polmerase δ (polδ) are important intermediates in DNA metabolism and displaced structures represent good substrates for FEN-1,

which can be successively recognized and cleaved within their 5'-single-stranded arm.[16] In addition, flap removal by FEN-1 is required for Okazaki fragment processing,[17] in long-patch base excision repair,[13] and in homologous recombination.[18]

The FEN-1 gene has been demonstrated to be involved in mouse gastrointestinal tract cancer in a haplo-insufficient manner.[19] FEN-1 heterozygous mice generated by knockout appeared normal, but when combined with a mutation of adenomatous polyposis coli (APC) gene, they showed increased number of adenocarcinomas and decreased survival. Tumors from these mice demonstrated microsatellite instability, which suggests that decreased expression of FEN-1 may be attributable to microsatellite instability of these cancer cells. FEN-1 is responsible for DNA replication and base excision repair (BER) pathways and has been shown to play an important role in the integrity of genome.[20] However, our study and prior microarray data suggest that alterations of FEN-1 through decreased expression or mutation are not likely to contribute to the development of prostate cancer.

There are possible explanations for the increased expression of FEN-1. FEN-1 is involved in DNA replication through its function in the processing of 5' ends of Okazaki fragments in the lagging DNA strand and thus increased expression of FEN-1 may reflect the increased proliferation rate of cancer cells compared to normal cells.[21, 22] In fact, upregulation of FEN-1 expression has been shown to be associated with normal proliferating cells and malignant cell lines.[23, 24] FEN-1 expression in serum-starved 3T3 cells has been shown to be induced by refeeding, indicating that progression from a quiescent state into the cell cycle results in increased FEN-1 expression.[24] Furthermore, our study demonstrated that FEN-1 expression was significantly correlated with high Gleason score prostate cancer, which may be more proliferative than low Gleason score prostate cancer. Some cells can also adapt to DNA alkylating agent

exposure by increasing the expression of DNA polymerase β-pol mRNA, which functions in the BER pathway.[25] Thus, increased FEN1 expression may be a response caused by increased DNA damage in cancer compared to normal cells.

High-throughput IHC provides a large amount of valuable information on expression of proteins within tissues at a cellular and subcellular level in a relatively short period of time. However, it is important to consider that the protein level in the tissue microarray may not necessarily depict protein activity and/or correct protein structure, which may be truncated or posttranslationally modified.[26] Other issues to consider include alteration of the epitope preventing recognition by the antibody or the epitope may be inaccessible to the antibody (e.g. through protein–protein interactions, cross-linking or modification). Alternatively, the antigen may be present at levels below the sensitivity limits of the detection system or within background generated by the detection system. In addition, cross-reactivity with related or unrelated epitopes can occur.

Fluorescence in situ hybridization (FISH) analysis of FEN-1 has been performed and 11q12 was found to be the location of FEN-1 confirmed by radiation-reduced hybrid cell analysis.[27] Its upregulation in a variety of malignant cell lines is intriguing and may suggest chromosomal amplification of this genomic region in many cancers. Further investigations such as search for alterations in other components of the DNA repair system are needed to clarify the underlying mechanisms of microsatellite alterations and other signs of genetic abnormalities found in prostate cancer.

CONCLUSIONS

FEN-1 is overexpressed in primary prostate cancers with a Gleason score of 7 and higher. FEN-1 expression appears to be similar between matched pairs of primary and metastatic prostate cancer. Overexpression of FEN-1 may reflect the increased proliferation rate of cancer cells compared to normal cells. These results suggest that FEN-1 may be a tumor marker for the selection of patients at high risk for progression and may be a useful target for prostate cancer diagnosis and therapy. To our knowledge, this is the first study to analyze the clinical significance of FEN-1 expression in a large panel of prostate cancer specimens.

LEGEND

FIG. 1. Mean percentage of cells with positive staining for FEN-1 in prostate cancer (CaP), benign prostatic hyperplasia (BPH), normal prostate, and prostatic intraepithelial neoplasia (PIN). Total of 1,083 spots were available. Error bars represent 1 standard error.

FIG. 2. Immunohistochemical analysis of a prostate tissue microarray using anti-FEN-1 antibody. A. normal, B. benign prostatic hyperplasia (BPH), C. prostatic intraepithelial neoplasia (PIN), D. low grade prostate cancer, E. high grade prostate cancer. Reduced from x10 (A to E) and x40 (inserts).

FIG. 3. Mean percent positive expression of FEN-1 according to Gleason score shown in a box plot graph. The middle line represents the median; the upper and lower hinges of the box show the medians of the upper and lower halves of the data. The width of the boxes represents the number of tumor spots. The ends of the line segments attached to the box extend to the smallest data value and the largest data value. All data values are shown.

Figure 1.

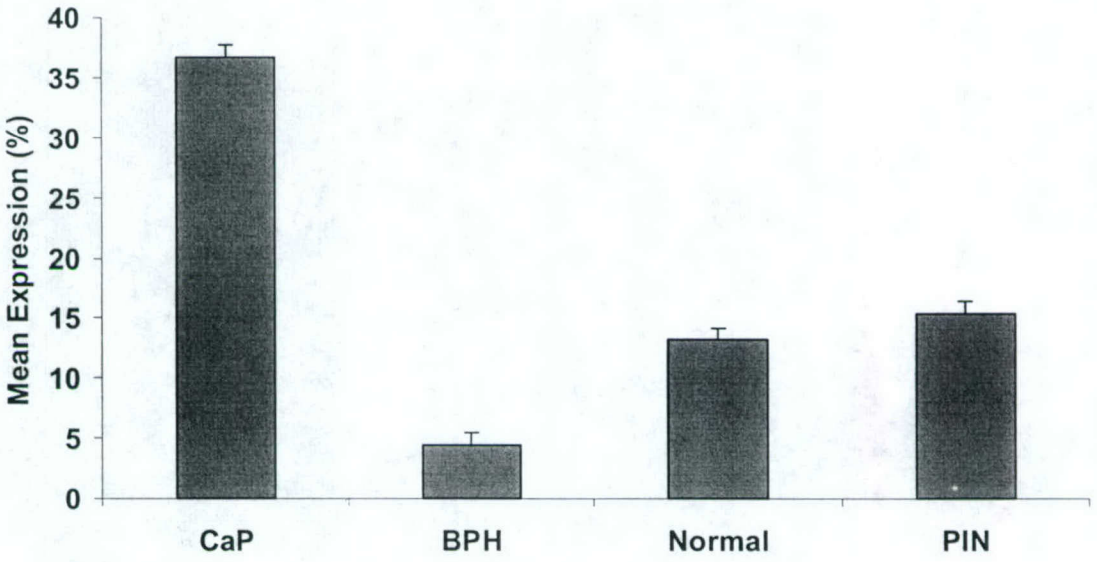

Figure 2A.

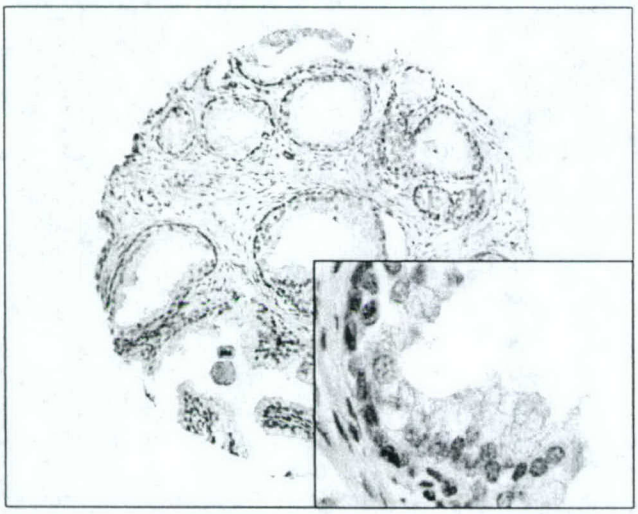

Figure 2B.

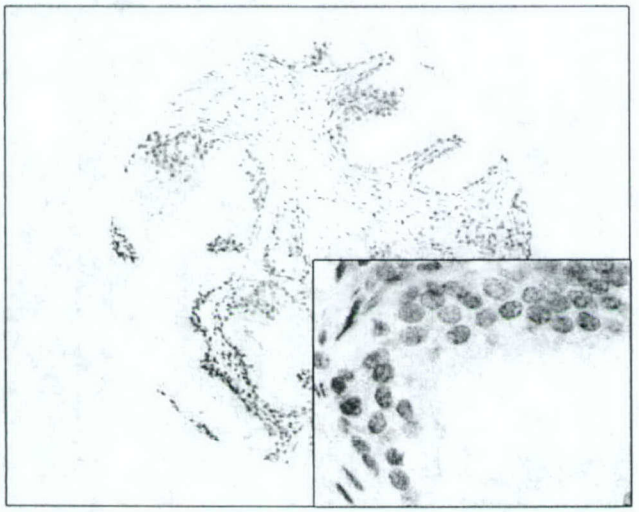

Figure 2C.

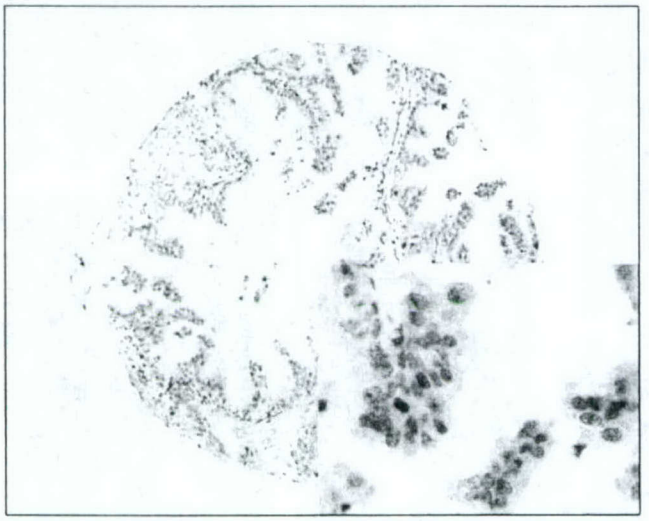

Figure 2D.

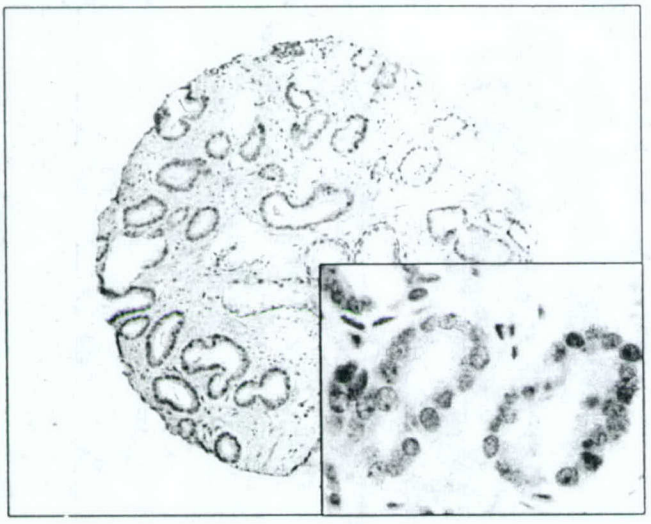

Figure 2E.

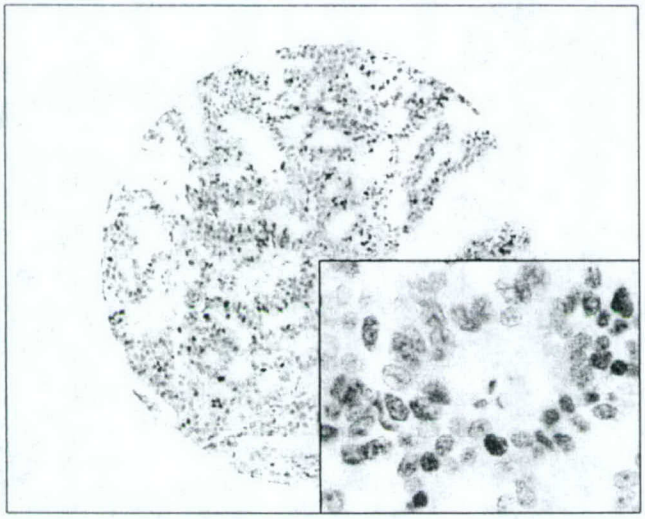

Figure 3.

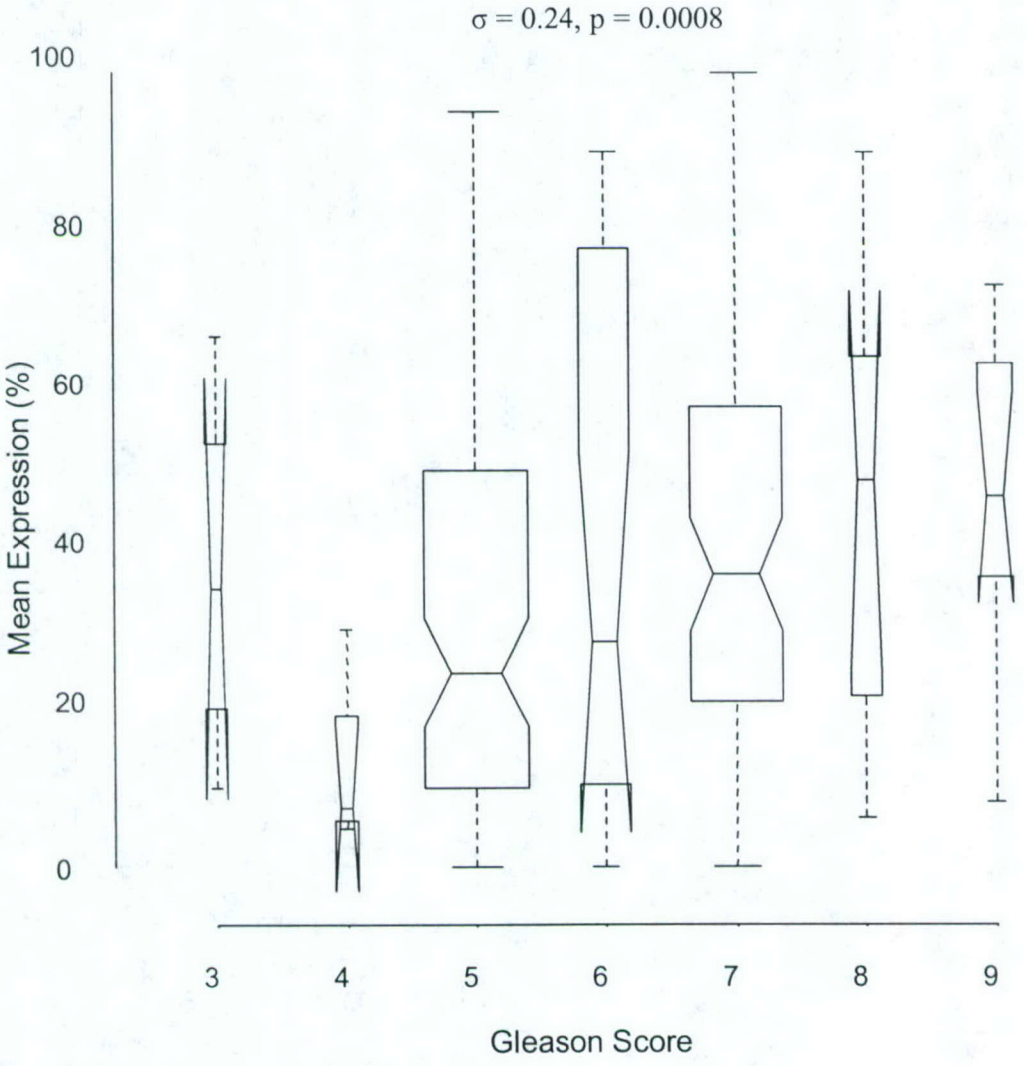
σ = 0.24, p = 0.0008
100
80
60
40
20
0
Mean Expression (%)
3
4
5
6
7
8
9
Gleason Score

Table 1. Mean FEN-1 expression of paired primary and metastatic prostate cancers.

	Mean expression FEN-1 (%)
Matched pair 1	
Primary prostate cancer	12
Metastatic lesion	10
Matched pair 2	
Primary prostate cancer	53
Metastatic lesion	40
Matched pair 3	
Primary prostate cancer	8
Metastatic lesion	0

Table 2. Mean FEN-1 expression and clinical prognostic factors.

	Mean expression FEN-1 (%) ± SE	p value*
Gleason score		0.004
6 or less	32.2 ± 26.7	
7 or greater	41.7 ± 24.5	
Seminal vesicle invasion		0.36
No	35.6 ± 26.4	
Yes	39.3 ± 25.0	
Organ confined		0.6
Yes	35.7 ± 26.3	
No	37.2 ± 25.3	
Capsular involvement		0.77
None	36.0 ± 24.8	
Capsular invasion	35.4 ± 26.3	
Extraprostatic extension	38.7 ± 27.4	
PSA (ng/ml)		0.9
Less than 10	36.9 ± 26.8	
10 or greater	37.0 ± 25.8	
Nodal involvement		0.72
No	36.4 ± 26.1	
Yes	33.2 ± 23.8	

* p value from a Kruskal-Wallis test.

Table 3. Cox regression analysis for PSA recurrence-free survival.

	Hazard Ratio	95% CI	p value
Univariate			
Preoperative PSA	1.02	1.01 – 1.03	0.0052
Seminal vesicle invasion	4.58	2.78 – 7.55	<0.0001
Gleason score ≥7	3.93	2.39 – 6.45	<0.0001
Extraprostatic extension	1.82	1.26 – 2.62	0.0013
FEN-1	1.00	0.99 – 1.01	0.99
Multivariate			
Preoperative PSA	1.00	0.99 – 1.02	0.66
Seminal vesicle invasion	2.43	1.33 – 4.45	0.004
Gleason score ≥7	3.00	1.59 – 5.67	0.0007
Extraprostatic extension	1.85	1.17 – 2.93	0.0084
FEN-1	1.00	0.98 – 1.00	0.2

REFERENCES

1. Jemal, A., Tiwari, R. C., Murray, T., Ghafoor, A., Samuels, A., Ward, E. et al: Cancer statistics, 2004. CA Cancer J Clin, **54:** 8, 2004
2. Hernandez, J. and Thompson, I. M.: Prostate-specific antigen: A review of the validation of the most commonly used cancer biomarker. Cancer, **101:** 894, 2004
3. Tso, C. L., McBride, W. H., Sun, J., Patel, B., Tsui, K. H., Paik, S. H. et al: Androgen deprivation induces selective outgrowth of aggressive hormone-refractory prostate cancer clones expressing distinct cellular and molecular properties not present in parental androgen-dependent cancer cells. Cancer J, **6:** 220, 2000
4. Patel, B. J., Pantuck, A. J., Zisman, A., Tsui, K. H., Paik, S. H., Caliliw, R. et al: CL1-GFP: an androgen independent metastatic tumor model for prostate cancer. J Urol, **164:** 1420, 2000
5. Freedland, S. J., Pantuck, A. J., Paik, S. H., Zisman, A., Graeber, T. G., Eisenberg, D. et al: Heterogeneity of molecular targets on clonal cancer lines derived from a novel hormone-refractory prostate cancer tumor system. Prostate, **55:** 299, 2003
6. Fleming, I. D., Cooper, J. S., Hensen, D. E., Hutter, R. V. P., Kennedy, B. J. and Murphy, G. P.: AJCC Cancer Staging Manuel, 5th ed. Philadelphia: Lippincott-Raven, 1997
7. Gleason, D. F. and Mellinger, G. T.: Prediction of prognosis for prostatic adenocarcinoma by combined histological grading and clinical staging. J Urol, **111:** 58, 1974
8. Kononen, J., Bubendorf, L., Kallioniemi, A., Barlund, M., Schraml, P., Leighton, S. et al: Tissue microarrays for high-throughput molecular profiling of tumor specimens. Nat Med, **4:** 844, 1998
9. Liao, S. Y., Brewer, C., Zavada, J., Pastorek, J., Pastorekova, S., Manetta, A. et al: Identification of the MN antigen as a diagnostic biomarker of cervical intraepithelial squamous and glandular neoplasia and cervical carcinomas. Am J Pathol, **145:** 598, 1994
10. Harrell, F. E.: Regression Modeling Strategies with Applications to Linear Models, Logistic Regression, and Survival Analysis. New York: Springer Publishing, 2001
11. Harrington, J. J. and Lieber, M. R.: The characterization of a mammalian DNA structure-specific endonuclease. Embo J, **13:** 1235, 1994
12. Lindahl, T., Gally, J. A. and Edelman, G. M.: Deoxyribonuclease IV: a new exonuclease from mammalian tissues. Proc Natl Acad Sci U S A, **62:** 597, 1969
13. Klungland, A. and Lindahl, T.: Second pathway for completion of human DNA base excision-repair: reconstitution with purified proteins and requirement for DNase IV (FEN1). Embo J, **16:** 3341, 1997
14. Lieber, M. R.: The FEN-1 family of structure-specific nucleases in eukaryotic DNA replication, recombination and repair. Bioessays, **19:** 233, 1997
15. Tishkoff, D. X., Filosi, N., Gaida, G. M. and Kolodner, R. D.: A novel mutation avoidance mechanism dependent on S. cerevisiae RAD27 is distinct from DNA mismatch repair. Cell, **88:** 253, 1997
16. Kaiser, M. W., Lyamicheva, N., Ma, W., Miller, C., Neri, B., Fors, L. et al: A comparison of eubacterial and archaeal structure-specific 5'-exonucleases. J Biol Chem, **274:** 21387, 1999
17. Rumbaugh, J. A., Henricksen, L. A., DeMott, M. S. and Bambara, R. A.: Cleavage of substrates with mismatched nucleotides by Flap endonuclease-1. Implications for mammalian Okazaki fragment processing. J Biol Chem, **274:** 14602, 1999
18. Wu, X., Wilson, T. E. and Lieber, M. R.: A role for FEN-1 in nonhomologous DNA end joining: the order of strand annealing and nucleolytic processing events. Proc Natl Acad Sci U S A, **96:** 1303, 1999
19. Kucherlapati, M., Yang, K., Kuraguchi, M., Zhao, J., Lia, M., Heyer, J. et al: Haploinsufficiency of Flap endonuclease (Fen1) leads to rapid tumor progression. Proc Natl Acad Sci U S A, **99:** 9924, 2002
20. Henneke, G., Friedrich-Heineken, E. and Hubscher, U.: Flap endonuclease 1: a novel tumour suppresser protein. Trends Biochem Sci, **28:** 384, 2003
21. Bambara, R. A., Murante, R. S. and Henricksen, L. A.: Enzymes and reactions at the eukaryotic DNA replication fork. J Biol Chem, **272:** 4647, 1997
22. Waga, S. and Stillman, B.: The DNA replication fork in eukaryotic cells. Annu Rev Biochem, **67:** 721, 1998
23. Otto, C. J., Almqvist, E., Hayden, M. R. and Andrew, S. E.: The "flap" endonuclease gene FEN1 is excluded as a candidate gene implicated in the CAG repeat expansion underlying Huntington disease. Clin Genet, **59:** 122, 2001

24. Warbrick, E., Coates, P. J. and Hall, P. A.: Fen1 expression: a novel marker for cell proliferation. J Pathol, **186:** 319, 1998
25. Chen, K. H., Yakes, F. M., Srivastava, D. K., Singhal, R. K., Sobol, R. W., Horton, J. K. et al: Up-regulation of base excision repair correlates with enhanced protection against a DNA damaging agent in mouse cell lines. Nucleic Acids Res, **26:** 2001, 1998
26. Liotta, L. A., Espina, V., Mehta, A. I., Calvert, V., Rosenblatt, K., Geho, D. et al: Protein microarrays: meeting analytical challenges for clinical applications. Cancer Cell, **3:** 317, 2003
27. Hiraoka, L. R., Harrington, J. J., Gerhard, D. S., Lieber, M. R. and Hsieh, C. L.: Sequence of human FEN-1, a structure-specific endonuclease, and chromosomal localization of the gene (FEN1) in mouse and human. Genomics, **25:** 220, 1995

Drug Interactions between the Proteasome Inhibitor Bortezomib and Cytotoxic Chemotherapy, Tumor Necrosis Factor (TNF) α, and TNF-Related Apoptosis-Inducing Ligand in Prostate Cancer

Jiabin An, Yi-Ping Sun, Julian Adams, Myrna Fisher, Arie Belldegrun, and Matthew B. Rettig[1]

Veterans Administration Greater Los Angeles Healthcare System, Los Angeles, California 90073 [J. An, Y-P. S., M. F., M. B. R.]; Millennium Pharmaceuticals, Inc., Cambridge, Massachusetts 02139 [J. Ad.]; and University of California at Los Angeles School of Medicine, Los Angeles, CA 90095 [A. B., M. B. R.]

ABSTRACT

Purpose: **Proteasome inhibition has been shown to be an effective anticancer therapy in many tumor models, including prostate cancer. We sought to identify drug interactions between the proteasome inhibitor bortezomib and other apoptotic stimuli, including cytotoxic chemotherapy and tumor necrosis factor-related apoptosis-inducing ligand (TRAIL). In addition, we wanted to gain insight into the role of nuclear factor κB inhibition as a mediator of bortezomib cytotoxic effects.**

Experimental Design: **Prostate cancer cell lines (LNCaP, LAPC4, CL1, and DU145) were treated with bortezomib and apoptotic stimuli (TRAIL, chemotherapy, and tumor necrosis factor α), alone or in combination. Apoptosis and cell viability were measured, and median effect/combination index analyses were used to quantitate drug interactions. Nuclear factor κB activity at baseline and in response to drug treatment was determined by gel shift and reporter gene assays.**

Results: **Bortezomib induced cell death of androgen-dependent (LNCaP and LAPC4) and androgen-independent (CL1 and DU145) prostate cancer cell lines, although androgen-dependent cells were more sensitive to proteasome inhibition. Bortezomib synergized with TRAIL and tumor necrosis factor α to induce death in both androgen-dependent and androgen-independent cells.**

Conclusions: **Bortezomib and TRAIL represent a synergistic drug combination that warrants further evaluation in *in vivo* models of prostate cancer.**

INTRODUCTION

The ubiquitin-proteasome pathway represents the principal mechanism whereby cytosolic proteins are degraded. Proteins degraded by the proteasome are targeted by ubiquitination, which subsequently results in protein degradation by the proteasome, a large complex of proteins that are the executioners of the degradation process. The degradation of proteins is crucial for maintenance of cellular homeostasis. The proteasome plays a critical role in modulating intracellular levels of proteins that are involved in cell cycle regulation, including cyclins and cyclin-dependent kinase inhibitors (1, 2). The proteasome also regulates the activity of signal transduction pathways, such as the NF-κB[2] pathway, in that the degradation of the inhibitor of nuclear factor-κB, the NF-κB inhibitory protein, is also dependent on the ubiquitin-proteasome pathway (3). Degradation of tumor suppressor genes, such as *p53*, and oncogenes, including c-*jun* and c-*myc*, is also modulated by the proteasome (4–6).

Proteasome inhibitors have been actively studied for their antitumor effects and have been shown to induce cytotoxicity of many tumor models both *in vitro* and *in vivo*. In prostate cancer, the proteasome inhibitor bortezomib is active against AD prostate cancer cells (LNCaP cell line) as well as AI lines (PC3 and DU-145; Refs. 7 and 8). In addition, bortezomib reduces prostate cancer tumor growth in murine tumor models (8). Importantly, the activity of proteasome inhibitors does not seem to be influenced by the low growth fractions of tumors, including prostate cancer, which is in contradistinction to cytotoxic chemotherapy, which is more often cell cycle dependent (8–10). In addition, proteasome inhibitors seem to induce cytotoxicity of prostate cancer cells independent of *p53* status and *bcl*-2 expression (11). Thus, proteasome inhibition represents a suitable approach to treatment of prostate cancer.

The interactions between proteasome inhibitors and other apoptotic stimuli in prostate cancer have not been studied. In other tumor models, such as colon cancer, proteasome inhibition sensitizes cancer cells both *in vitro* and *in vivo* to cytotoxic chemotherapy (12). TNFα, TRAIL, and chemotherapy consistently induce apoptosis of prostate cancer cells *in vitro*, although

Received 3/25/03; revised 6/17/03; accepted 6/18/03.
The costs of publication of this article were defrayed in part by the payment of page charges. This article must therefore be hereby marked *advertisement* in accordance with 18 U.S.C. Section 1734 solely to indicate this fact.

[1] To whom requests for reprints should be addressed, at Veterans Administration Greater Los Angeles Healthcare System, Building 304, Room E1-113, 11301 Wilshire Boulevard, Los Angeles, CA 90073. Phone: (310) 478-3711, ext. 44761; Fax: (310) 268-4508; E-mail: matthew.rettig@med.va.gov.

[2] The abbreviations used are: NF-κB, nuclear factor κB; AD, androgen-dependent; AI, androgen-independent; TNFα, tumor necrosis factor α; TRAIL, tumor necrosis factor-related apoptosis-inducing ligand; CI, combination index; MTT, 3-(4,5-dimethylthiazol-2-yl)-2,5-diphenyltetrazolium bromide; EMSA, electrophoretic mobility shift assay.

the activity of these cytokines can vary depending on the cell line or hormone-dependency status (13–17). Thus, we investigated the potential of the proteasome inhibitor bortezomib to sensitize AD and AI prostate cancer cells to these apoptosis-inducing agents. In these studies, we specifically tested chemotherapeutic agents that are in clinical use for prostate cancer patients. In addition, because TNFα, TRAIL, and chemotherapy can activate NF-κB (13, 16, 18–22) and inhibition of NF-κB is thought to play a critical role in the mechanism of action of proteasome inhibitors, we also studied the relationship between activation of NF-κB and sensitization to bortezomib-induced death.

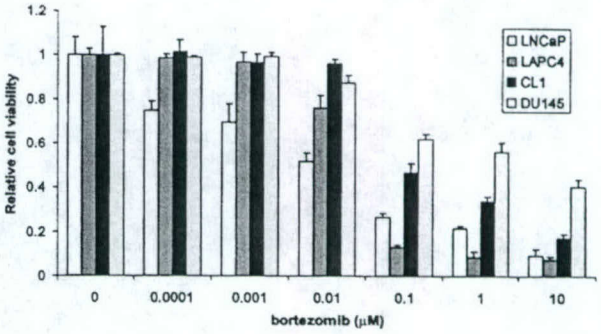

Fig. 1 Cytotoxicity of bortezomib in AD and AI prostate cancer cell lines. Prostate cancer cell lines were plated in 96-well plates. Bortezomib or vehicle control was added the next morning. After 48 h, MTT assays were performed. Results are means of four experiments +/− SD and are normalized to that of vehicle control.

Table 1 IC_{50} values (μM) for bortezomib

	IC_{50}
LAPC4	0.054
LNCaP	0.0070
CL1	0.42
DU145	1.7

MATERIALS AND METHODS

Cell Culture and Prostate Cancer Cell Lines. AD LNCaP cells (American Type Culture Collection, Manassas, VA) and LAPC4 cells (a gift from Dr. Charles Sawyers, University of California, Los Angeles, CA) were maintained in RPMI 1640 supplemented with 10% fetal bovine serum and penicillin (100μg/ml) and streptomycin (100μg/ml). CL1 cells represent an AI subclone of LNCaP that was generated by culturing LNCaP in charcoal-stripped, androgen-depleted serum, as described (23). CL1 cells were maintained as for LNCaP cells, but continuously in charcoal-stripped serum. AI DU145 cells (American Type Culture Collection) were maintained in DMEM containing 10% fetal bovine serum and antibiotics. All culture media were purchased from Omega Scientific (Thousand Oaks, CA).

Reagents. The proteasome inhibitor bortezomib was provided by Millennium, Inc. (Cambridge, MA) and dissolved in DMSO. Recombinant human TNFα (R&D Systems, Minneapolis, MN) and recombinant human TRAIL (Calbiochem, San Diego CA) were dissolved in PBS. Methyltrienolone (R1881) was purchased from New England Nuclear Life Science Products (Boston, MA) and dissolved in ethanol. For subsequent experiments, the final concentration of all solvents was maintained at 0.1%. A κB-responsive plasmid (p4x-κB-luc), in which four copies of the κB-response element drives expression of firefly luciferase, was purchased from Invitrogen (Carlsbad, CA). The pRL-SV40 plasmid, in which *Renilla* luciferase is constitutively expressed under the regulation of the SV40 promoter/enhancer, was purchased from Promega Corp. (Madison, WI) and was used for normalization of firefly luciferase activity.

Transient Transfections and Reporter Gene Assays. Cells were plated at 10^5 cells/well in 24-well plates the day before transfection. The plasmids were transfected with Lipofectamine Plus (Life Technologies, Inc., Gaithersburg, MD) according to the manufacturer's instructions. Protein was extracted 48 h after transfection, and firefly and *Renilla* luciferase were measured on a TD20/20 tube luminometer (Turner Designs, Sunnyvale, CA) using a Dual Luciferase Assay kit (Promega Corp.), according to the manufacturer's instructions. Firefly luciferase activity was normalized to *Renilla* luciferase expression.

EMSAs. Wild-type and mutant κB oligonucleotide probes were purchased from Santa Cruz Biotechnology. Fifteen micrograms of nuclear protein were combined with end-labeled, double-stranded κB oligonucleotide probe, 1 μg of poly-dIdC (Amersham Pharmacia Biotech, Piscataway, NJ), 1 μg of BSA, and 5 mM spermidine in a final reaction volume of 20 μl for 20 min at room temperature. The DNA protein complex was run on a 4% nondenaturing polyacrylamide gel with 0.4× Tris-borate EDTA running buffer before subsequent autoradiography. Cold-competition experiments were performed with a 100-fold molar excess of cold wild-type or cold mutant κB oligonucleotides. For supershift assays, nuclear protein was preincubated with specific or control antibodies (6 μg) for 20 min at room temperature.

Assessment of Cytotoxicity. LNCaP, LAPC4, CL1, and DU145 cells were seeded in 96-well plates the day before chemical treatment at concentrations of 4×10^4, 4×10^4, 1×10^4, and 2×10^4 cells per well, respectively. Various combinations of bortezomib and apoptotic stimuli were added to cells, and 48 h later, cell viability was assessed by the thiazolyl blue (MTT) assay. All experiments were performed in quadruplicate.

Assessment of Apoptosis. Cells were plated in 10-cm dishes (2×10^6 cells/dish). The next day, cells were treated with various concentrations of bortezomib or vehicle control for 48 h. Cells were harvested and then stained with an annexin V-FITC kit (BD Biosciences, Palo Alto, CA) according to the manufacturer's instructions. Cells were analyzed on a Becton Dickinson FACS Caliber flow cytometer with CellQuest software (BD Biosciences).

Median Effect/CI Isobologram Method for Multiple Drug Effect Analysis. The effect of drug combinations on cytotoxicity was performed by the median effect method using Calcusyn software, version 1.1.1 (Biosoft, Ferguson, MO; Ref. 24). CI values were calculated using the most conservative assumption of mutually nonexclusive drug interactions. CI val-

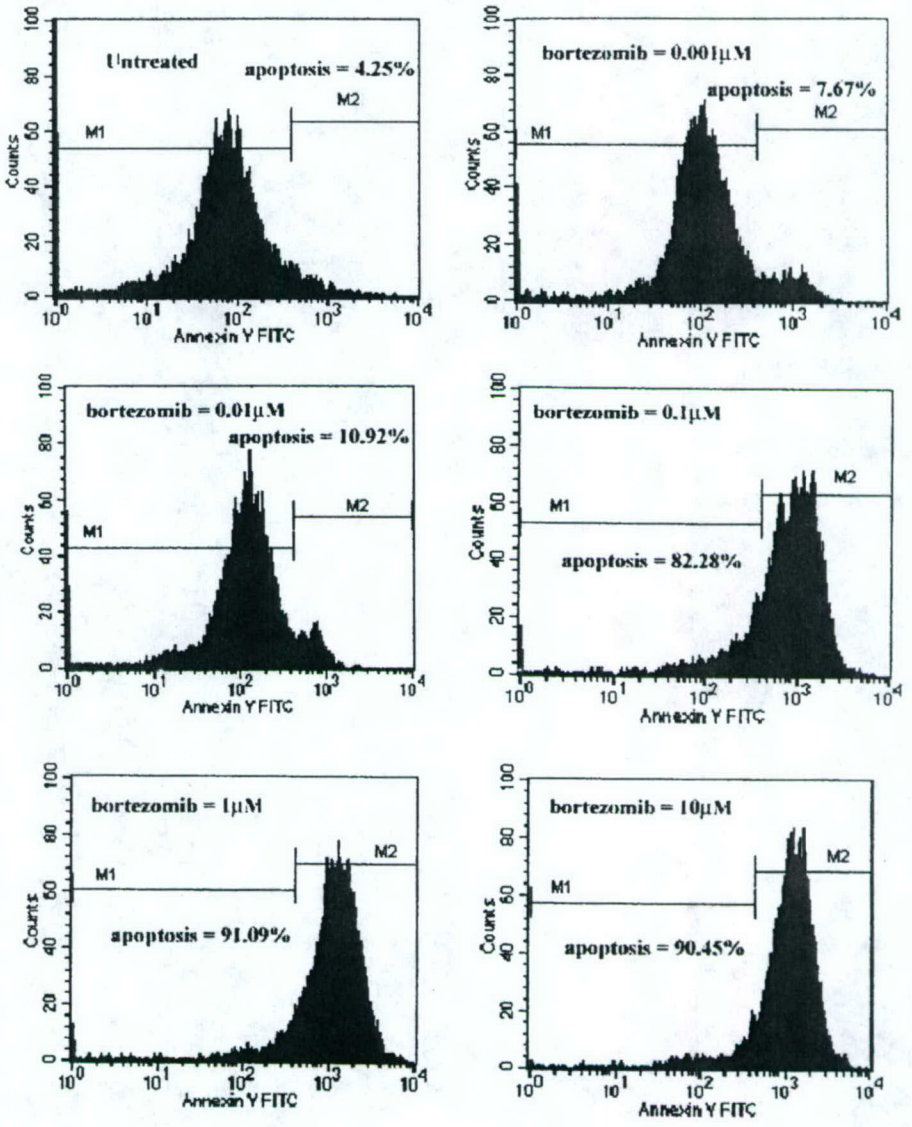

Fig. 2 Bortezomib induces apoptosis. CL1 cells were plated in 6-well dishes (1×10^6 cells/well) and incubated overnight. Cells were subsequently treated with bortezomib or vehicle control for 48 h before harvesting cells for assessment of apoptosis by annexin V-FITC staining.

ues were calculated from median results of the cytotoxicity (MTT) assays, which were performed in quadruplicate. CI values significantly greater than 1 indicate drug antagonism, CI values significantly less than 1 are indicative of synergy, and CI values not significantly different than 1 indicate an additive drug effect. Linear regression correlation coefficients of the median effects plots were required to be >0.90 to demonstrate that the effects of the drugs follow the law of mass action, which is required for a median effect analysis.

RESULTS

Cytotoxicity of Bortezomib. We confirmed the ability of bortezomib to induce cytotoxicity as measured by a MTT assay in AD (LNCaP and LAPC4) and AI (CL1 and DU145) prostate cancer cell lines. After 48 h of treatment, bortezomib potently induced cytotoxicity of all cell lines tested (Fig. 1). The IC_{50} values were substantially lower for the AD cell lines compared with the AI cell lines (Table 1). Induction of apoptosis was confirmed in all four cell lines by annexin V staining. Fig. 2 shows a representative experiment in CL1 cells treated with various concentrations of bortezomib. As shown in Fig. 2, a concentration-dependent increase in apoptosis was identified, which correlated with the effective concentrations of bortezomib in the MTT assays (Fig. 1).

Androgen Does Not Protect AD Prostate Cancer Cells from Bortezomib. Androgens have been shown to protect androgen-responsive prostate cancer cells from apoptotic stimuli, including Fas activation and TNFα (25). Consequently, we tested whether androgen could block bortezomib-induced apoptosis in the AD cell lines LAPC4 and LNCaP. Pilot studies demonstrated that the optimal concentration of the synthetic androgen R1881 to induce reporter gene expression driven by the androgen-response element was 1.0 nM for LAPC4 and 0.1 nM for LNCaP cells. Pretreatment of LAPC4 and LNCaP cells

with R1881 had no effect on protecting cells from bortezomib-induced apoptosis/death (data not shown). In these experiments, cells were stained with annexin V to detect cells in the early stages of apoptosis and with propidium iodide to identify dead cells.

Proteasome Inhibition Sensitizes AD and AI Prostate Cancer Cells to TRAIL-induced Cytotoxicity. TRAIL is a member of the TNFα superfamily that induces apoptosis in tumor cell lines by engaging and activating death receptors (26–28). We studied the ability of bortezomib to sensitize AD and AI prostate cancer cells to TRAIL-induced death. TRAIL (0–200 ng/ml) alone had virtually no cytotoxic effect on LNCaP and CL1 cells and only modest cytotoxic effects on LAPC4 and DU145 cells, as measured in a MTT assay (Fig. 3). However, when bortezomib and TRAIL were used in combination, median effect analysis demonstrated synergistic interactions across all concentrations of both bortezomib and TRAIL in both AD (LNCaP and LAPC4) and AI (DU145) cell lines (Fig. 4). Up to 90% cell death was observed at concentrations well below those that induced death by either agent alone in both AD and AI cells (Fig. 3). Bortezomib and TRAIL were antagonistic in CL1 cells (Fig. 4).

Like TRAIL, TNFα can induce apoptosis in a wide variety of cells by activating signaling pathways through death receptors (16, 29). Thus, we also tested the drug interactions between TNFα and bortezomib. By itself, TNFα (20 ng/ml) had modest cytotoxic effects on AD LNCaP and LAPC4 cells, as measured by the MTT assay, but no significant effect on AI CL1 and DU145 cell lines (data not shown). Combinations of TNFα and bortezomib demonstrated similar interactions by median effect analysis as TRAIL and bortezomib, although the synergy between TNFα and bortezomib was observed in CL1 cells rather than DU145 cells (Fig. 4). The synergistic interaction between TNFα and bortezomib in CL1 cells was of borderline statistical significance ($P = 0.08$).

Because the effects of drug interactions may be schedule dependent, we studied the effects of varying the duration of preincubation with bortezomib. In the experiments described above, cells were exposed to bortezomib for 90 min before the addition TRAIL or TNFα. When we used CL1 cells to study the effects of extending the preincubation period to 24 h, we did not observe any difference in the drug interaction profiles between bortezomib and either TRAIL or TNFα (data not shown). In addition, reversing the sequence of drugs by adding TRAIL or TNFα for 24 h before bortezomib did not affect the drug interaction data (data not shown).

Bortezomib Does Not Sensitize Prostate Cancer Cells to Cytotoxic Chemotherapy. We studied the interactions between bortezomib and cytotoxic chemotherapeutic agents (doxorubicin, paclitaxel, and vinblastine) used in the treatment of prostate cancer patients and their potential interaction with bortezomib. Paclitaxel and vinblastine as single agents were significantly more cytotoxic than doxorubicin (Table 2 and Fig. 5). When we assessed the effects of drug combinations by median effect/CI analysis, there were no consistent interactions for any of the chemotherapeutic agents and bortezomib (Fig. 6). None of the drugs displayed synergy across the many concentrations tested. As described for TRAIL and TNFα, neither a more prolonged preincubation with bortezomib (24 h *versus* 90

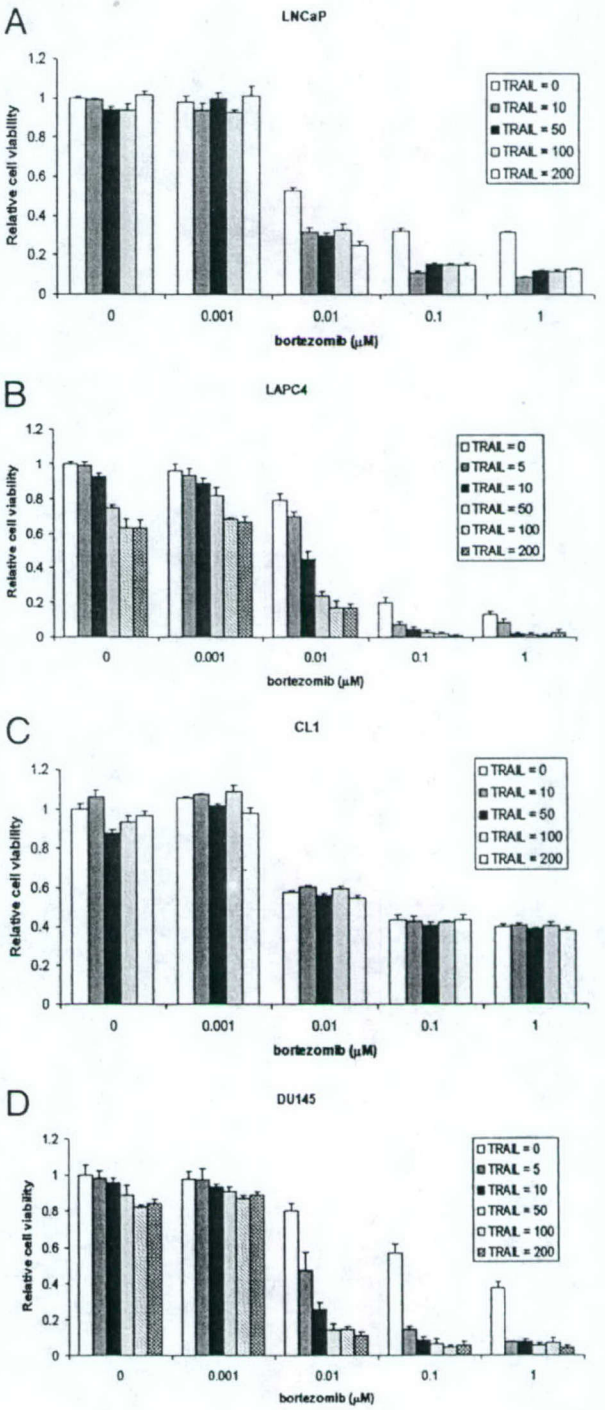

Fig. 3 Cytotoxicity of combinations of TRAIL or TNFα and bortezomib in AD and AI prostate cancer cells. Prostate cancer cells were plated in the 96-well format and incubated overnight. TRAIL or TNFα alone or in combination with bortezomib or appropriate vehicle controls were added at the indicated concentrations for 48 h, and cell viability was measured by the MTT assay. For drug combinations, bortezomib was added 90 min before TRAIL. Experiments were performed in quadruplicate and are reported as means +/− SD. *A*, LNCaP; *B*, LAPC4; *C*, CL1; *D*, DU145.

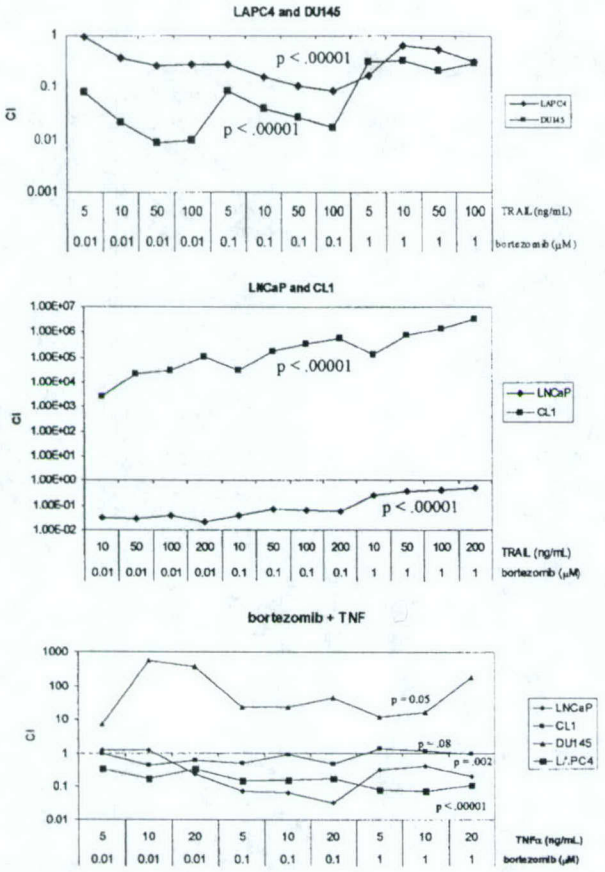

Fig. 4 Drug interactions between TRAIL or TNFα and bortezomib. Data were analyzed by the median effect/CI method (see "Materials and Methods" for details). CI values >1 indicate antagonistic effect, CI values <1 indicate synergy, and CI values ≅1 indicate an additive effect. Note the logarithmic scales. *P*s are two tailed and represent differences between all CI values and 1.

Table 2 IC_{50} values (nM) for chemotherapy

	CL1	DU145	LNCaP	LAPC4
Doxorubicin	1.2×10^5	1.5×10^4	9.1×10^3	2.9×10^4
Paclitaxel	32	5.6×10^3	1.5×10^2	1.5×10^2
Vinblastine	22	0.08	93	58

min) before chemotherapy treatment nor reversing the order with which we added the chemotherapeutic agents and bortezomib influenced the cytotoxicity or median effect analysis of drug interactions (data not shown).

The Relationship between NF-κB Activation and Effects of Bortezomib Alone or in Combination with other Cytotoxic Agents. Inhibition of NF-κB has been postulated as a mechanism of action of bortezomib. We assayed NF-κB activation by EMSA in CL1 cells and found that a concentration of 10 μM bortezomib was required to inhibit basal NF-κB activation (Fig. 7*A*). Modest reduction in TNFα-induced NF-κB activation was observed at 0.25 μM, and further, but not complete, inhibition was observed at a concentration of up to 10 μM

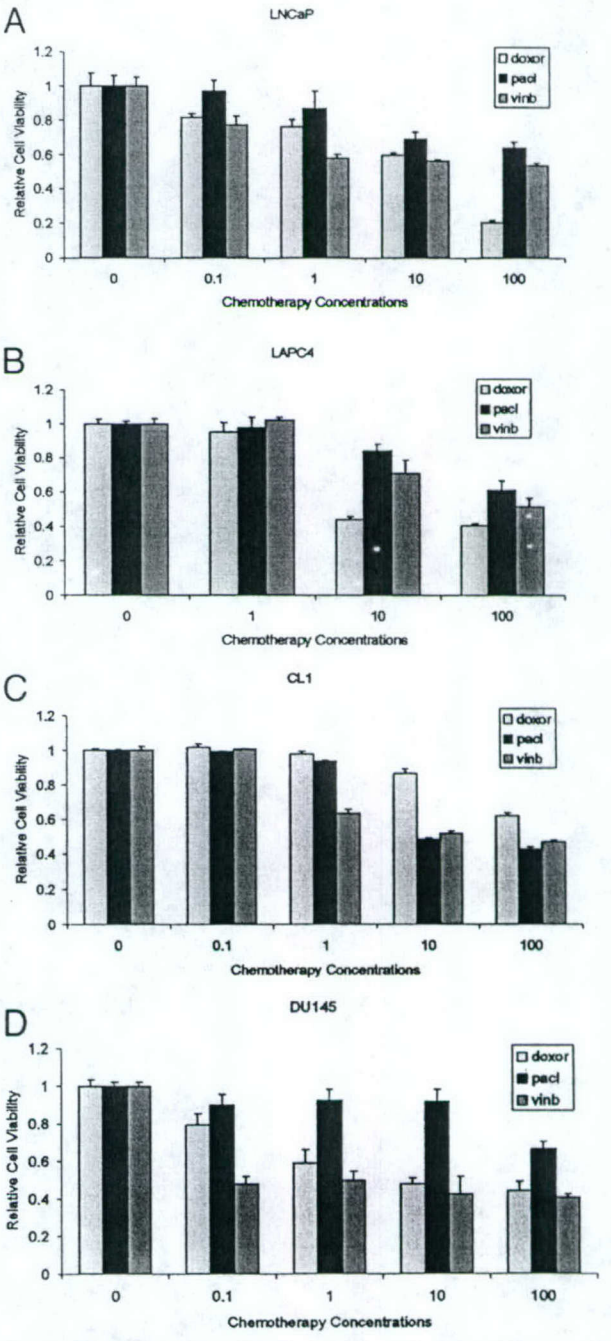

Fig. 5 Cytotoxicity of combinations of chemotherapy and bortezomib in AD and AI prostate cancer cells. Prostate cancer cells were plated in the 96-well format and incubated overnight. Chemotherapy (*doxor*, doxorubicin; *pacl*, paclitaxel; *vinb*, vinblastine), bortezomib, or appropriate vehicle controls were added at the indicated concentrations for 48 h, and cell viability was measured by the MTT assay. For drug combinations, bortezomib was added 90 min before the indicated chemotherapeutic agent. Experiments were performed in quadruplicate and are reported as means +/− SD. Units of concentration are nanomoles for paclitaxel and vinblastine and micromolars for doxorubicin. *A*, LNCaP; *B*, LAPC4; *C*, CL1; *D*, DU145.

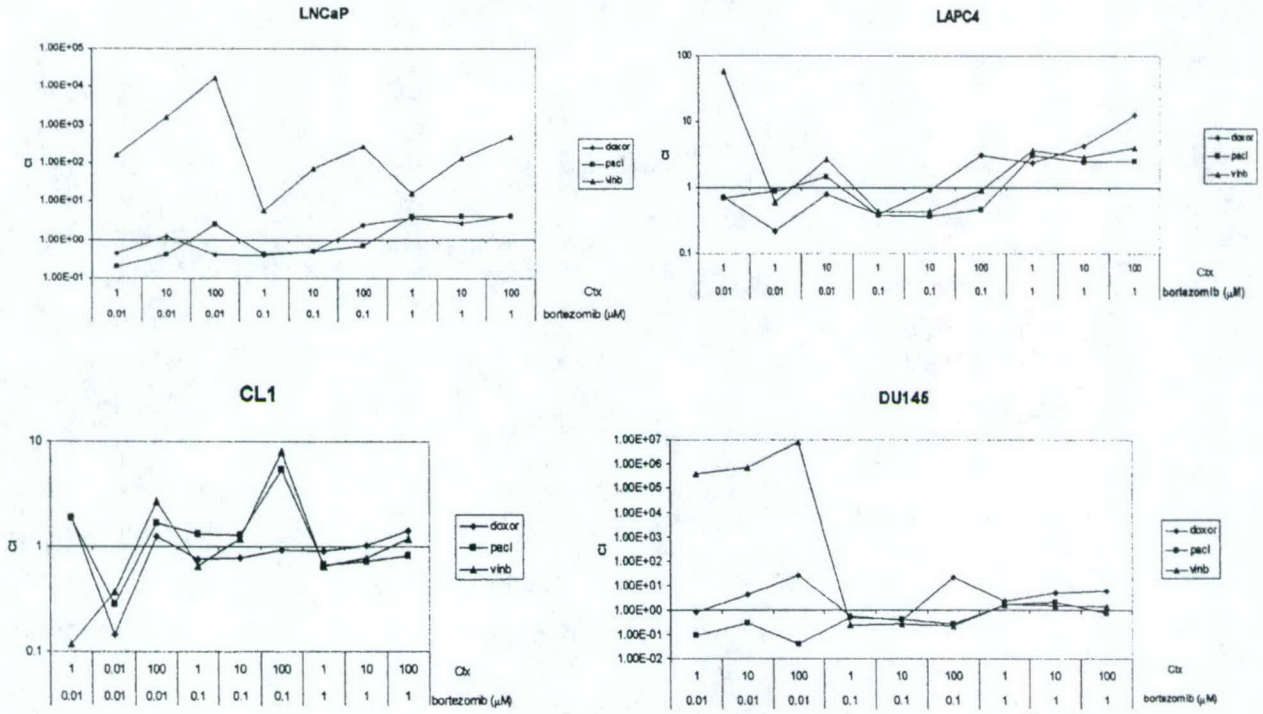

Fig. 6 Drug interactions between chemotherapy and bortezomib. CI values for combinations of various chemotherapeutic agents and bortezomib were determined. Note the logarithmic scales. Units of concentration are nanomoles for paclitaxel and vinblastine and micromolars for doxorubicin.

bortezomib (Fig. 7*A*). Similar results were obtained for all other cell lines (data not shown). The bandshift pattern was characterized with the addition of various antibodies to the EMSA reaction and demonstrated that the NF-κB protein complexes consisted of a p65/p50 heterodimer and a p50/p50 homodimer (Fig. 7*B*). We also used a reporter gene assay to assess bortezomib-mediated inhibition of basal NF-κB activity. Bortezomib induced partial blockade of basal κB-driven reporter gene expression at 0.1 μM and complete inhibition at 10 μM (Fig. 7*C*). Given that the IC_{50} of bortezomib is 0.42 μ M in CL1 cells, there is a good correlation between the concentrations of bortezomib required to induce cytotoxicity and inhibit NF-κB.

We next investigated the importance of heightened NF-κB activation induced by apoptotic stimuli as a determinant of sensitivity to bortezomib. Fig. 8 shows the effects of various apoptotic stimuli on activation of NF-κB in DU145 cells. We demonstrated that neither chemotherapy nor TRAIL activated NF-κB, whereas TNFα did augment NF-κB activity. Similar results were obtained for the other cell lines (data not shown). Thus, given the aforementioned drug interactions with bortezomib, there does not seem to be a correlation between the ability of an apoptotic stimulus to activate NF-κB and to synergize with bortezomib.

DISCUSSION

Proteasome inhibition has been demonstrated to be an effective antitumor agent for prostate cancer both *in vitro* and in mouse models (7, 12, 30, 31). In this study, we evaluated the potential synergistic effects of the proteasome inhibitor bortezomib alone and in combination with various apoptotic stimuli. Our results demonstrate that bortezomib was synergistic with TRAIL and TNFα, but chemotherapeutic agents had no consistent effect. We have shown that bortezomib is a potent apoptotic stimulus in LNCaP and DU145 cells, as described previously (7, 32), as well as the LAPC4 and CL1 prostate cancer cell lines. Interestingly, the synthetic androgen R1881, which blocks apoptosis induced by Fas activation and TNFα (25), did not prevent bortezomib-mediated apoptosis. This suggests that bortezomib may not require androgen deprivation to achieve its maximal effect in patients with prostate cancer.

The concentrations of bortezomib required to inhibit NF-κB correlated with those required to induce cytotoxicity. In addition, the IC_{50} values for bortezomib were substantially higher for AI, which manifest significantly greater basal NF-κB activity compared with their AD counterparts (19, 20, 33, 34). These latter results indicate that NF-κB activation status may represent one factor that predicts for sensitivity to bortezomib. However, many other factors are likely to be involved, especially given the understanding that there are a multitude of differences in the biochemical and gene expression profiles of AD and AI prostate cancer cells and that bortezomib affects the degradation of a multitude of proteins that regulate proliferation and apoptosis.

TRAIL is a death receptor ligand that effectively induces apoptosis in a wide variety of tumor types, although the studies in prostate cancer have yielded variable results (13, 35–37). TRAIL seems to spare normal tissues from its apoptotic effects, although hepatotoxicity caused by TRAIL has been noted when TRAIL is synthesized with an epitope tag for the purpose of

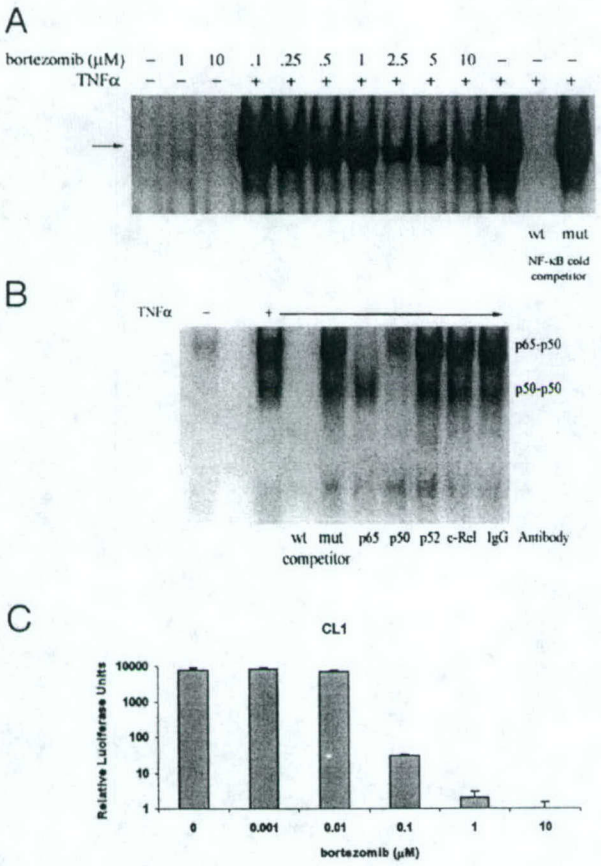

Fig. 7 Bortezomib inhibits both basal and TNFα-induced NF-κB activation. *A*, EMSA for NF-κB activity. CL1 cells (5×10^7 cells) were plated in 150-mm dishes and incubated overnight. Cells were then pretreated with bortezomib or vehicle control for 90 min before the addition of TNFα (20 ng/ml) for 30 min. Nuclear protein was then harvested for EMSA. Cold competition experiments were performed with a 100-fold molar excess of cold wild-type or mutant κB probes. *B*, EMSA on CL1 cells. Cells were plated as in *A* but treated with TNFα or vehicle control only. EMSA was performed as in A, but nuclear extracts were preincubated with the indicated antibodies. Note that the p65 and p50 antibodies bind to the DNA-binding domains of the p65 and p50, respectively, and consequently cause abrogation of the shifted band rather than a supershift. *C*, NF-κB reporter gene assay. CL1 cells were transfected with the p4x-κB-luc reporter construct (and pRL-SV40 for normalization of transfection efficiency). After 24 h, cells were treated with bortezomib at the indicated concentrations. After an additional 24 h, Dual Luciferase assays were performed. Experiments were performed in triplicate and are reported as means +/− SD.

purification (38, 39). Recombinant TRAIL produced without an epitope tag has been successfully administered to animals, including mice and primates, without significant systemic toxicity (38, 39). Because of the promise of both TRAIL and bortezomib as single antitumor agents, we tested drug interactions between these compounds. We found TRAIL and bortezomib synergize to induce cytotoxicity in LNCaP, LAPC4, and DU145 cells across many concentrations. The synergistic interaction was quite significant for LAPC4, LNCaP, and DU145, as exemplified by the fact that the combination of TRAIL and bortezomib induced >90% cytotoxicity at concentrations that induced minimal cytotoxicity with either drug alone. Moreover, because synergy was observed in AD (LNCaP and LAPC4) and AI (DU145) cell lines, hormone-dependency status does not seem to be a predictor for synergistic interactions between TRAIL and bortezomib. However, given that TRAIL and bortezomib may be antagonistic in some cell prostate cancer cells (*i.e.*, CL1 cells), there must be molecular and/or biochemical predictors for synergy between TRAIL and bortezomib.

Similar to TRAIL, synergistic interactions between bortezomib and TNFα were observed for AD cell lines. In addition, the combination of bortezomib and TNFα demonstrated modest synergy in CL1 cells, whereas bortezomib and TRAIL potently synergized in DU145 cells. The discrepancy in synergy between bortezomib and these two death ligands in DU145 and CL1 cells cannot be attributed to differences in NF-κB activation, because both cell lines manifested similar baseline and induced NF-κB activation. It is possible that the ability of TNFα and TRAIL to activate the extrinsic caspase cascade via binding to their respective cellular receptors varies among different cell lines.

When bortezomib was used in combination with cytotoxic chemotherapeutic agents (*i.e.*, doxorubicin, paclitaxel, and vinblastine) that are commonly used in the treatment of patients with prostate cancer, we did not observe any consistent synergistic interactions. We rigorously assessed the effects of these drug interactions with the use of median effect/CI analysis. These drug interactions observed in prostate cancer are in contradistinction to the synergistic interaction between bortezomib and cytotoxic chemotherapy in colon cancer (12). Interestingly, a synergistic interaction between bortezomib and chemotherapy in colon cancer was observed for SN38, the active metabolite of the topoisomerase I inhibitor irinotecan, which activates NF-κB in colon cancer cells (21). However, none of the chemotherapeutic agents we tested augmented NF-κB activity in prostate cancer cells. Given that NF-κB inhibition represents a putative mechanism of action of bortezomib, the discrepancy in the drug interactions between bortezomib and chemotherapy in colon and prostate cancer may, thus, reflect the difference in the ability of chemotherapy to induce NF-κB in these tumor models and/or that resistance to chemotherapy in prostate cancer is mediated by biochemical pathways other than NF-κB. In addition, we excluded the possibility that the outcome of our drug interaction studies were the result of the scheduling of drug exposure. In particular, neither a more prolonged preincubation with bortezomib (24 h *versus* 90 min) nor reversing the order with which we added the bortezomib and the other agents influenced the cytotoxicity or median effect analysis of drug interactions.

In summary, bortezomib is active in AD and AI prostate cancer cell lines, although AD cells, which have lower levels of basal NF-κB activity, seem to be more sensitive to proteasome inhibition. In addition, androgen does not protect prostate cancer cells from bortezomib. No consistent interactions were demonstrated between bortezomib and cytotoxic chemotherapeutic agents, including paclitaxel, doxorubicin, and vinblastine. Bortezomib synergizes with TRAIL and TNFα to inhibit growth of prostate cancer cells. Although TNFα causes major toxicity when administered systemically to animals, TRAIL has been given safely to animals (38, 39). Thus, bortezomib and TRAIL represent a drug combination that should be explored in *in vivo* models.

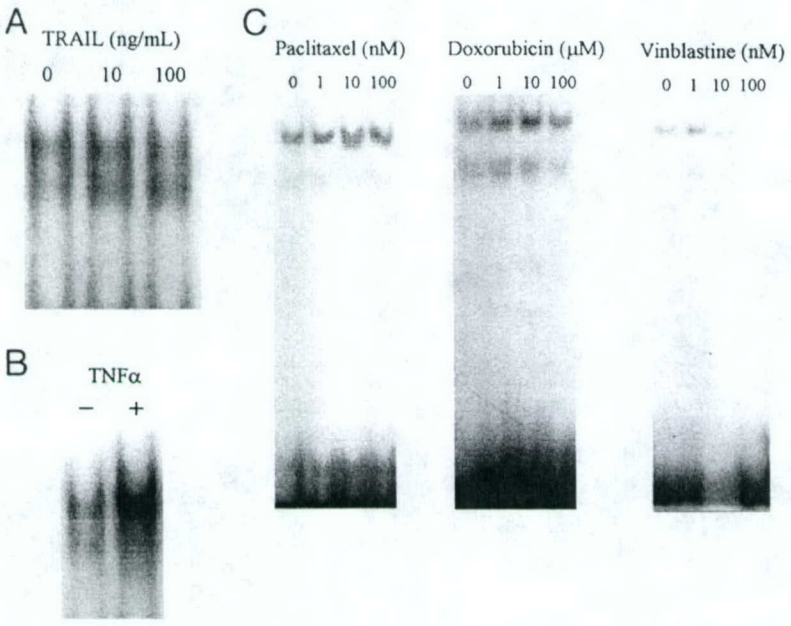

Fig. 8 Effects of various apoptotic stimuli on NF-κB activity in DU145 cells. DU145 cells (3×10^7) were plated in 10-cm dishes and incubated overnight. After treatment with the indicated agents, nuclear protein was harvested and EMSAs were performed. *A*, TRAIL was added at the indicated concentrations for 30 min. *B*, TNFα (20 ng/ml) was added for 30 min. *C*, chemotherapeutic agents were added for 1 h before extraction of nuclear protein. Similar results were obtained when cells were treated with the indicated chemotherapeutic agents for 24 h.

ACKNOWLEDGMENTS

We are grateful to Drs. Mark Pegram and Gottfried Konecny for assistance in median effect/combination index analyses.

REFERENCES

1. Sudakin, V., Ganoth, D., Dahan, A., Heller, H., Hershko, J., Luca, F. C., Ruderman, J. V., and Hershko, A. The cyclosome, a large complex containing cyclin-selective ubiquitin ligase activity, targets cyclins for destruction at the end of mitosis. Mol. Biol. Cell, *6:* 185–197, 1995.

2. Pagano, M., Tam, S. W., Theodoras, A. M., Beer-Romero, P., Del Sal, G., Chau, V., Yew, P. R., Draetta, G. F., and Rolfe, M. Role of the ubiquitin-proteasome pathway in regulating abundance of the cyclin-dependent kinase inhibitor p27. Science (Wash. DC), *269:* 682–685, 1995.

3. Palombella, V. J., Rando, O. J., Goldberg, A. L., and Maniatis, T. The ubiquitin-proteasome pathway is required for processing the NF-κB1 precursor protein and the activation of NF-κB. Cell, *78:* 773–785, 1994.

4. Maki, C. G., Huibregtse, J. M., and Howley, P. M. *In vivo* ubiquitination and proteasome-mediated degradation of p53(1). Cancer Res., *56:* 2649–2654, 1996.

5. Treier, M., Staszewski, L. M., and Bohmann, D. Ubiquitin-dependent c-Jun degradation in vivo is mediated by the delta domain. Cell, *78:* 787–798, 1994.

6. Ciechanover, A., and Schwartz, A. L. The ubiquitin-proteasome pathway: the complexity and myriad functions of proteins death. Proc. Natl. Acad. Sci. USA, *95:* 2727–2730, 1998.

7. Frankel, A., Man, S., Elliott, P., Adams, J., and Kerbel, R. S. Lack of multicellular drug resistance observed in human ovarian and prostate carcinoma treated with the proteasome inhibitor PS-341. Clin. Cancer Res., *6:* 3719–3728, 2000.

8. Adams, J., Palombella, V. J., Sausville, E. A., Johnson, J., Destree, A., Lazarus, D. D., Maas, J., Pien, C. S., Prakash, S., and Elliott, P. J. Proteasome inhibitors: a novel class of potent and effective antitumor agents. Cancer Res., *59:* 2615–2622, 1999.

9. Sutherland, R. M. Cell and environment interactions in tumor microregions: the multicell spheroid model. Science (Wash. DC), *240:* 177–184, 1988.

10. Olive, P. L., and Durand, R. E. Drug and radiation resistance in spheroids: cell contact and kinetics. Cancer Metastisis Rev., *13:* 121–138, 1994.

11. Herrmann, J. L., Briones, F., Jr., Brisbay, S., Logothetis, C. J., and McDonnell, T. J. Prostate carcinoma cell death resulting from inhibition of proteasome activity is independent of functional Bcl-2 and p53. Oncogene, *17:* 2889–2899, 1998.

12. Cusack, J. C., Jr., Liu, R., Houston, M., Abendroth, K., Elliott, P. J., Adams, J., and Baldwin, A. S., Jr. Enhanced chemosensitivity to CPT-11 with proteasome inhibitor PS-341: implications for systemic nuclear factor-κB inhibition. Cancer Res., *61:* 3535–3540, 2001.

13. Yu, R., Mandlekar, S., Ruben, S., Ni, J., and Kong, A. N. Tumor necrosis factor-related apoptosis-inducing ligand-mediated apoptosis in androgen-independent prostate cancer cells. Cancer Res., *60:* 2384–2389, 2000.

14. Nimmanapalli, R., Perkins, C. L., Orlando, M., O'Bryan, E., Nguyen, D., and Bhalla, K. N. Pretreatment with paclitaxel enhances apo-2 ligand/tumor necrosis factor-related apoptosis-inducing ligand-induced apoptosis of prostate cancer cells by inducing death receptors 4 and 5 protein levels. Cancer Res., *61:* 759–763, 2001.

15. Nesterov, A., Lu, X., Johnson, M., Miller, G. J., Ivashchenko, Y., and Kraft, A. S. Elevated AKT activity protects the prostate cancer cell line LNCaP from TRAIL-induced apoptosis. J. Biol. Chem., *276:* 10767–10774, 2001.

16. Muenchen, H. J., Lin, D. L., Walsh, M. A., Keller, E. T., and Pienta, K. J. Tumor necrosis factor-α-induced apoptosis in prostate cancer cells through inhibition of nuclear factor-κB by an IκBα "super-repressor". Clin. Cancer Res., *6:* 1969–1977, 2000.

17. Nakajima, Y., DelliPizzi, A. M., Mallouh, C., and Ferreri, N. R. TNF-mediated cytotoxicity and resistance in human prostate cancer cell lines. Prostate, *29:* 296–302, 1996.

18. Palayoor, S. T., Youmell, M. Y., Calderwood, S. K., Coleman, C. N., and Price, B. D. Constitutive activation of IκB kinase α and NF-κB in prostate cancer cells is inhibited by ibuprofen. Oncogene, *18:* 7389–7394, 1999.

19. Huang, S., Pettaway, C. A., Uehara, H., Bucana, C. D., and Fidler, I. J. Blockade of NF-κB activity in human prostate cancer cells is associated with suppression of angiogenesis, invasion, and metastasis. Oncogene, *20:* 4188–4197, 2001.

20. Chen, C. D., and Sawyers, C. L. NF-κB activates prostate-specific antigen expression and is upregulated in androgen-independent prostate cancer. Mol. Cell. Biol., *22:* 2862–2870, 2002.

21. Cusack, J. C., Jr., Liu, R., and Baldwin, A. S., Jr. Inducible chemoresistance to 7-ethyl-10-[4-(1-piperidino)-1-piperidino]-carbonyloxycamptothe cin (CPT-11) in colorectal cancer cells and a xenograft model is overcome by inhibition of nuclear factor-κB activation. Cancer Res., *60:* 2323–2330, 2000.

22. Das, K. C., and White, C. W. Activation of NF-κB by antineoplastic agents. Role of protein kinase C. J. Biol. Chem., *272:* 14914–14920, 1997.

23. Patel, B. J., Pantuck, A. J., Zisman, A., Tsui, K. H., Paik, S. H., Caliliw, R., Sheriff, S., Wu, L., deKernion, J. B., Tso, C. L., and Belldegrun, A. S. CL1-GFP: an androgen independent metastatic tumor model for prostate cancer. J. Urol., *164:* 1420–1425, 2000.

24. Chou, T. C., and Talalay, P. Quantitative analysis of dose-effect relationships: the combined effects of multiple drugs or enzyme inhibitors. Adv. Enzyme Regul., *22:* 27–55, 1984.

25. Kimura, K., Markowski, M., Bowen, C., and Gelmann, E. P. Androgen blocks apoptosis of hormone-dependent prostate cancer cells. Cancer Res., *61:* 5611–5618, 2001.

26. Wiley, S. R., Schooley, K., Smolak, P. J., Din, W. S., Huang, C. P., Nicholl, J. K., Sutherland, G. R., Smith, T. D., Rauch, C., and Smith, C. A. Identification and characterization of a new member of the TNF family that induces apoptosis. Immunity, *3:* 673–682, 1995.

27. Marsters, S. A., Pitti, R. M., Donahue, C. J., Ruppert, S., Bauer, K. D., and Ashkenazi, A. Activation of apoptosis by Apo-2 ligand is independent of FADD but blocked by CrmA. Curr. Biol., *6:* 750–752, 1996.

28. Pitti, R. M., Marsters, S. A., Ruppert, S., Donahue, C. J., Moore, A., and Ashkenazi, A. Induction of apoptosis by Apo-2 ligand, a new member of the tumor necrosis factor cytokine family. J. Biol. Chem., *271:* 12687–12690, 1996.

29. Wang, C. Y., Mayo, M. W., and Baldwin, A. S., Jr. TNF- and cancer therapy-induced apoptosis: potentiation by inhibition of NF-κB. Science (Wash. DC), *274:* 784–787, 1996.

30. Adams, J. Preclinical and clinical evaluation of proteasome inhibitor PS-341 for the treatment of cancer. Curr. Opin. Chem. Biol., *6:* 493–500, 2002.

31. Hideshima, T., Richardson, P., Chauhan, D., Palombella, V. J., Elliott, P. J., Adams, J., and Anderson, K. C. The proteasome inhibitor PS-341 inhibits growth, induces apoptosis, and overcomes drug resistance in human multiple myeloma cells. Cancer Res., *61:* 3071–3076, 2001.

32. Herrmann, J. L., Briones, F., Jr., Brisbay, S., Logothetis, C. J., and McDonnell, T. J. Prostate carcinoma cell death resulting from inhibition of proteasome activity is independent of functional Bcl-2 and p53. Oncogene, *17:* 2889–2899, 1998.

33. Gasparian, A. V., Yao, Y. J., Kowalczyk, D., Lyakh, L. A., Karseladze, A., Slaga, T. J., and Budunova, I. V. The role of IKK in constitutive activation of NF-κB transcription factor in prostate carcinoma cells. J. Cell Sci., *115:* 141–151, 2002.

34. Suh, J., Payvandi, F., Edelstein, L. C., Amenta, P. S., Zong, W. X., Gelinas, C., and Rabson, A. B. Mechanisms of constitutive NF-κB activation in human prostate cancer cells. Prostate, *52:* 183–200, 2002.

35. Munshi, A., Pappas, G., Honda, T., McDonnell, T. J., Younes, A., Li, Y., and Meyn, R. E. TRAIL (APO-2L) induces apoptosis in human prostate cancer cells that is inhibitable by Bcl-2. Oncogene, *20:* 3757–3765, 2001.

36. Zisman, A., Ng, C. P., Pantuck, A. J., Bonavida, B., and Belldegrun, A. S. Actinomycin D and gemcitabine synergistically sensitize androgen-independent prostate cancer cells to Apo2L/TRAIL-mediated apoptosis. J. Immunother., *24:* 459–471, 2001.

37. Eid, M. A., Lewis, R. W., Abdel-Mageed, A. B., and Kumar, M. V. Reduced response of prostate cancer cells to TRAIL is modulated by NFκB-mediated inhibition of caspases and Bid activation. Int. J. Oncol., *21:* 111–117, 2002.

38. Ashkenazi, A., Pai, R. C., Fong, S., Leung, S., Lawrence, D. A., Marsters, S. A., Blackie, C., Chang, L., McMurtrey, A. E., Hebert, A., DeForge, L., Koumenis, I. L., Lewis, D., Harris, L., Bussiere, J., Koeppen, H., Shahrokh, Z., and Schwall, R. H. Safety and antitumor activity of recombinant soluble Apo2 ligand. J. Clin. Invest., *104:* 155–162, 1999.

39. Lawrence, D., Shahrokh, Z., Marsters, S., Achilles, K., Shih, D., Mounho, B., Hillan, K., Totpal, K., DeForge, L., Schow, P., Hooley, J., Sherwood, S., Pai, R., Leung, S., Khan, L., Gliniak, B., Bussiere, J., Smith, C. A., Strom, S. S., Kelley, S., Fox, J. A., Thomas, D., and Ashkenazi, A. Differential hepatocyte toxicity of recombinant Apo2L/TRAIL versions. Nat. Med., *7:* 383–385, 2001.

[CANCER RESEARCH 63, 2306–2311, May 1, 2003]

Overexpression of Vimentin: Role in the Invasive Phenotype in an Androgen-independent Model of Prostate Cancer[1]

Sadmeet Singh, Skanda Sadacharan, Scott Su, Arie Belldegrun, Sujata Persad, and Gurmit Singh[2]

Hamilton Regional Cancer Centre, Hamilton, Ontario, L8V 5C2 Canada [S. Si., S. Sa., S. Su, S. P., G. S.], and Department of Urology, University of California Los Angeles, Los Angeles, California 90095 [A. B.]

ABSTRACT

The androgen-sensitive LNCaP prostate cancer cell line is less invasive than hormone-insensitive lines. CL1, an aggressive, hormone-insensitive LNCaP subline derived by continuous passaging in hormone-depleted medium, was compared with the parental cell line by cDNA microarray analysis. The gene coding for the intermediate filament protein vimentin was found to be highly up-regulated in the CL1 subline. This difference was confirmed by Northern and Western blots and visualized by immunofluorescence microscopy. To assess the contribution of vimentin to the invasive phenotype, LNCaP cells were stably transfected to overexpress vimentin, and the CL1 cells were transfected with vimentin antisense construct. The invasiveness of the transfected cells was tested using an *in vitro* invasion assay. We were able to demonstrate that decreasing vimentin expression in the constitutively vimentin-expressing CL1 cells led to a significant decrease in their invasiveness but that forcing expression of vimentin in the LNCaP cells did not augment their invasiveness. These findings imply that vimentin expression contributes to the invasive phenotype but cannot confer it alone.

INTRODUCTION

With the advent of prostate-specific antigen testing for prostate cancer, this disease is increasingly being detected at a potentially curable stage. There remain, however, major challenges to the successful management of this, the most commonly diagnosed cancer in men in the Western world. Although the number of men diagnosed with extraprostatic disease is decreasing, a significant proportion of those treated with curative intent go on to develop advanced disease. For these patients, androgen ablation is the mainstay of treatment, and although the initial response rate approaches 80%, most patients demonstrate biochemical or clinical relapse within 18 months (1). Moreover, the heterogeneity of the disease, in which cancer cells within the same patient may have different histological features and metastatic potential, means that outcome after treatment is extremely unpredictable. At a fundamental biological level, very little is known about what makes the disease aggressive in some and relatively indolent in others. The purpose of this study was to elucidate factors making an androgen-independent prostate cancer cell line much more aggressive than the androgen-sensitive line from which it was derived.

The model used compared the androgen-sensitive LNCaP prostate cancer cell line and an aggressive, androgen-independent subline, CL1. The CL1 cell line was derived by continuous subculturing of LNCaP cells in media deprived of androgen by supplementation with charcoal-stripped serum (2). Although a number of molecular characteristics of the CL1 line have been documented, we sought to compare it with the parental line using a limited, human cancer-specific cDNA microarray. Among the differentially expressed genes between the two cell lines, one coding for an intermediate filament cytoskeletal protein, vimentin, was overexpressed 20-fold in the CL1 cells. Among actin filaments, microtubules, and intermediate filaments, the three major classes of cytoskeletal proteins found in eukaryotic cells, intermediate filaments are the most complex (3). There are around 50 types of intermediate filament proteins that are categorized into 5 subtypes, and vimentin belongs to type III.

Having established that vimentin expression was up-regulated in the transition of LNCaP to CL1 cells, our aim was to determine the importance of vimentin expression to the aggressive phenotype of prostate cancer cells. LNCaP cells were stably transfected with a vimentin sense cDNA construct, and CL1 cells were transfected with the corresponding antisense construct. An *in vitro* invasion assay using Matrigel reconstituted basement membrane was then used to test the resulting cell lines.

MATERIALS AND METHODS

Cell Culture. The androgen-responsive human prostate cancer LNCaP and nonresponsive DU145 and PC3 cell lines were obtained from the American Type Culture Collection (Manassas, VA). The MatLyLu anaplastic Dunning rat prostate cancer cell line was a generous gift of Dr. S. A. Rabbani (McGill University, Montreal, Canada). The cell lines were maintained in RPMI 1640 (Life Technologies, Inc.) supplemented with 10% fetal bovine serum (Life Technologies, Inc.), 1% antibiotic-antimycotic solution (Life Technologies, Inc.), 10 mM HEPES, and 1.0 mM sodium pyruvate. The CL1 androgen-independent subline derived from the LNCaP line, a generous gift from Dr. A. S. Belldegrun (University of California Los Angeles Medical School, Los Angeles, CA), was maintained in RPMI 1640 supplemented with 10% charcoal-stripped FBS. Cells were kept at 37°C in a humidified atmosphere with 5% CO_2.

DNA Microarray Analysis. Total RNA was extracted from LNCaP and CL1 cell lines using the Qiagen RNeasy Minikit. Radioactively labeled cDNA probes were created from total RNA and hybridized to Clontech human cancer cDNA nylon arrays containing 588 genes (Clontech, Palo Alto, CA) according to the manufacturer's instructions. After a series of washes, the hybridized membranes were exposed to a phosphorimager plate for 48 h and imaged using the Storm PhosphorImaging system (Molecular Dynamics Inc., Sunnyvale, CA). The signal intensity of each cDNA pair of spots was quantified using ImageQuant software (Amersham Biosciences) by subtracting the local regional background intensity from each spot. The two membranes were normalized to each other by using the signal of housekeeping genes provided.

Northern Blot Analysis. Total RNA was extracted separately for analysis by Northern blot. Ten μg of total RNA were separated on a RNA gel and transferred overnight to a nylon membrane (Boehringer Mannheim). A cDNA probe was created from a 1.1-kb vimentin clone obtained from the American Type Culture Collection (catalogue number 59160). The probe was labeled with [α-^{32}P]dCTP (New England Nuclear, Boston, MA) using the RTS RadPrime DNA Labeling system (Life Technologies, Inc.). The membrane was washed after hybridization, exposed for 48 h to a phosphorimager plate, and imaged using the Storm PhosphorImaging system. The 18S and 28S ribosomal bands were used to assess equal loading of RNA.

Western Blot Analysis. Cells were treated with lysis buffer containing 15% NP40, 5 M NaCl, 2 M Tris base (pH 7.4), and 0.5 M EDTA (pH 8.0). Protein concentrations were determined using the Bio-Rad protein assay. Equal amounts of protein denatured in SDS sample buffer [2% SDS, 62.5 mM Tris base (pH 6.8), 10% glycerol, 5% β-mercaptoethanol, and 0.005% bromphenol blue] were loaded onto 10% SDS-PAGE, and gels were transferred onto nitrocellulose membranes (Amersham Biosciences). Equal loading of protein

Received 10/7/02; accepted 2/20/03.

The costs of publication of this article were defrayed in part by the payment of page charges. This article must therefore be hereby marked *advertisement* in accordance with 18 U.S.C. Section 1734 solely to indicate this fact.

[1] Supported by a grant from the Canadian Institute of Health Research (to G. S.).

[2] To whom requests for reprints should be addressed, at The Hamilton Regional Cancer Centre, 699 Concession Street, Hamilton, Ontario, L8V 5C2 Canada. Phone: (905) 387-9711, ext. 67007; Fax: (905) 575-6330; E-mail: gurmit.singh@hrcc.on.ca.

was confirmed by staining the membrane with Ponceau S (Sigma). The membranes were blocked overnight in Tris-buffered saline containing 5%(w/v) skimmed milk powder, and after a series of washes, blots were stained with the recommended dilution of primary antibodies against vimentin (V9; Santa Cruz Biotechnology, Santa Cruz, CA), anti-CK directed against CK7 and CK8 (Cam 5.2; Becton Dickinson), or β-actin (C2; Santa Cruz Biotechnology). After further washing, the blots were incubated with a 1:1000 dilution of goat antimouse IgG antibody conjugated to horseradish peroxidase (Santa Cruz Biotechnology) and developed using the enhanced chemiluminescence Western blot detection kit (Amersham Biosciences).

Immunofluorescence Microscopy. Cells were seeded on sterile glass coverslips to 50% confluence. After 24 h of attachment, they were fixed at room temperature in 4% paraformaldehyde in PBS for 10 min and then washed three times in PBS. Cells were permeabilized for 10 min in a 0.2% solution of Triton X-100 and blocked in a 1:20 normal goat serum solution (Vector Laboratories, Burlingame, CA). After a series of washes, the coverslips were incubated with primary antibody (1 μg/ml vimentin V9 or 0.5 μg/ml anti-CK Cam 5.2) for 1 h and then washed in PBS. This was followed by a 1-h incubation with Alexa Fluor 488 goat antimouse secondary antibody (Molecular Probes, Eugene, OR). Nuclei were stained by a 10-min incubation with DAPI[3] (Sigma).

Expression Vector Construction. A 1.8-kb vimentin cDNA fragment was excised from the pCMV-SPORT6 phagemid vector supplied by the American Type Culture Collection. This was cloned into the *Kpn*I/*Not*I (sense orientation) and *Eco*RI/*Hin*dIII (antisense orientation) sites of pcDNA3.1 vector (Invitrogen, Carlsbad, CA).

DNA Transfection and Clone Selection. LNCaP cells were transfected with 3 μg of the pcDNA3 vector with the vimentin insert in the sense orientation, and CL1 cells were transfected with the vector containing vimentin in the antisense orientation, according to the protocol supplied with the LipofectAMINE transfection reagent (Life Technologies, Inc.). Briefly, 2×10^5 cells were plated in 6-well dishes and incubated with the appropriate DNA and LipofectAMINE in serum-free media for 5 h, and then equal volumes of media containing 20% FBS were added. At 24 h, the media were replaced with media containing 1 mg/ml G418. Surviving colonies were selected after 2 weeks and then maintained in 350 μg/ml G418 (CL1 cells) or 185 μg/ml G418 (LNCaP cells). Changes in vimentin levels were assayed for by both Western blotting and immunofluorescence microscopy.

Motility and Invasion Assays. Cell motility was assessed using 24-well Biocoat Control Insert Chambers (Becton Dickinson) with polycarbonate filters containing 8-μm pores. Cells were plated at 1.0×10^5 cells/well (LNCaP) and 1.5×10^4 cells/well (CL1) in 0.5 ml of serum-free medium. The outer chambers were filled with 0.5 ml of media containing 10% FBS. After 48 h (LNCaP) or 24 h (CL1), cells migrating to the undersurface of the filters were counted. The top surface of the membrane was gently scrubbed with a cotton bud, and cells on the undersurface were fixed in methanol and stained with H&E before undergoing a series of washes. The same five microscopic fields were used to count the number of cells passing to the undersurface of each filter. For invasion assays, the control insert chambers were replaced with Biocoat Invasion Chambers (Becton Dickinson) containing a Matrigel reconstituted basement membrane layer.

RESULTS

Up-Regulation of Vimentin in CL1 Cells. The derivation of CL1 hormone-refractory prostate cancer cells from the parental hormone-sensitive LNCaP cell line has been described previously (2). The CL1 cells were shown to have an accelerated growth rate, resistance to radiation/cytotoxic anticancer drugs, and highly tumorigenic behavior even in castrated and female mice when compared with the parental cell line. In addition, up-regulation of particular molecules, including interleukin 6, fibroblast growth factor, and vascular endothelial growth factor, associated with aggressive cancer cell lines was sought and observed. Both LNCaP and CL1 cells expressed high levels of the epidermal growth factor receptor, although levels were higher in the CL1 cells. To establish whether other classes of molecules were involved in the acquisition of an aggressive, invasive phenotype, the cells were compared using the Clontech Atlas Human Cancer array. RNA was extracted from both cell lines, and radiolabeled cDNA probes were prepared for hybridization to the arrays. A 10-fold difference in expression was set as the minimum difference to be further investigated. The signal for one gene, vimentin, met this criterion, being overexpressed 20-fold in the CL1 cells with respect to the LNCaP cells. An image of a pair of hybridized cDNA membranes with the site of the cDNA spot for vimentin outlined on the membrane hybridized with CL1 RNA is shown in Fig. 1*A*.

The findings from the microarray were confirmed by Northern and Western analyses as shown in Fig. 1, *B* and *C*. Dual staining of LNCaP and CL1 cells with the vimentin V9 antibody and DAPI for nuclear staining is shown in Fig. 2, *A* and *B*. A network of vimentin intermediate filaments is clearly seen in the CL1 cells, whereas in the LNCaP cells, under the same conditions, only the nuclear staining is visible.

In addition, the expression of vimentin was sought in both DU145 and PC3 androgen-insensitive, invasive human prostate cancer cell lines as well as the MatLyLu rat prostate cancer cell line. High levels of vimentin in comparison with those seen in LNCaP cells are shown by Western analysis in Fig. 1*C*. Immunocytochemical staining of these cells (Fig. 2, *G*–*I*) demonstrates a dense network of vimentin filaments, similar to that seen in CL1 cells.

CK Distribution in LNCaP and CL1 Cells. Earlier reports of vimentin expression in invasive breast cancer cell lines have suggested that coexpression of vimentin and CK intermediate filaments is necessary to confer the invasive phenotype (3). Cells of epithelial origin would be expected to express CK intermediate filaments (3). A Western blot (Fig. 3) comparing amounts of CK7 and CK8 in the CL1 and LNCaP cells demonstrates higher levels in the LNCaP cells, although immunofluorescence microscopy (Fig. 2, *C* and *D*) shows that both cell lines do have a network of CK filaments.

Stable Transfection of Sense and Antisense Vimentin Constructs. Three clones of LNCaP cells transfected with the vimentin sense vector and four clones of CL1 cells transfected with the antisense vector were established by ring cloning. Protein levels of vimentin in the clones were assayed for by Western blot as well as by immunofluorescence microscopy. The CL1 clone that demonstrated the lowest level of vimentin expression by Western blot

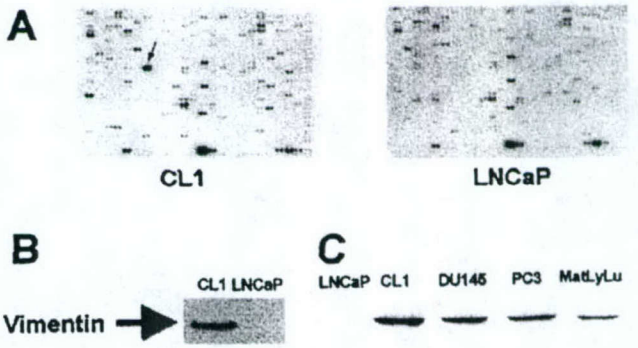

Fig. 1. CL1 cells express higher levels of vimentin than the parental LNCaP cells. *A*, a pair of hybridized Atlas Human Cancer Array cDNA membranes. The site of the cDNA spot for vimentin is shown by an *arrow* on the membrane hybridized with RNA from CL1 cells. The signal intensity of the vimentin cDNA spot on the CL1 membrane was 20 times that seen on the LNCaP membrane. *B*, Northern blot comparing vimentin expression in CL1 and LNCaP cells. Equal loading of RNA was confirmed by staining of 28S and 18S ribosomal bands. *C*, Western blot comparing levels of vimentin in LNCaP cells with levels of vimentin in CL1, DU145, PC3, and MatLyLu cells. Equal loading of protein was confirmed by staining the blot with Ponceau S stain.

[3] The abbreviations used are: DAPI, 4′,6-diamidino-2-phenylindole-2HCl; EMT, epithelial-mesenchymal transition; ER, estrogen receptor; CK, cytokeratin.

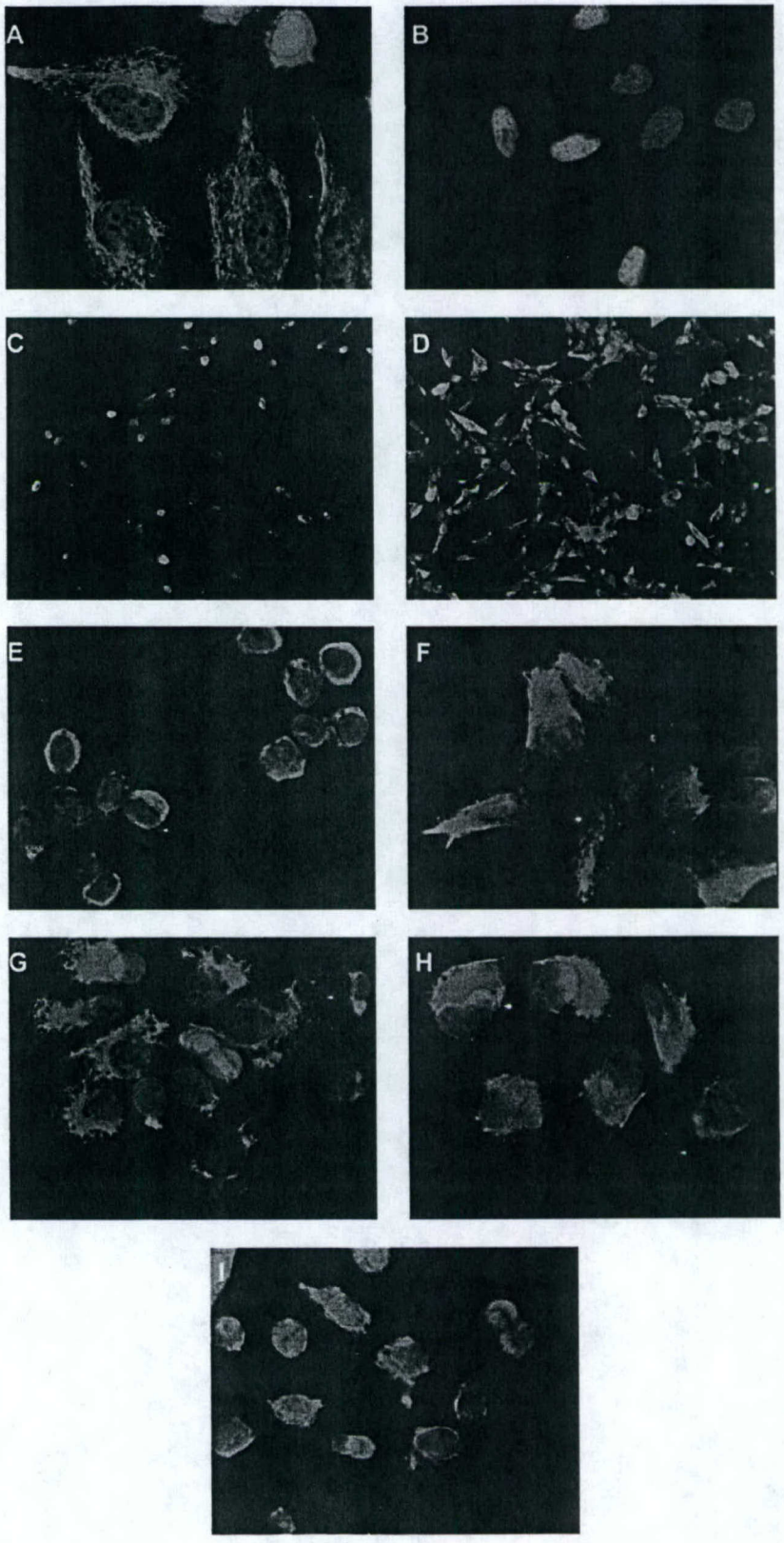

Fig. 2. Immunocytochemical staining with vimentin V9 antibody. *A*, distribution of vimentin in CL1 cells. *B*, distribution of vimentin in LNCaP cells. *Blue*, nuclear staining with DAPI. A dense network of vimentin intermediate filaments is seen in the CL1 cells, whereas under the same conditions, only nuclear staining is seen in LNCaP cells. *C* and *D*, immunocytochemical staining of CL1 (*C*) and LNCaP (*D*) cells with Cam 5.2 anti-CK primary antibody. CK is seen in the CL1 cells, although a denser network of filaments is observed in LNCaP cells. *E*, decreased vimentin distribution and altered morphology in CL1-AS4 cells. *F*, vimentin network seen in LNCaP-S2 cells. DU145 (*G*), PC3 (*H*), and MatLyLu (*I*) cells demonstrating vimentin cytoskeleton.

(Fig. 4*A*) is designated CL1-AS4. These cells have a rounded morphology and loss of discrete vimentin filaments (Fig. 2*E*) when compared with the wild-type cells (Fig. 2*A*). Increased expression in the LNCaP clone with the highest levels of vimentin expression is shown by Western blot in Fig. 4*B*. This is demonstrated most graphically by immunofluorescence microscopy in Fig. 2*F*. Vimentin filaments that are not identifiable in the wild-type cells are clearly seen here.

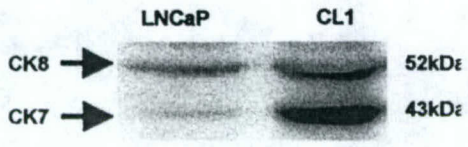

Fig. 3. Comparison of CK expression in CL1 and LNCaP cells. Western blot was detected with Cam 5.2 antibody. CK7 and CK8 bands are demonstrated at higher levels in the LNCaP cells.

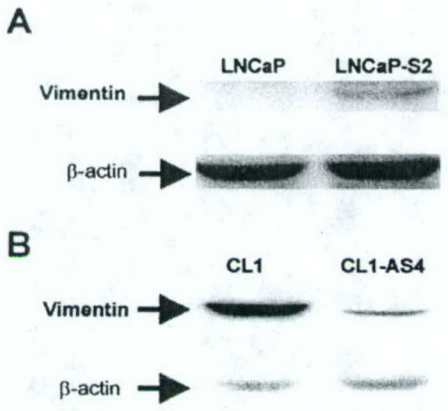

Fig. 4. Vimentin levels in stably transfected cells. *A*, CL1 cells and CL1-AS4 clone transfected with vimentin antisense vector. *B*, LNCaP and LNCaP-S2 clone transfected with sense vimentin vector.

Motility and Invasive Potential of Wild-type Cells Compared with Transfected Cells. The motility of cells was tested by counting the number of cells passing through an uncoated filter containing 8-μm pores in response to a serum gradient. To test invasive potential, a similar assay was performed with filters coated with reconstituted basement membrane (Matrigel). The motility and invasion assays were carried out on three filters for each cell line, and cells were counted from the same five fields of each filter under $\times 200$ magnification. Growth curves comparing wild-type with transfected cells showed no difference in proliferation over the time course during which the assays took place (data not shown). Fig. 5*A* shows the motility of the wild-type and transfected cell lines represented as the mean number of cells counted on the undersurface of each filter per field counted. The motility of the transfected cells is not altered with respect to the wild-type cells under these conditions. The invasion assay data are presented in Fig. 5*B*. It is clear that in the CL1-AS4 cells, with decreased expression of vimentin, invasion through the Matrigel reconstituted basement membrane is effectively abolished ($P < 0.001$). However, when the wild-type LNCaP cells were compared with the transfected clone demonstrating the highest levels of vimentin (LNCaP-S2), no increase in invasive potential was seen. Both cell lines were unable to invade through the Matrigel membranes in appreciable numbers over the 48-h period in which the assay was carried out.

DISCUSSION

The aim of this study was to identify factors involved in the conversion of noninvasive, hormone-dependent prostate cancer to aggressive, hormone-independent cancer. The model used was an *in vitro* analogue of the situation seen during prostate cancer treatment, in which initially successful therapeutic hormone deprivation is followed by unresponsive, highly invasive disease. To identify differentially expressed genes, a cDNA hybridization analysis of 588 well-characterized genes covering a broad range of cellular functions was used. Other investigators have used microarrays bearing thousands of genes to compare prostate cancer cell lines and RNA from tissue samples to search for genetic differences (4–6). Our approach was directed at establishing differences emerging specific to the process of hormone deprivation and their effect on the invasive potential of prostate cancer cells. Given the heterogeneity of prostatic biopsy samples and the great differences between even cell lines established from the same organ, this targeted approach is valid. The gene demonstrating the greatest differential expression between the cell lines, vimentin, was selected for further study.

Early work suggested that the expression of intermediate filament proteins was tissue type specific, with normal and tumor tissue expressing a single class of intermediate filament (7). In this context, vimentin is considered to be the intermediate filament of mesenchymal tissue (8), and as such, it has been used as a tumor marker in the diagnosis of melanoma (9). Epithelial tissues and tumors have traditionally been characterized by their CK expression (10). However, coexpression of both vimentin and CK intermediate filaments has been shown in prostate cancer (11) and a variety of other tumor cell lines and tissues (12–15).

The coexpression of vimentin and CKs has been strongly associated with a more aggressive and metastatic phenotype in breast cancer. Data from breast cancer cell lines have demonstrated that ER-negative, aggressively behaving cell lines express vimentin, whereas ER-positive, noninvasive cell lines do not (13). In an immunohistochemical analysis of breast cancer specimens (16), vimentin immunopositivity was inversely related to keratin and ER expression but positively correlated to tumor

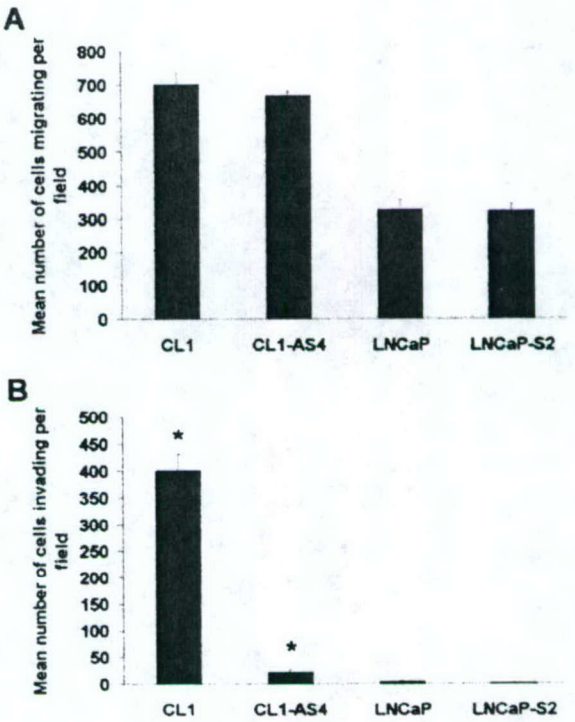

Fig. 5. Motility and invasion assays. In both assays, 1.5×10^4 CL1/CL1-AS4 and 1.0×10^5 LNCaP/LNCaP-S2 cells were seeded per filter. Assays in CL1/CL1-AS4 cells were carried out over 24 h, and assays in LNCaP/LNCaP-S2 cells were carried out over 48 h. *A*, motility assay represented by numbers of cells counted per field passing through uncoated 8-μm filter. *Error bars*, SE. Motility was not affected by transfection of antisense vimentin or vimentin in CL1 or LNCaP cells, respectively. *B*, invasion assay represented by numbers of cells passing through Matrigel-coated filters. Invasive potential significantly decreased in CL1-AS4 cells with respect to CL1 wild-type cells (*, $P < 0.001$, Student's t test). LNCaP-S2 cells remained unable to invade through Matrigel-coated membrane.

grade. Tumors in which vimentin and CKs were expressed in approximately similar amounts were those with the worst prognosis. Coexpression of keratins and vimentin is also associated with recurrent and metastatic disease in melanoma (15).

Our data demonstrate an increase in vimentin expression of the CL1 cells accompanied by a decrease in the levels of CKs. This type of change in the expression profile of intermediate filaments in epithelial cells is referred to as EMT. This transition of cell phenotype occurs physiologically during normal developmental processes that require cell migration and extracellular matrix invasion and during wound healing (17). EMT is now becoming well recognized as a hallmark of tumor progression, characterizing invasive and metastatic carcinomas (18). As well as a switch from CK to vimentin intermediate filament expression, EMT involves a reduction in expression of cell adhesion molecules, particularly E-cadherin. It has been proposed that EMT represents a permanent switch in certain tumors (19), and this was the finding in mammary epithelial cells that underwent EMT in response to transfection with the matrix metalloproteinase stromelysin 1 (20). This is consistent with the finding that the transition in phenotype undergone by CL1 cells is not reversible by replacing the charcoal-stripped serum in which they grow with untreated FBS (2).

Data to show that vimentin expression in prostate cancer is associated with a more aggressive phenotype have been contradictory. Our data confirm the findings of previous studies in which the phenotypes of prostate cancer cell lines have been examined and in which LNCaP cells show low levels of vimentin expression in contrast to the high expression seen in their more aggressive DU145 and PC3 counterparts (21, 22). In a differential hybridization analysis of rat prostate carcinoma sublines from the Dunning model, a protein with 96% homology to human vimentin was found to be highly expressed in all of the hormone-independent, anaplastic tumors. Its expression was very low in normal prostate and in the well- or moderately differentiated Dunning sublines. Our results using the anaplastic MatLyLu cells, the most aggressive of the Dunning sublines, corroborate these data. This finding was similar to that of the earlier study of breast cancer cell lines, in which hormone receptor status and invasiveness were considered with vimentin expression (13). A subsequent immunohistochemical study of 15 cases of tumor and 49 cases of nodular hyperplasia found vimentin expression in both tissues, but no correlation could be made between vimentin expression and tumor grade (23). This led to the conclusion that vimentin expression could not be used to help distinguish high-grade from low-grade tumors. However, a recent, more elaborate study concerned with factors associated with motility in prostate cancer cell lines and poorly differentiated metastatic prostate cancer did point to the importance of vimentin expression in prostate cancer (24). Here it was reported that among a number of adhesion molecules, cytoskeletal elements, and prostate-specific markers, vimentin expression alone correlated with motility of prostate cancer cell lines. However, levels of vimentin expression did not necessarily correlate with invasiveness in all of the cell lines tested. Immunohistochemical studies showed that vimentin expression was found in poorly differentiated prostatic tumors and in prostate tissue from patients with metastatic disease identified by bone scan. In addition, bone metastases resulting from prostate cancer were analyzed, and the majority of these were shown to stain positively for vimentin.

Having established that vimentin expression was barely detectable in LNCaP cells and highly expressed in the faster-growing and more aggressive CL1 subline, we wanted to assess the contribution of vimentin to the invasive phenotype. We found that experimentally reducing the expression of vimentin in the CL1 cell line effectively abolished the invasive potential of CL1 cells in the *in vitro* Matrigel invasion assay. In experiments conducted with breast cancer cell lines (3), transient down-regulation of vimentin in MDA-MB-231 cells led to a decrease in their migratory ability that the authors considered to be indicative of decreased metastatic potential. The MDA-MB-231 cell line shares characteristics of the CL1 cell line in that both constitutively coexpress vimentin and CKs and are unresponsive to hormonal stimulation.

When vimentin expression was forced in LNCaP cells by stable transfection, we were not able to observe acquisition of an invasive phenotype using the Matrigel invasion assay. Similar experiments conducted in the MCF-7 breast cancer cell line have produced controversial results. This cell line, like the LNCaP cell line (25, 26), does not constitutively express vimentin, is hormone sensitive, and has a slow growth pattern in nude mice (27). Sommers *et al.* (28) were unable to increase the invasiveness of MCF-7 cells by stable transfection with vimentin, whereas Hendrix *et al.* (3), using a different expression vector and experimental conditions, were able to increase the invasive and tumorigenic potential in *in vitro* assays. However, artificial expression of vimentin in these cells was not sufficient to confer the metastatic phenotype of MDA-MB-231 cells when they were inoculated into severe combined immunodeficient (SCID) mice.

The immunohistochemical studies of vimentin in prostate cancer to date have been performed with a view to evaluating its expression as a marker for aggressive or metastatic disease. Although vimentin itself may not be the marker that investigators had hoped for, the experimental evidence surrounding vimentin and other intermediate filament proteins indicates that this is an important field in prostate cancer tumor biology and the development of metastases. The finding that vimentin expression is up-regulated in this model of androgen-deprived prostate cancer cells, in the hormone-refractory Dunning rat prostate cancer sublines (29), and in ER-negative breast cancer cell lines (13) raises the issue of its influence in the aggressiveness of hormone-independent disease. Recently, in a study considering the role of vimentin as a tool for cellular immortalization, 1757 bp of the human vimentin promoter were sequenced (30). Androgen response elements were not among the transcription factor binding sites identified, so it would seem that the effect of hormonal regulation on vimentin expression is an indirect one.

There is growing evidence that the extracellular matrix can regulate gene expression and that it does this via certain cell surface integrin receptors (31, 32). Importantly, intermediate filaments including vimentin seem to act as mechanical transducers between cell surface integrins and nuclei (33, 34). Furthermore, the finding that inappropriate expression of intermediate filament proteins may be involved in the conference of drug resistance (35) is of great relevance to the treatment of advanced, metastatic disease.

Our data, like those of others presented in different tumor types, suggest that constitutive coexpression of vimentin with CK in prostate cancer cell lines is associated with an invasive phenotype that can be reversed by reducing vimentin expression. However, it would seem that vimentin is likely to function with other proteins or is likely to act in one of the later stages in the invasion process, given the results seen in the LNCaP-S2 cells and previous data obtained from breast cancer cell lines (28). Additional studies to establish the function and interactions of vimentin in prostate cancer, particularly with regard to advanced, metastatic, and hormone-refractory disease, are warranted.

REFERENCES

1. Turkes, A. O., and Griffiths, K. Endocrine treatment of prostate cancer. Prog. Med. Chem., *26:* 299–321, 1989.
2. Tso, C. L., McBride, W. H., Sun, J., Patel, B., Tsui, K. H., Paik, S. H., Gitlitz, B., Caliliw, R., Ophoven, A., Wu, L., deKernion, J., and Belldegrun, A. Androgen deprivation induces selective outgrowth of aggressive hormone-refractory prostate cancer clones expressing distinct cellular and molecular properties not present in parental androgen-dependent cancer cells. Cancer J., *6:* 220–233, 2000.

3. Hendrix, M. J., Seftor, E. A., Seftor, R. E., and Trevor, K. T. Experimental co-expression of vimentin and keratin intermediate filaments in human breast cancer cells results in phenotypic interconversion and increased invasive behavior. Am. J. Pathol., *150:* 483–495, 1997.
4. Singh, D., Febbo, P. G., Ross, K., Jackson, D. G., Manola, J., Ladd, C., Tamayo, P., Renshaw, A. A., D'Amico, A. V., Richie, J. P., Lander, E. S., Loda, M., Kantoff, P. W., Golub, T. R., and Sellers, W. R. Gene expression correlates of clinical prostate cancer behavior. Cancer Cell, *1:* 203–209, 2002.
5. Welsh, J. B., Sapinoso, L. M., Su, A. I., Kern, S. G., Wang-Rodriguez, J., Moskaluk, C. A., Frierson, H. F., Jr., and Hampton, G. M. Analysis of gene expression identifies candidate markers and pharmacological targets in prostate cancer. Cancer Res., *61:* 5974–5978, 2001.
6. Mousses, S., Bubendorf, L., Wagner, U., Hostetter, G., Kononen, J., Cornelison, R., Goldberger, N., Elkahloun, A. G., Willi, N., Koivisto, P., Ferhle, W., Raffeld, M., Sauter, G., and Kallioniemi, O. P. Clinical validation of candidate genes associated with prostate cancer progression in the CWR22 model system using tissue microarrays. Cancer Res., *62:* 1256–1260, 2002.
7. Osborn, M., and Weber, K. Intermediate filaments: cell-type-specific markers in differentiation and pathology. Cell, *31:* 303–306, 1982.
8. Steinert, P. M., Steven, A. C., and Roop, D. R. The molecular biology of intermediate filaments. Cell, *42:* 411–420, 1985.
9. Huszar, M., Halkin, H., Herczeg, E., Bubis, J., and Geiger, B. Use of antibodies to intermediate filaments in the diagnosis of metastatic amelanotic malignant melanoma. Hum. Pathol., *14:* 1006–1008, 1983.
10. Moll, R., Franke, W. W., Schiller, D. L., Geiger, B., and Krepler, R. The catalog of human cytokeratins: patterns of expression in normal epithelia, tumors and cultured cells. Cell, *31:* 11–24, 1982.
11. Leong, A. S., Gilham, P., and Milios, J. Cytokeratin and vimentin intermediate filament proteins in benign and neoplastic prostatic epithelium. Histopathology, *13:* 435–442, 1988.
12. Ramaekers, F. C., Haag, D., Kant, A., Moesker, O., Jap, P. H., and Vooijs, G. P. Coexpression of keratin and vimentin type intermediate filaments in human metastatic carcinoma cells. Proc. Natl. Acad. Sci. USA, *80:* 2618–2622, 1983.
13. Sommers, C. L., Walker-Jones, D., Heckford, S. E., Worland, P., Valverius, E., Clark, R., McCormick, F., Stampfer, M., Abularach, S., and Gelmann, E. P. Vimentin rather than keratin expression in some hormone-independent breast cancer cell lines and in oncogene-transformed mammary epithelial cells. Cancer Res., *49:* 4258–4263, 1989.
14. Azumi, N., and Battifora, H. The distribution of vimentin and keratin in epithelial and nonepithelial neoplasms. A comprehensive immunohistochemical study on form. Am. J. Clin. Pathol., *88:* 286–296, 1987.
15. Hendrix, M. J., Seftor, E. A., Chu, Y. W., Seftor, R. E., Nagle, R. B., McDaniel, K. M., Leong, S. P., Yohem, K. H., Leibovitz, A. M., Meyskens, F. L., Jr., *et al.* Coexpression of vimentin and keratins by human melanoma tumor cells: correlation with invasive and metastatic potential. J. Natl. Cancer Inst. (Bethesda), *84:* 165–174, 1992.
16. Thomas, P. A., Kirschmann, D. A., Cerhan, J. R., Folberg, R., Seftor, E. A., Sellers, T. A., and Hendrix, M. J. Association between keratin and vimentin expression, malignant phenotype, and survival in postmenopausal breast cancer patients. Cancer Res., *5:* 2698–2703, 1999.
17. Hay, E. D. An overview of epithelio-mesenchymal transformation. Acta Anat., *154:* 8–20, 1995.
18. Birchmeier, C., Birchmeier, W., and Brand-Saberi, B. Epithelial-mesenchymal transitions in cancer progression. Acta Anat., *156:* 217–226, 1996.
19. Gilles, C., Polette, M., Birembaut, P., Brunner, N., and Thompson, E. W. Expression of c-ets-1 mRNA is associated with an invasive, EMT-derived phenotype in breast carcinoma cell lines. Clin. Exp. Metastasis, *15:* 519–526, 1997.
20. Lochter, A., Galosy, S., Muschler, J., Freedman, N., Werb, Z., and Bissell, M. J. Matrix metalloproteinase stromelysin-1 triggers a cascade of molecular alterations that leads to stable epithelial-to-mesenchymal conversion and a premalignant phenotype in mammary epithelial cells. J. Cell Biol., *139:* 1861–1872, 1997.
21. Nagle, R. B., Ahmann, F. R., McDaniel, K. M., Paquin, M. L., Clark, V. A., and Celniker, A. Cytokeratin characterization of human prostatic carcinoma and its derived cell lines. Cancer Res., *47:* 281–286, 1987.
22. Mitchell, S., Abel, P., Ware, M., Stamp, G., and Lalani, E. Phenotypic and genotypic characterization of commonly used human prostatic cell lines. BJU Int., *85:* 932–944, 2000.
23. Heatley, M., Maxwell, P., Whiteside, C., and Toner, P. Vimentin and cytokeratin expression in nodular hyperplasia and carcinoma of the prostate. J. Clin. Pathol., *48:* 1031–1034, 1995.
24. Lang, S. H., Hyde, C., Reid, I. N., Hitchcock, I. S., Hart, C. A., Bryden, G. A. A., Villette, J. M., Stower, M. J., and Maitland, M. J. Enhanced expression of vimentin in motile prostate cancer cell lines and in poorly differentiated and metastatic prostate carcinoma. Prostate, *52:* 253–263, 2002.
25. Lim, D. J., Liu, X. L., Sutkowski, D. M., Braun, E. J., Lee, C., and Kozlowski, J. M. Growth of an androgen-sensitive human prostate cancer cell line, LNCaP, in nude mice. Prostate, *22:* 109–118, 1993.
26. Veldscholte, J., Ris-Stalpers, C., Kuiper, G. G., Jenster, G., Berrevoets, C., Claassen, E., van Rooij, H. C., Trapman, J., Brinkmann, A. O., and Mulder, E. A mutation in the ligand binding domain of the androgen receptor of human LNCaP cells affects steroid binding characteristics and response to anti-androgens. Biochem. Biophys. Res. Commun., *173:* 534–540, 1990.
27. Thompson, E. W., Paik, S., Brunner, N., Sommers, C. L., Zugmaier, G., Clarke, R., Shima, T. B., Torri, J., Donahue, S., and Lippman, M. E., *et al.* Association of increased basement membrane invasiveness with absence of estrogen receptor and expression of vimentin in human breast cancer cell lines. J. Cell. Physiol., *150:* 534–544, 1992.
28. Sommers, C. L., Heckford, S. E., Skerker, J. M., Worland, P., Torri, J. A., Thompson, E. W., Byers, S. W., and Gelmann, E. P. Loss of epithelial markers and acquisition of vimentin expression in adriam. Cancer Res., *52:* 5190–5197, 1992.
29. Bussemakers, M. J., Verhaegh, G. W., van Bokhoven, A., Debruyne, F. M., and Schalken, J. A. Differential expression of vimentin in rat prostatic tumors. Biochem. Biophys. Res. Commun., *182:* 1254–1259, 1992.
30. Kryszke, M. H., and Vicart, P. Regulation of the expression of the human vimentin gene: application to cellular immortalization. Pathol. Biol. (Paris), *46:* 39–45, 1998.
31. Ginsberg, M. H., Du, X., and Plow, E. F. Inside-out integrin signalling. Curr. Opin. Cell Biol., *3:* 841–848, 1992.
32. Juliano, R. L., and Haskill, S. Signal transduction from the extracellular matrix. J. Cell Biol., *120:* 577–585, 1993.
33. Maniotis, A. J., Chen, C. S., and Ingber, D. E. Control of cell and nuclear shape by mechanical stresses transmitted from integrins to the nucleus over direct cytoskeletal interconnections. Proc. Natl. Acad. Sci. USA, *94:* 849–854, 1997.
34. Miyamato, S., Teramoto, H., Coso, O. A., Gutkind, J. S., Burbelo, P. D., Akiyama, S. K., and Yamada, K. M. Integrin function: molecular hierarchies of cytoskeletal and signaling molecules. J. Cell Biol., *131:* 791–805, 1995.
35. Cress, A. E., and Dalton, W. S. Multiple drug resistance and intermediate filaments. Cancer Metastisis Rev., *15:* 499–506, 1996.

The Prostate 55:299–307 (2003)

Heterogeneity of Molecular Targets on Clonal Cancer Lines Derived From a Novel Hormone-Refractory Prostate Cancer Tumor System

Stephen J. Freedland,[1] Allan J. Pantuck,[1] Sun H. Paik,[1] Amnon Zisman,[1] Thomas G. Graeber,[2] David Eisenberg,[2] William H. McBride,[3] David Nguyen,[1] Cho-Lea Tso,[1] and Arie S. Belldegrun[1]*

[1]*Department of Urology, UCLA, Los Angeles, California*
[2]*UCLA-Department of Energy, Laboratory of Structural Biology and Molecular Medicine, UCLA, Los Angeles, California*
[3]*Department of Radiation Oncology, UCLA, Los Angeles, California*

OBJECTIVE. We recently described a new hormone refractory prostate cancer cell line, CL1, derived from LNCaP via in vitro androgen deprivation. To study gene expression during prostate cancer progression and to identify molecular targets for therapy, a pure clonal tumor system was generated.

METHODS. Limiting dilution of CL1 stably transfected with a green fluorescent protein, generated 35 single-cell clones, which were expanded into stable cell lines. In vitro responses to various therapeutic modalities were assessed in each clone. Gene expression was determined using reverse transcriptase-polymerase chain reaction and oligonucleotide microarrays. In vivo biology was assessed following orthotopic injection into intact and castrated severe combined immunodeficient mice.

RESULTS. In vitro, all clones demonstrated similar resistance to traditional therapeutic efforts including chemotherapy and radiation therapy, but differential sensitivity to cell-mediated cytotoxicity. The clones demonstrated differential gene expression relative to each other and to the parental CL1 and LNCaP cell lines. Following orthotopic injection into mice, three distinct growth patterns were observed: fast growth with widespread metastasis; slower grower with widespread metastasis; and no tumor formation. Using oligonucleotide microarrays, several genes were identified as differentially expressed between the most aggressive and the non-tumorigenic clone.

CONCLUSIONS. We have described a novel fluorescent-labeled clonal hormone refractory prostate cancer tumor system that exhibited marked heterogeneity in its response to various therapeutic modalities, gene expression, and in vivo biology. Our data suggests that given the marked clonal heterogeneity, multi-modality approaches directed against multiple molecular targets rather than single agent therapy will be necessary to adequately eradicate the entire malignant cell population. Clonal tumor lines may allow more accurate examination of

Abbreviations: AR, androgen receptor; bFGF, basic fibroblast growth factor; EGFR, epidermal growth factor; GFP, green fluorescent protein; HGF, hepatocyte growth factor; HRPC, hormone refractory prostate cancer; IL, interleukin; LAK, IL-2 activated killer; LU, lytic units; NK, natural killer; PBL, peripheral blood lymphocytes; PSA, prostate specific antigen; PSMA, prostate specific membrane antigen; RT-PCR, reverse transcriptase polymerase chain reaction; SCID, severe combined immunodeficient; TGF, transforming growth factor; VEGF, vascular epithelial growth factor.

Grant sponsor: Department of Defense; Grant sponsor: The J.B. (Bert) Ladd Foundation; Grant sponsor: Abe Zarem Research Fellowship (to S.J.F.); Grant sponsor: Alfred P. Sloan Foundation/ Department of Energy Postdoctoral Fellowship (to T.G.G.).

*Correspondence to: Arie S. Belldegrun, Department of Urology, UCLA School of Medicine, Box 951738, Los Angeles, CA 90095-1738. E-mail: abelldegrun@mednet.ucla.edu

Received 9 November 2002; Accepted 22 November 2002
DOI 10.1002/pros.10226

molecular pathways involved in tumor progression and resistance to treatment. *Prostate 55: 299–307, 2003.*

KEY WORDS: **prostate cancer; clones; tumor model; hormone refractory**

INTRODUCTION

While various treatment modalities for clinically localized prostate cancer are available, androgen deprivation remains the standard of care for metastatic disease. However, androgen independence invariably develops. The exact mechanisms involved in this progression to a hormone refractory state remain unknown.

In order to study progression from androgen sensitive to HRPC, we recently developed a new HRPC model (Fig. 1) [1,2]. In vitro androgen deprivation of the slow growing and poorly tumorigenic androgen sensitive human prostate cancer cell line, LNCaP, was carried out. This resulted in the emergence of a fast growing, chemo- and radio-therapy resistant androgen independent derivative, CL1. When stably transfected with the *Aequorea victoria* GFP and transplanted orthotopically into SCID mice, CL1–GFP shows aggressive local growth with metastases detected by fluorescence microscopy in multiple organs. CL1–GFP is characterized by an over-expression relative to that of the parental LNCaP of the growth and pro-angiogenic factors IL-6, IL-8, VEGF, and TGF-β2. There was concomitant down-regulation of the prostate related genes *PSA*, *AR*, and *PSMA* as well as the tumor suppressor genes *E-cadherin* and *p53*.

To identify potential molecular targets relevant to prostate cancer progression while avoiding potential limitations related to the heterogeneous expression of many genes in a nonclonal population, we studied differential gene expression in a pure clonal tumor system based upon single-cell derived clones of CL1–GFP.

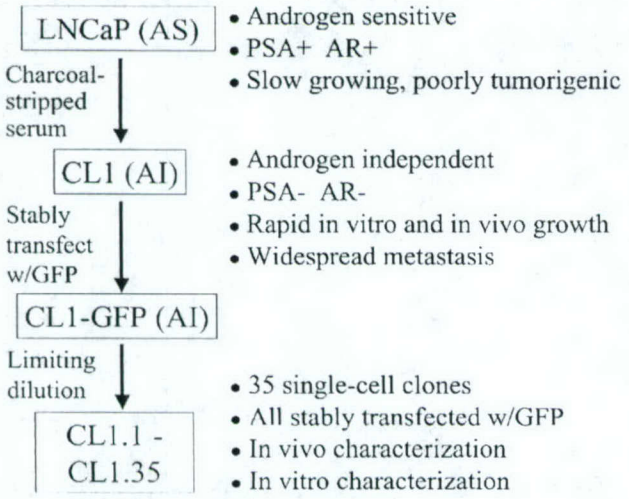

Fig. 1. Schematic of the relationship between LNCaP, CL1, and the CL1 clones.

MATERIALS AND METHODS

Cell Culture

The human prostate cancer cell line LNCaP was provided by the American Type Culture Collection (Rockville, MD) and CL1 was derived as previously described [1]. LNCaP was maintained in RPMI 1640 medium (Life Technologies, Gaithersburg, MD) with 10% fetal bovine serum, glutamine, and antibiotics (50 IU/ml penicillin; 50 μg/ml streptomycin). CL1 and its clones were maintained in RPMI 1640 medium with 10% charcoal-stripped fetal bovine serum, glutamine, and antibiotics. CL1 was stably transfected with the GFP gene as previously described [1]. Limiting dilution of CL1–GFP was used to obtain single-cell derived clones that each expressed GFP.

Limiting Dilution and Growth Assays

CL1–GFP was plated at 0.3 cells/well in 200 μl of media with 10% charcoal-stripped serum in a 96-well plate. The plate was incubated until individual colonies were seen. Thirty five single cell clones (36%) were expanded. Proliferation assays were performed by ^{3}H-thymidine incorporation as previously described [1].

Chemotherapeutic Assays

Cells in semi-logarithmic phase of growth were plated at 2×10^4 cells/ml/well in 24-well plates in triplicate and allowed to adhere overnight. The cells were treated the following day with varying concentrations of doxorubicin, ketoconazole, paclitaxel, or vinblastine and cell viability/number was assayed using an 3-(4,5-dimethylthiazol-2-yl)2,5-diphenyl tetrazolium bromide (MTT) assay 48 hr thereafter [3]. A standard number of CL1 cells was plated and immediately assayed in a similar fashion to establish a standard curve, which was used to convert absorbance to cell number. Numbers are presented as percent inhibition. All experiments were run in triplicate with the results representing the mean.

Cytotoxicity Assays

The immunogenicity of the clones to stimulate cytolytic activity by NK cells and LAK cells was determined by an 18 hr chromium-51 (^{51}Cr) release assay. Fresh PBL, harvested with ficoll centrifugation, were used to assay for NK activity. To assay for LAK cell activity, fresh PBL were expanded in vitro in RPMI with 10% autologous serum and 100 U/ml of IL-2 for 4 days. Five thousand ^{51}Cr-labeled target cells per well were seeded in 96-well plates in triplicate and mixed with lymphocytes at effector-target ratios of 40:1, 20:1, 10:1, and 5:1. Cytotoxicity is expressed as LU per 10^6 effector cells. LU are defined as the number of effector cells capable of inducing 30% lysis.

Radiation

Cells in semi-logarithmic phase of growth were harvested and irradiated with 0, 2, 4, or 6 Gy using a Mark 1 cesium irradiator (Shepherd Associates, San Fernando Valley, CA) with a dose rate of approximately 450 cGy/min. Cells were then plated in triplicate in 100 mm Petri dishes at numbers predetermined to yield between 50 and 100 colonies per dish. After 12 days incubation at 37°C in 10% CO_2, colonies were stained with 1% crystal violet and those containing >50 cells were counted to obtain the surviving fraction. The surviving fraction was plotted against dose on a log-linear scale.

RT-PCR

Total RNA was extracted from LNCaP, CL1, and CL1 clones by acid guanidine isothiocyanate-phenol-chloroform and reverse transcribed into cDNA. The amount of diluted cDNA that expressed equivalent signal intensity of β-actin was used to perform PCR for the other markers. The oligonucleotide primer pair sequences and cycle settings used for β-actin, PSA, AR, PSMA, caveolin, p53, E-cadherin, IL-8, VEGF, TGF-β2, IL-6, bFGF, bcl-2, EGFR, and HER2 were previously described [1]. The primers pair sequences and cycle settings used for HGF and its tyrosine kinase receptor, c-met [4] were previously described. The primers pair sequences for TGF-α were CGCTCTGGGTATTGTGTTGG and TCTCTTCTTTAGTCGCCTGG and the cycle settings consisted of 94°C for 2 min followed by 30 cycles (94°C for 1 min, 65°C for 2 min).

Animal Studies

Male 6–8-week-old SCID (CB.17 scid/scid) mice were obtained from the breeding program at the University of California, Los Angeles. All animals were anesthetized with ketamine before inoculation with cancer cells. The prostate gland was exposed following a lower midline incision. Five mice per treatment group were inoculated with 5×10^4 cells in 10 μl RPMI 1640 into the dorsolateral lobe of the prostate using a 30-gauge needle and a calibrated push-button syringe. For the castrated group, castration was performed at the same time as tumor implantation. Tumor growth was measured by palpation. When a large easily palpable tumor was evident and prior to deterioration in the health of the animal, the mice were sacrificed. This correlated to an approximately 1–1.5 cm^3 primary tumor size. Tumor invasion was examined grossly on necroscopy and histologically by evaluation of the primary tumor and multiple organs. Micrometastases were detected by fluorescence microscopy for GFP positive cells.

Oligonucleotide Microarrays

Total RNA was extracted from LNCaP, CL1, and CL1 clones by acid guanidine isothiocyanate-phenol-chloroform and purified by column isolation. RNA was transcribed into cDNA, labeled with biotin and hybridized separately to oligonucleotide microarrays (human U95A chip, Affymetrix, Santa Clara, CA) according to the manufacturers recommendations. Samples from CL1.31 were run once, and samples from CL1.1 were run in duplicate with gene expression determined by the average expression across the two samples. Conversion of raw data into numeric values of expression was done using software provided by Affymetrix. The independent measurements of expression for each gene from the two identically prepared CL1.1 samples were used to estimate parameters describing a probabilistic error model for gene-expression measurement variation. In the error model, fluctuations in observed gene expression values were generated by assuming inefficiencies in counting the true number of gene transcripts, and thus the fluctuations were described by Poisson statistics. Counts were converted to expression values by multiplicative scaling. The scale factor was assumed to be identical for all genes and was determined using maximum-likelihood estimation. Synthetic data generated using this model accurately reproduced the relationship between expression values and their variation seen in experimental data with smaller expression values having larger relative variation. The error model was then used to calculate the likelihood that the expression of a gene differed by at least fivefold between two samples given the observed expression values and their modeled error.

RESULTS

CL1 Clones

In vitro limiting dilution of CL1-GFP was undertaken to generate 35 single-cell clones (Fig. 1).

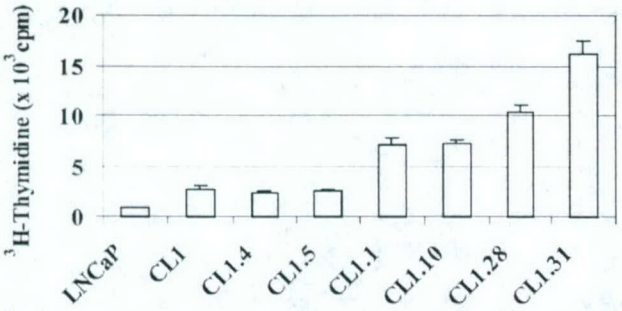

Fig. 2. Growth activity of CL1 clones. In vitro ^{3}H-thymidine incorporation assay for LNCaP, CL1, and CL1 clones. Error bars are the standard deviation. Proliferation activity of the clones ranged from 0.8 to 6-fold that of CL1, with CL1 having a twofold increase relative to LNCaP.

Proliferative activity as measured by ^{3}H-thymidine incorporation was determined for all 35 clones, and based upon this, six clones with differential in vitro growth were chosen for detailed characterization (Fig. 2). The six clones were chosen to encompass the entire spectrum of proliferative activity from slow growing (CL1.4 and CL1.5) to rapid growing clones (CL1.31 and CL1.28). Proliferative activity of the six clones ranged from 0.8 to 6-fold that of the parental CL1.

Sensitivity to Cytotoxic Agents

All six clones showed a similar relative resistance to the chemotherapeutic agents doxorubicin, ketoconazole, paclitaxel, vinblastine (Fig. 3). This compares to the chemotherapy sensitive cell line LNCaP, which showed 70–80% growth inhibition at doses of paclitaxel (0.625 nM) and vinblastine (0.625 nM) that resulted in minimal to no growth inhibition among the CL1 clones [1]. All six clones showed similar responsiveness to ionizing radiation (Fig. 4A). At physiologic dose of 2 Gy, all clones had a greater than 50% surviving fraction. This compares to less than 20% surviving fraction for the radiation sensitive LNCaP cell line [5]. At 6 Gy, all clones had a surviving fraction between 0.5% and 2%. The clones demonstrated a heterogeneous sensitivity to both NK cell and LAK cell-mediated cytotoxicity (Fig. 4B–C). Although there was 2.5-fold differential sensitivity between the most and least sensitive clones in NK cell-mediated cytotoxicity, the parental CL1 and all clones demonstrated a NK resistant phenotype. Overall, all clones had greater sensitivity to LAK cell-mediated cytotoxicity than NK cell-mediated cytotoxicity, however, the parental cell line, CL-1 was less sensitive to LAK mediated killing than any of the CL1-derived clones.

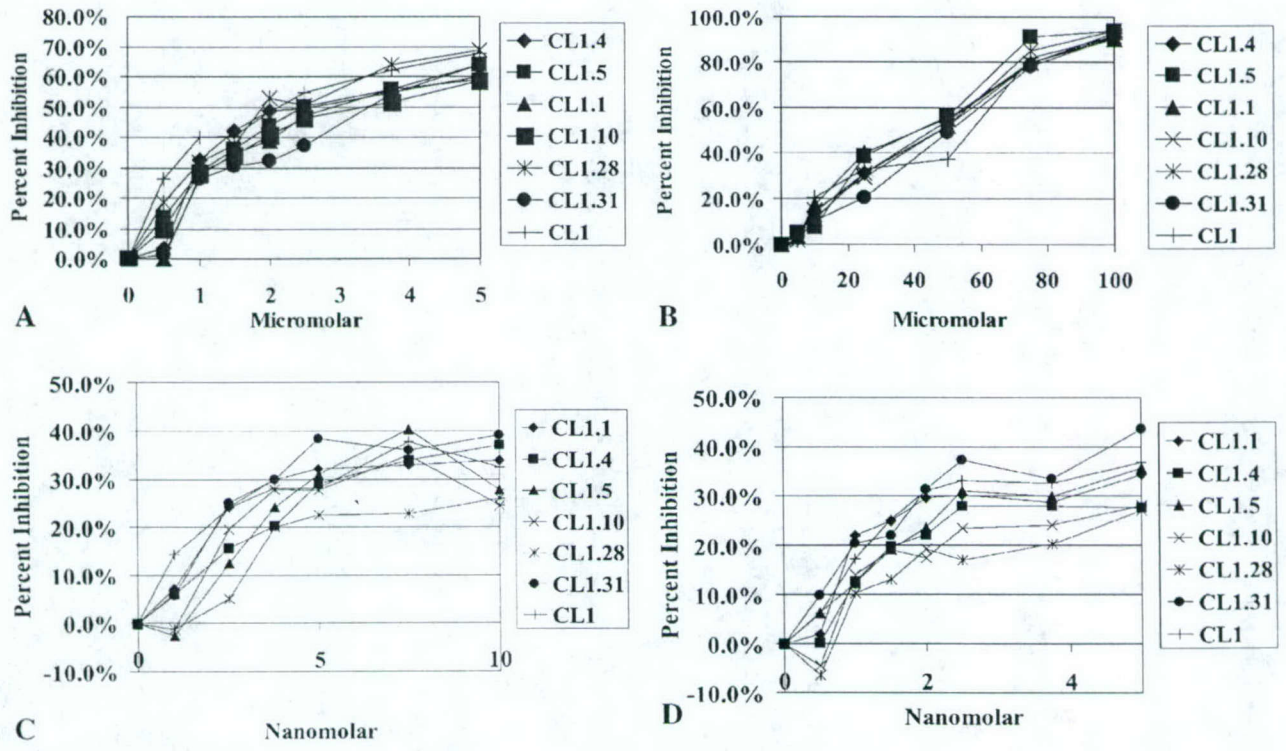

Fig. 3. Response of CL1 and its clones to chemotherapeutic agents. **A**: Doxorubicin. **B**: Ketoconazole. **C**: Paclitaxel. **D**: Vinblastine. Percent inhibition is indicated on the Y-axis, and drug concentrations tested on the X-axis.

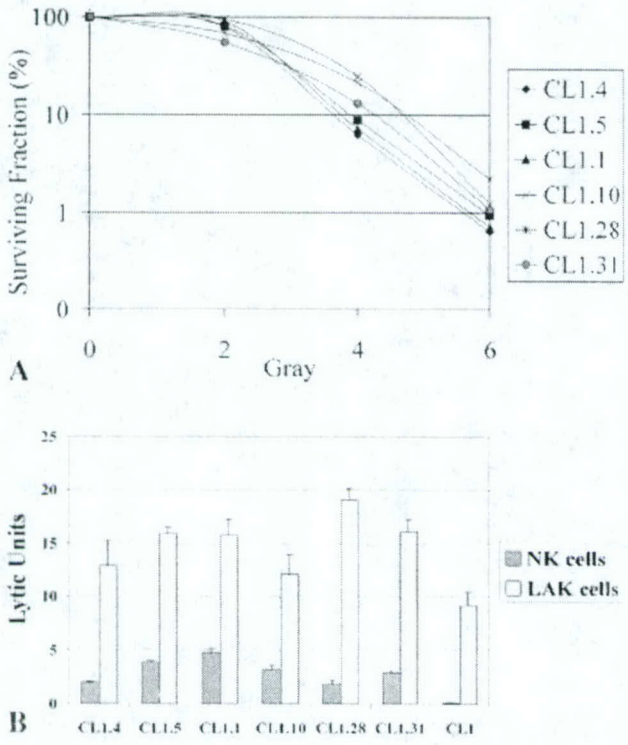

Fig. 4. Response of CL1 and its clones to cytotoxic agents. **A**: Response to ionizing radiation. The surviving fraction is indicated in log-scale on the Y-axis and the radiation dose on the X-axis. **B**: Response to cell-mediated cytotoxicity from NK cells and LAK cells. The lytic units are indicated on the Y-axis and the various cell line on X-axis. All clones were more sensitive to cell-mediated cytotoxicity that the parental CL-1.

Gene Expression Analyzed by RT-PCR

All six clones, CL1 and LNCaP were characterized for gene expression of various prostate related genes, tumor suppressors, and growth and angiogenic factors using RT-PCR (Fig. 5). The prostate related genes PSA, AR, and PSMA were downregulated in CL1 and its clonal derivatives, though expression was heterogeneous among the clones. There was a uniform upregulation of caveolin in CL1 and the clones relative to very low expression in LNCaP. Expression of the tumor suppressor genes E-cadherin and p53 was heterogeneously decreased in CL1 and the clones. The proangiogenic factor IL-8 as well as the growth factors HGF and c-met were expressed in CL1 and the clones, but not in LNCaP. The angiogenic factor VEGF, the growth factor bFGF, and the growth factor receptors EGFR and HER2 were expressed by all cell lines. There was marked heterogeneity of expression of the growth factors TGF-α and TGF-β2 with some clones having higher expression and others lower expression than LNCaP. IL-6 and bcl-2 were expressed by CL1 but expression was heterogeneous among the clones.

Tumor Growth in Mice

Following orthotopic implantation of tumor cells into SCID mice, three distinct patterns of in vivo growth were identified: CL1.1 was characterized as a fast growing clone (FGC) with tumor formation and development of distant metastases within 5 weeks; CL1.4, CL1.5, CL1.10, and CL1.28 were characterized as slow growing clones (SGC) with tumor formation and development of distant metastases by 7–12 weeks; and CL1.31 was characterized as a non-growing clone (NGC), with no demonstrable tumor development in any of 10 mice injected (5 castrated, 5 intact) (Fig. 6A,B, Table II). CL1.4 and CL1.10 from the SGC group demonstrated tumor development only in intact mice. Once a palpable tumor was present, tumor growth was rapid for both FGC and SGC necessitating sacrifice of the mice within 1–2 weeks. Upon sacrifice, aggressive local growth, invasion of adjacent organs, spread to regional lymph nodes, and distant metastases could all be detected (Fig. 7A,B). Histological evaluation of the primary tumors revealed poorly differentiated high-grade, anaplastic tumor cells (Fig. 7C,D). With GFP stably transfected, metastases could be detected by fluorescence microscopy in the femur, lungs, kidneys, liver, spleen, pancreas, and lymph nodes (Fig. 7E–J).

Gene Expression Using Oligonucleotide Microarrays

Gene expression measurements from oligonucleotide microarrays were used to identify genes that were differentially expressed between the most aggressive clone, CL1.1, and the nontumorigenic clone, CL1.31. Using a statistical error model, we were able to determine which genes had a five-fold or greater difference in expression level between any two samples ($P < 0.01$). Using these criteria, we identified 10 genes that were differentially expressed between the NGC, CL1.31, and the FGC, CL1.1 (Table I). Three of these genes (prostate differentiation factor, flap structure-specific endonuclease 1 and DNA polymerase delta 1 catalytic subunit) were overexpressed in the FGC, CL1.1, whereas the remaining seven genes (8-oxoguanine DNA glycosylase, paralemmin, filamin C gamma, skin-specific protein (XP5), calponin 3 acidic, DDX21, and KIAA0690 protein) were overexpressed in the NGC, CL1.31. The most differentially expressed gene was 8-oxoguanine DNA glycosylase, which was over-expressed in the NGC, CL1.31 relative to the FGC, CL1.1.

DISCUSSION

In order to study gene expression during prostate cancer progression and thus identify molecular targets for advanced disease, we created a clonal tumor system

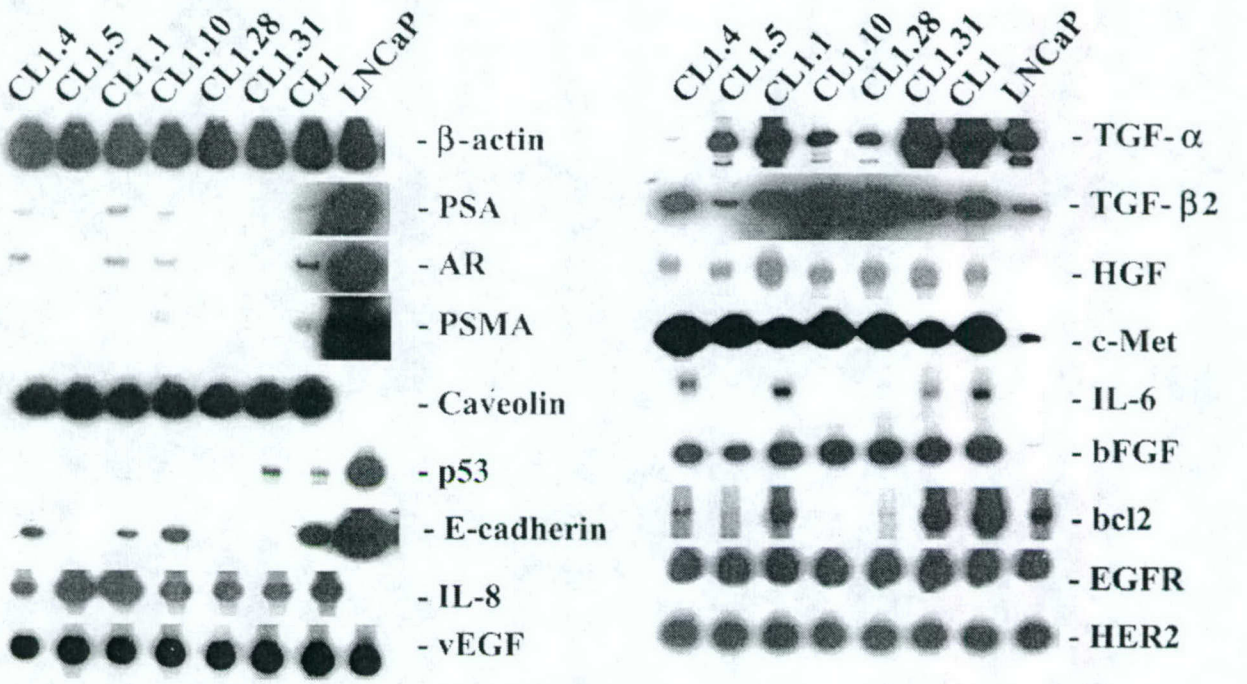

Fig. 5. Gene expression of LNCaP, CLI, and CLI clones. There is marked down-regulation of PSA, AR, PSMA, E-cadherin, and p53; and up-regulation of caveolin IL-8, HGF, c-met, IL-6, and bFGF as estimated from the band intensities.

based upon single-cell derived clones from the aggressive HRPC cell line CL1. Though the clones all demonstrated similar resistance to standard chemotherapy and radiation therapy in vitro there was differential sensitivity to cell-mediated cytotoxicity. Moreover, the clones had differential gene expression and heterogeneous in vitro and in vivo growth. Using oligonucleotide microarrays, several genes that were differentially expressed between the most and least aggressive clones were identified. The marked heterogeneity in the sensitivity to cell-mediated cytotoxicity, gene expression, and in vitro and in vivo biological growth exhibited by clonal cells derived from the same tumor cell line underscores the potential pitfalls of using single agent therapy as treatment for advanced prostate cancer. Given this marked heterogeneity, multi-modality therapy directed against several molecular targets may be required to control HRPC. This model may serve as a valuable tool to define the optimal molecular targets.

Advanced prostate cancer is often characterized by loss of tumor suppressor genes and expression of various growth/angiogenic factors [6]. The HRPC cell line CL1 exhibits many of these changes, with reduced

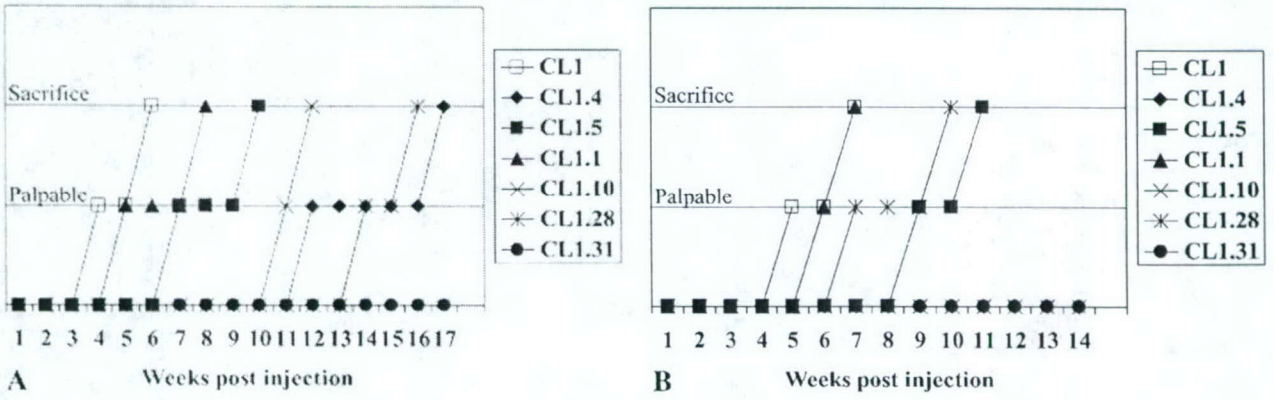

Fig. 6. In vivo growth curve of CLI and the clones following orthotopic injection into intact (**A**) and castrated (**B**) SCID mice. Note three patterns of growth: fast growing clones (CLI.I); slow growing clones (CLI.4, CLI.5, CLI.10, and CLI.28), and non-growing clones (CLI.3I).

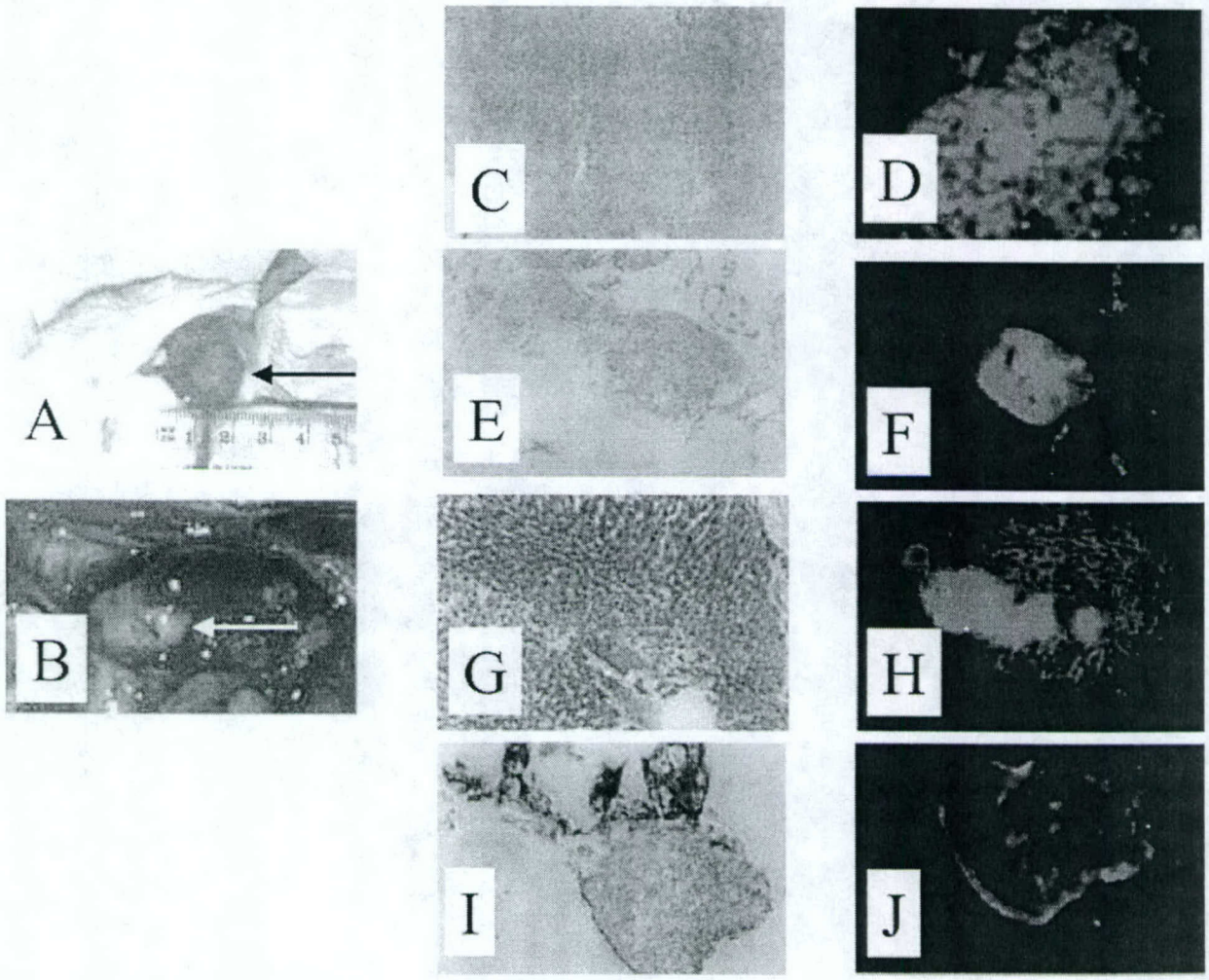

Fig. 7. Gross necroscopy and histology 6 weeks after orthotopic injection of CL1.1 into castrated mice. In (**A**), a large primary tumor is present (arrow), which measures approximately 1 × 1 × 1.5 cm. In (**B**), a gross metastasis to the left kidney is seen (arrow). In (**C–J**), hematoxylin and eosin (100×) staining of specimens from sacrificed mice with corresponding fluorescence microscopy (100×) from primary tumor (C and D), lung (E and F), liver (G and H), and femur (I and J) metastases.

p53 and E-cadherin expression and an associated increased expression of several growth/angiogenic factors such as IL-8, IL-6, bFGF, and HGF/c-met relative to LNCaP [1]. However, the identification of the ideal molecular target is confounded by tumor heterogeneity [7]. This heterogeneity is clearly evident in our tumor system by the isolation of single-cell derived clones with differing gene expression and

TABLE 1. Differentially Expressed Genes Between the Most Aggressive Clone, CL1.1 and the Nontumorigenic Clone, CL1.31

Overexpressed in CL1.1	Overexpressed in CL1.31
Prostate differentiation factor	8-Oxoguanine DNA glycosylase
Flap structure-specific endonuclease 1	Paralemmin
DNA polymerase, delta 1, catalytic subunit	Filamin C, gamma
	Skin-specific protein (XP5)
	Calponin 3, acidic
	DDX21
	KIAA0690 protein

TABLE II. Comparison of the Six Clones for Time to Palpable Tumor and Time to Sacrifice Following Orthotopic Injection

Clone	Days to palpable tumor (mean)	Days to sacrifice (mean)
Intact mice		
CL1	22–32 (25)	28–39 (32)
CL1.1	37 (37)	51–64 (58)
CL1.4	77–119 (89)	87–139 (122)
CL1.5	37–56 (47)	56–77 (67)
CL1.10	77 (77)	80 (80)
CL1.28	77–125 (101)	84–139 (112)
CL1.31	No tumors	No tumors
Castrated mice		
CL1	24–37 (31)	35–51 (44)
CL1.1	35–46 (41)	39–56 (48)
CL1.4	No tumors	No tumors
CL1.5	56–64 (61)	78 (78)
CL1.10	No tumors	No tumors
CL1.28	46 (46)	78 (78)
CL1.31	No tumors	No tumors

differing in vivo biology. Not every clone examined expressed every growth factor or lost expression of every tumor suppressor gene. For example, there was marked heterogeneity in the expression of the growth factor, IL-6. Only three of the six clones expressed IL-6 at detectable levels. Therefore, any treatment aimed at blocking IL-6 expression may have no or minimal impact on those cells that did not express IL-6, and thus may leave a significant proportion of the cell population untreated. It is this marked heterogeneity that likely underlies most tumors' resistance to monotherapy. However, several candidate targets such as the growth factors VEGF, EGFR, and HER2 were expressed by all the clones, CL1, and LNCaP, and thus may prove to be valuable therapeutic targets.

CL1 and all the clones demonstrated relative resistance to radiation therapy and the various chemotherapeutic agents tested. There was no relationship between bcl-2 expression and sensitivity to these cytotoxic agents. Specifically, CL1.10, CL1.28, and CL1.5 had very low to no bcl-2 expression by RT-PCR, but displayed similar resistance to these agents as those clones with higher bcl-2 expression. Thus, it appears that aggressive, treatment resistant HRPC is not always associated with significant expression of bcl-2 and therefore, treatment aimed at blocking bcl-2 expression using anti-sense molecules [8] may fall short of eliminating the entire malignant cell population. Moreover, the relative resistance to traditional approaches such as chemotherapy and radiation therapy argues for the need for novel approaches such as gene or immunotherapy. The fact that the CL1 clones demonstrated relative sensitivity to LAK cell-mediated cytotoxicity further suggests that immunotherapy may be a useful treatment for HRPC. The differential sensitivity of the clones to cell-mediated cytotoxicity may also explain why immunotherapy protocols are often associated with a marked tumor response, but are unable to completely eradicate the malignant cell population [9]. In gene-based approaches, it is essential to define the optimal molecular target or combination of targets. Based upon the current tumor model, it is clear that treatment aimed solely at a single genetic locus is apt to leave a significant proportion of the malignant population untreated, and thus, genetic therapy may be most successful when multiple genes are targeted simultaneously.

Microarrays are a new high-throughput technique that allows the measurement of gene expression simultaneously across thousands of genes [10]. Microarrays have been used to identify genes that can accurately differentiate prostate cancer from benign prostate tissue [11]. Using oligonucleotide microarrays, we identified several genes that were differentially expressed between the most and least aggressive clones. The most significantly differentially expressed gene was 8-oxoguanine DNA glycosylase, which was over-expressed by the NGC, CL1.31 relative to the aggressive FGC, CL1.1. 8-Oxoguanine DNA glycosylase is an enzyme involved in DNA repair that removes 8-oxoguanine, a highly mutagenic oxidative DNA adduct [12]. This enzyme has been shown to undergo mutation during cancer progression [13]. Therefore, the reduced expression of this gene in the FGC, CL1.1 may allow further genetic alterations to accumulate, thus helping to contribute to cancer progression. However, the exact role or significance of these differentially expressed genes in the current tumor model is currently unknown.

The biologic aggressiveness of our clones did not correlate with their in vitro proliferative activity. The NGC, CL1.31, demonstrated the greatest in vitro proliferative activity, yet was unable to develop tumors in any of the 10 mice injected. The FGC, CL1.1, demonstrated modest in vitro proliferative activity. Therefore, it is clear that the factors that are important for rapid in vitro growth are not necessarily important for in vivo tumor development.

In contrast to the Dunning R-3327 model of rat prostate cancer [14], our prostate cancer model has the advantage that it is of human origin, being derived from LNCaP, which was originally established from a lymph node metastasis. Moreover, all CL1 clones are derived from single cells, unlike the polyclonal cell lines of the Dunning model. The use of single-cell clones provides a significant advantage for study and

avoids potential problems related to heterogeneous expression of many genes in a nonclonal population, making interpretation of results equivocal. Moreover, unlike the Dunning model, all CL1 clones can be grown in vitro. On the other hand the NGC, CL1.31, demonstrated no in vivo tumor development. To date, we have not identified any clones that are similar to the Dunning sublines that show distinct differences in their metastatic potential and organ specificity, nor have we identified any clones that are analogous to sublines that form tumors without widespread metastasis [15]. However, we have only characterized 6 of the 35 single-cell clones. Therefore, it remains to be seen whether one of the remaining 29 clones will demonstrate the ability to develop tumors without metastasis or show distinct organ specificity in their metastatic potential.

A different LNCaP-based prostate tumor model system was established in the laboratory of Chung and colleagues [16]. This system was developed through in vivo androgen deprivation of LNCaP co-inoculated with a bone stromal cell line. With the co-inoculation of a bone stromal cell line, a prostate cancer cell line, C4-2, was generated that showed preferential metastasis to the bone [17]. The advantage of the current model is that all of our clones are stably transfected with GFP to increase the sensitivity for detection of metastasis in vivo, and most importantly, all of our clones are single-cell derived as opposed to a heterogeneous population of clones each with their own distinct cellular and molecular properties.

CONCLUSIONS

Using limiting dilution, we developed a fluorescent-labeled prostate tumor model based upon single-cell derived clones of the aggressive HRPC cell line, CL1. All clones showed resistance to radiation, chemotherapy, NK mediated killing, but differential sensitivity to LAK cell-mediated cytotoxicity. The clones demonstrated heterogeneous in vitro and in vivo growth with differential gene expression. The marked heterogeneity among the clones underscores the importance of multimodality therapy simultaneously directed against multiple molecular targets. This model may help elucidate these ideal therapeutic targets.

ACKNOWLEDGMENTS

We thank Robert Grothe for assistance with the statistical error model.

REFERENCES

1. Tso CL, McBride WH, Sun J, Patel B, Tsui KH, Paik SH, Gitlitz B, Caliliw R, van Ophoven A, Wu L, deKernion J, Belldegrun A. Androgen deprivation induces selective outgrowth of aggressive hormone-refractory prostate cancer clones expressing distinct cellular and molecular properties not present in parental androgen-dependent cancer cells. Cancer J Sci Am 2000;6:220–233.
2. Patel BJ, Pantuck AJ, Zisman A, Tsui KH, Paik SH, Caliliw R, Sheriff S, Wu L, deKernion JB, Tso CL, Belldegrun AS. CL1-GFP: An androgen independent metastatic tumor model for prostate cancer. J Urol 2000;164:1420–1425.
3. Mosmann T. Rapid colorimetric assay for cellular growth and survival: Application to proliferation and cytotoxicity assays. J Immunol Methods 1983;65:55–63.
4. Oda Y, Sakamoto A, Saito T, Kinukawa N, Iwamoto Y, Tsuneyoshi M. Expression of hepatocyte growth factor (HGF)/scatter factor and its receptor c-MET correlates with poor prognosis in synovial sarcoma. Hum Pathol 2000;31:185–192.
5. Colletier PJ, Ashoori F, Cowen D, Meyn RE, Tofilon P, Meistrich ME, Pollack A. Adenoviral-mediated p53 transgene expression sensitizes both wild-type and null p53 prostate cancer cells in vitro to radiation. Int J Radiat Oncol Biol Phys 2000;48:1507–1512.
6. Abate-Shen C, Shen MM. Molecular genetics of prostate cancer. Genes Dev 2000;14:2410–2434.
7. Pettaway CA, Pathak S, Greene G, Ramirez E, Wilson MR, Killion JJ, Fidler IJ. Selection of highly metastatic variants of different human prostatic carcinomas using orthotopic implantation in nude mice. Clin Cancer Res 1996;2:1627–1636.
8. Gleave ME, Miayake H, Goldie J, Nelson C, Tolcher A. Targeting *bcl-2* gene to delay androgen-independent progression and enhance chemosensitivity in prostate cancer using antisense bcl-2 oligodeoxynucleotides. Urology 1999;54:36–46.
9. Murphy GP, Tjoa BA, Simmons SJ, Ragde H, Rogers M, Elgamal A, Kenny GM, Troychak MJ, Salgaller ML, Boynton AL. Phase II prostate cancer vaccine trial: Report of a study involving 37 patients with disease recurrence following primary treatment. Prostate 1999;39:54–59.
10. Lockhart DJ, Winzeler EA. Genomics, gene expression and DNA arrays. Nature 2000;405:827–836.
11. Luo J, Duggan DJ, Chen Y, Sauvageot J, Ewing CM, Bittner ML, Trent JM, Isaacs WB. Human prostate cancer and benign prostatic hyperplasia: Molecular dissection by gene expression profiling. Cancer Res 2001;61:4683–4688.
12. Boiteux S, Radicella JP. The human *OGG1* gene: Structure, functions, and its implication in the process of carcinogenesis. Arch Biochem Biophys 2000;377:1–8.
13. Chevillard S, Radicella JP, Levalois C, Lebeau J, Poupon MF, Oudard S, Dutrillaux B, Boiteux S. Mutations in *OGG1*, a gene involved in the repair of oxidative DNA damage, are found in human lung and kidney tumours. Oncogene 1998;16:3083–3086.
14. Tennant TR, Kim H, Sokoloff M, Rinker-Schaeffer CW. The Dunning model. Prostate 2000;43:295–302.
15. Isaacs JT, Isaacs WB, Feitz WF, Scheres J. Establishment and characterization of seven Dunning rat prostatic cancer cell lines and their use in developing methods for predicting metastatic abilities of prostatic cancers. Prostate 1986;9:261–281.
16. Wu HC, Hsieh JT, Gleave ME, Brown NM, Pathak S, Chung LW. Derivation of androgen-independent human LNCaP prostatic cancer cell sublines: Role of bone stromal cells. Int J Cancer 1994;57:406–412.
17. Thalmann GNN, Sikes RA, Wu TT, Degeorges A, Chang SM, Ozen M, Pathak S, Chung LW. LNCaP progression model of human prostate cancer: Androgen-independence and osseous metastasis. Prostate 2000;44:91–103.

The Prostate 55:71–80 (2003)

Loss of CD10 (Neutral Endopeptidase) Is a Frequent and Early Event in Human Prostate Cancer

Stephen J. Freedland,[1] David B. Seligson,[2] Alvin Y. Liu,[3] Allan J. Pantuck,[1] Sun H. Paik,[1] Steve Horvath,[4] Jeffrey A. Wieder,[1] Amnon Zisman,[1] David Nguyen,[1] Cho-Lea Tso,[1] Aarno V. Palotie,[2,4] and Arie S. Belldegrun[1]*

[1]*Department of Urology, UCLA School of Medicine, Los Angeles, California*
[2]*Department of Pathology and Laboratory Medicine, UCLA School of Medicine, Los Angeles, California*
[3]*Department of Urology, University of Washington, Seattle, Washington*
[4]*Department of Human Genetics, UCLA School of Medicine, Los Angeles, California*

BACKGROUND. We hypothesized that the aggressive LNCaP-derived androgen-independent cell line, CL1, might differ from LNCaP in their repertoire of cell surface markers and that these differences might typify changes that occur during clinical prostate cancer progression.
METHODS. The cell surface marker expression profiles of CL1 and LNCaP were examined using flow cytometry. Markedly differential gene expression was confirmed using RT-PCR and further examined using immunohistochemistry among the prostate cancer cell lines LAPC-4, LNCaP, CL1, CL2, DU145, and PC-3. The expression of the most markedly differentially expressed surface marker, CD10, was further explored in a tissue microarray containing radical prostatectomy samples from 219 hormone naïve prostate cancer patients.
RESULTS. There were marked differences in the expression of CD10, CD13, CD26, CD33, CD44, CD54, CD55, and CD104 between CL1 and LNCaP. Results from both the RT-PCR and immunohistochemistry confirmed the differential expression and found that CD10 demonstrated a pattern of expression in hormone sensitive but not hormone refractory cell lines. When CD10 expression was examined in a tissue microarray, CD10 expression was below the 25th percentile of matched normal prostate tissue in 68% of prostate cancers, below the median expression of matched normal prostate tissue in 86% of cancers, and completely absent in 34% of cancers. Samples of prostatic intraepithelial neoplasia demonstrated CD10 expression that was intermediate between normal prostatic tissue and prostate cancer. Among prostate cancer patients, CD10 expression did not correlate with Gleason score, pathological stage, or biochemical recurrence following radical prostatectomy.
CONCLUSIONS. These findings demonstrate that loss or decreased expression of CD10 is an early and frequent event in human prostate cancer and implicates CD10 as a potential therapeutic target for early stage hormone sensitive prostate cancer. *Prostate 55: 71–80, 2003.*

KEY WORDS: **prostate cancer; hormone refractory; CD10; CD44**

Abbreviations used: AR, androgen receptor; BPH, benign prostatic hypertrophy; EGFR, epidermal growth factor receptor; ^{18}FDG, ^{18}F-deoxyglucose; FBS, fetal bovine serum; fMLPR, formylmethionylleucylphenylalanine receptor; GFP, green fluorescent protein; HGF, hepatocyte growth factor; hK2, human kallikrein 2; HRPC, hormone refractory prostate cancer; IHC, immunohistochemistry; IL, interleukin; LAP, leukocyte alkaline phosphatase; NGFR, nerve growth factor receptor; PIN, prostatic intraepithelial neoplasia; PSA, prostate specific antigen; PSMA, prostate specific membrane antigen; RT-PCR; reverse transcriptase polymerase chain reaction; SCID, severe combined immunodeficient; TGF, transforming growth factor; VEGF, vascular endothelial growth factor.

Stephen J. Freedland and David B. Seligson contributed equally to this work.

Grant sponsor: Department Of Defense; Grant sponsor: The J.B. (Bert) Ladd Foundation; Grant sponsor: CaPCURE Foundation; Grant sponsor: NIH; Grant number: NIHGM08243-13.

*Correspondence to: Dr. Arie S. Belldegrun, Department of Urology, UCLA School of Medicine, Box 951738, Los Angeles, CA 90095-1738.
E-mail: abelldegrun@mednet.ucla.edu
Received 24 May 2002; Accepted 9 October 2002
DOI 10.1002/pros.10202

INTRODUCTION

Characterization of prostate cancer cell lines using a panel of cell surface antibodies showed prostate cancer cells have distinct CD expression profiles [1]. As a population, expression of these cell surface molecules is heterogeneous. CD molecules can be used to track changes that occur during prostate cancer progression. Specifically, a model of prostate cancer progression has been proposed in which cells acquire the expression of basal cell markers as the disease worsens [1,2]. However, much of this work was based upon cell lines. The prevalence and significance of expression of these various surface markers among clinical samples is unknown.

In order to study prostate cancer progression from androgen dependent to HRPC, we recently developed a new HRPC model [3,4]. In vitro androgen deprivation of the slow growing, poorly tumorigenic androgen sensitive human prostate cancer cell line, LNCaP, was carried out. This resulted in the emergence of a fast growing, chemo- and radiotherapy resistant androgen independent derivative, CL1 (Fig. 1). When stably transfected with GFP and transplanted orthotopically into SCID mice, CL1-GFP demonstrated aggressive local growth with metastases in multiple organs detected by fluorescence microscopy. CL1-GFP is characterized by an overexpression relative to the parental LNCaP of the growth and pro-angiogenic factors IL-6, IL-8, VEGF, and TGF-β2 and downregulation of PSA, AR, PSMA, and the tumor suppressor genes E-cadherin and p53. The cell line, CL2, which resulted from returning CL1 cells to androgen containing medium 6 weeks after emergence from LNCaP, had similar in vivo and in vitro biological properties as CL1 [3].

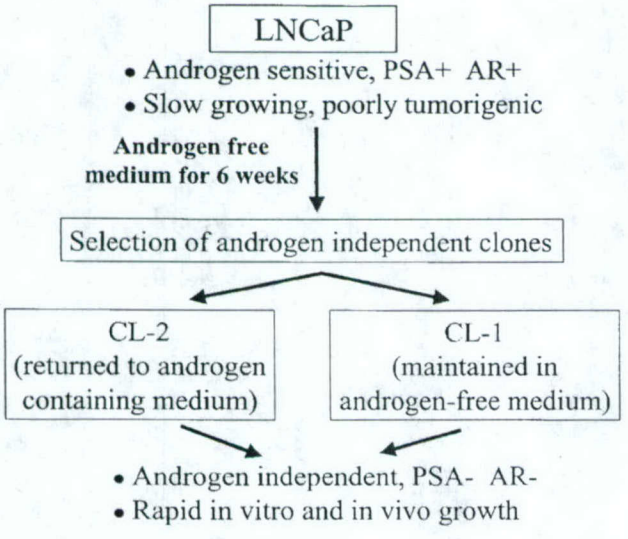

Fig. 1. Schematic of the relationship between LNCaP, CL1, and CL2.

We hypothesized that the hormone refractory cell line CL1 might differ from the parental LNCaP in their repertoire of cell surface molecules and that these differences might typify changes that occur during human clinical prostate cancer progression. To examine this, CL1 and LNCaP were screened for expression of 128 surface markers using flow cytometry. Several differentially expressed surface markers were further examined using RT-PCR and IHC among a set of well-characterized prostate cancer cell lines. Given that decreased CD10 expression appeared to correlate with hormone resistance in our limited cell line sampling, we sought to determine the prevalence of loss of CD10 in early, untreated clinical prostate cancer samples. Specifically, we sought to determine whether loss of CD10 was an early or late event in prostate cancer progression. To accomplish this, we determined CD10 expression in a tissue microarray of 219 radical prostatectomy specimens from hormone naïve patients.

MATERIALS AND METHODS

Cell Culture

Cell lines studied included the slow growing, androgen sensitive human prostate cancer cell line LNCaP and the rapid growing hormone resistant human prostate cancer cell lines PC-3, DU145, CL1, and CL2. We also studied LAPC-4, which was derived from a patient dying of HRPC, yet demonstrates slow growth and androgen sensitivity in vitro and in vivo as a xenograft [5]. The cell lines LNCaP, PC-3, DU145 were provided by the American Type Culture Collection (Rockville, MD). LAPC-4 was a generous gift from Dr. Robert E. Reiter (UCLA, Los Angeles, CA). CL1 and CL2 were derived from LNCaP as described (Fig. 1) [3]. LNCaP, PC-3, DU145, and CL2 were maintained in RPMI 1640 medium with 10% FBS. CL1 was maintained in RPMI 1640 medium with 10% charcoal-stripped FBS and LAPC-4 was maintained in Iscove's modified medium with 5% FBS.

Flow Cytometric Analysis and CD Antibodies

All CD antibodies were conjugated to either R-phycoerythrin or fluorescein isothiocyanate (PharMingen, San Diego, CA). Cells were labeled with CD antibodies as previously described [1]. A reaction without antibody was run first to delineate the unstained/autofluorescent population. Events registered outside this trace were scored as positive, and the percentage of positive events was calculated. Five thousand events were analyzed for each sample. Surface markers that were markedly differentially

expressed between CL1 and LNCaP (>60%) were repeated twice to confirm. Flow analysis was performed using a FACScan machine (Becton Dickinson, Mountain View, CA).

RT-PCR

Total RNA was extracted from cells by acid guanidine isothiocyanate-phenol-chloroform and reverse transcribed (Invitrogen, Carlsbad, CA) into cDNA. The amount of cDNA that expressed equivalent signal intensity of β-actin was used to perform PCR for other markers. The oligonucleotide primer sequences and cycle settings for CD10, CD13, CD26, and CD44 were previously described [1]. The primers pair sequences for CD33 were AACCTTACCTGCTCTGTGTCCTGGGC and GCCTGATGCTCTTGAGGGTTCCTCAC, CD54 were ATGGGGTTCCAGCCCAGCCACTGGG and CCGGGATAGGTTCAGGGAGGCGTGG, CD55 were ATCATGCCCTAATCCGGGAGAAATACGA and GACGGGTAGTACCTGAAGTGGTTCCAC, and CD104 were CGGGAGTCCCAGCCCTACCGCTACA and AGCCGATGCAGCTCACCGCCGTTCA. The cycle settings were 94°C for 2 min followed by 30 cycles (94°C at 1 min, 65°C at 2 min). cDNA samples were amplified using 30 ng of [^{32}P]-5′-oligonucleotide primer and separated on a polyacrylamide gel. The dried gels were autoradiographed to detect signal intensity. Because autoradiography times varied for the markers, comparisons of gene expression levels between different genes is impossible. However, because cell lines were assayed at the same time for each gene, comparison of gene expression between cell lines for the same gene is possible.

Tissue Microarray Construction

Following Internal Review Board approval, formalin-fixed paraffin-embedded tissue from primary radical prostatectomy specimens between 1984 and 1995 were randomly selected. To provide adequate sampling at least three replicate tumor (mean 3.4) and one matching normal tissue samples were taken in a widely representative fashion. When available, tumor samples were accompanied by matching benign (morphologically normal and hyperplastic) and PIN lesions. Ultimately, tissue from 246 prostatectomy specimens was arrayed into three blocks encompassing a total of 1,364 individual spots using the method of Kononen et al. [6].

Tissue Microarray Patient Data

Twenty patients treated with pre-operative hormonal therapy and seven with a lack of sufficient target tissue were excluded from analysis, resulting in 219 evaluable cases and 1,140 informative tissue spots (738 prostate cancer, 232 normal, 126 BPH, and 44 PIN spots). Median age was 64 years (range, 45–74 years). Pre-operative serum PSA was known for 193 patients, with a median of 8.9 ng/ml (range, 0.6–96.5 ng/ml). Two hundred-six (94%) patients were Caucasian. Biochemical recurrence, defined as a single postoperative serum PSA of 0.2 ng/ml or greater, occurred in 68 (31%) patients. Median follow-up for patients without biochemical recurrence was 75 months (range, 0–163 months).

Pathological Gleason score [7], as graded by a single pathologist (DBS), was 2–4 in 12 (6%) patients; 5–6 in 119 (54%) patients; 7 in 70 (32%) patients; and 8–9 in 18 (8%) patients. The majority of tumors (n = 144, 66%) were organ confined. Positive surgical margins were identified in 69 (32%) patients. Thirty-six (16%) patients had seminal vesicle invasion; 39 (18%) patients had tumor extending beyond the prostatic capsule; and 13 (6%) had lymph node metastases.

Cell Line Microarray Construction

A cell line microarray containing LNCaP, PC-3, DU-145, CL1, CL2, and LAPC-4 was constructed. Briefly, cells were cultured as described above, trypsin harvested, washed with PBS, formalin-fixed in suspension, embedded in low melt agarose, and then paraffin-embedded in the same manner as the archival whole tissues. Cores were taken from the resultant cell blocks and inserted in duplicate into a recipient cell array block in similar fashion as the tissue microarrays.

Immunohistochemistry

Four-micrometer thick tissue and cell line microarray sections were deparaffinized in three changes of xylene and rehydrated through a descending series of ethanol and standard two-step indirect avidin-biotin staining techniques (Vectastain ABC Elite mouse kit, Vector Laborartories, Burlingame, CA). Following endogenous peroxidase blocking, antigens were heat retrieved in a 95°C water bath for 25 min in 0.01 M citrate buffer (pH 6.0). Two blocking steps followed: blocking of non-specific protein binding by incubation for 30 min with 3% horse serum, and avidin/biotin blocking with consecutive application of avidin D and biotin. The sections were then incubated for 60 min at room temperature with the following primary mouse monoclonal antibodies: anti-CD10 (Neomarkers Ab-2, clone 56C6, 1:50 dilution, Fremont, CA); anti-CD13 (Neomarkers Ab-3, clone 13C03, 1:25 dilution); anti-CD44 (Neomarkers Ab-4, clone 156-3C11, 1:100 dilution); and anti-CD54 (Neomarkers Ab-4, clone 54C04, 1:10 dilution). For rat monoclonal anti-CD104 (Neomarkers Ab-1, clone 104C01, 1:10 dilution) heat

retrieval was performed with 1 mM EDTA 8.0 and rabbit normal serum was utilized for the protein blocking step. Subsequently, the sections were incubated with secondary antibody (Vector ABC Elite) for 30 min and thereafter with the avidin-biotin-peroxidase complexes for 30 min at room temperature followed by five times rinse with PBS for 3 min each. The sections were visualized with diaminobenzidine (DAB). After washing with water, they were counter-stained with hematoxylin. Primary CD10 antibody was replaced by non-immune pooled mouse or rat IgG (Santa Cruz Biotechnology, Santa Cruz, CA) at the same concentration as negative control.

A single pathologist (DBS) performed the semiquantitative assessment of antibody staining on the tissue microarray and cell line array in a blinded fashion. Cell lines stained with cell membrane predominance (Fig. 4A). For the tissue microarray, staining was predominantly membrane-based, apical-lateral in distribution with infrequent cytoplasm-based accentuation (Fig. 4B). Rarely, basal cells also stained with CD10. Only glandular elements of the prostate tissue were scored. Scoring of benign tissue was limited to secretory luminal epithelium. Tissue spot histology and grading were confirmed using H&E tissue microarray slides and only data from glandular regions corresponding to the appropriate histology and grade were included. Staining in the duplicate cell line spots was virtually identical, and no averaging of results was necessary.

Statistical Analysis

Three separate CD10 outcome measures were examined: maximum CD10 staining intensity on a 0–3 scale (0 = negative; 1 = weak; 2 = moderate, and 3 = strong staining), the percent of cells staining positive (0–100%), and their product (0–300). Boxplots and barplots were used to visualize the relationship between CD10 outcome measures and different groups defined by the pathological grade and stage. The nonparametric Kruskal–Wallis test was used to test whether the immunoreactivity of CD10 differed between different groups. To analyze the risk of biochemical recurrence, the clinical, pathological, and CD10 outcome measures were fit into univariate and multivariate logistic regression models. The adjusted odds ratios (relative risks) and their respective *P*-values were determined. Kaplan–Meier curves were used to estimate recurrence free survival, and the log rank test was used to test whether the curves differed between groups. To assess which covariates predicted recurrence free survival, we used univariate and multivariate Cox's proportional hazards models. The proportional hazards assumption was confirmed using Schoenfeld residuals. For each covariate, the relative hazard rate and the associated *P*-value was determined. For all analyses, a *P*-value of less than 0.05 was accepted as significant and the analyses were carried out with the software package R (URL: http://cran.r-project.org/). Patients with missing covariates or CD10 outcome measures were eliminated from analysis, resulting in a total of 169 evaluable patients.

RESULTS

CD Profiles of CL1 and LNCaP

To identify differential expression of surface markers that might typify changes that occur during clinical prostate cancer progression, a total of 128 CD specificities were screened by flow cytometry for reactivity to CL1 and the parental LNCaP from which CL1 was derived (Fig. 2A,B; Table I). Table II lists the most differentially expressed surface markers. Eight of the 128 CD specificities showed a difference in the percentage of cells staining positive of >60% (CD10, CD13, CD26, CD33, CD44, CD54, CD55, and CD104). In CL1, there was loss of the luminal cell marker CD10 and gain of the luminal cell markers CD13 and CD26, the basal cell markers CD44, CD55, and CD104, the non-prostate epithelial marker CD54, and the myeloid-associated antigen CD33 compared to LNCaP. To determine whether culturing CL1 cells in androgen-containing media affects CD expression, we compared the CD expression profile of a select group of 30 CD markers between CL1 and CL2 cells. CL2 are the cells that resulted from the return of CL1 to androgen containing medium 6 weeks after their emergence from LNCaP. The expression of the 30 CD specificities was nearly identical between CL1 and CL2 (data not shown).

Gene Expression Analyzed by RT-PCR

We sought to confirm the differential expression of the eight differentially expressed surface markers between CL1 and LNCaP and determine the expression of these eight genes in other well-characterized prostate cancer cell lines. To accomplish this, we used RT-PCR to determine the expression of these eight genes in the prostate cancer cell lines LAPC-4, LNCaP, DU145, PC-3, CL1, and CL2 (Fig. 3). Results of the RT-PCR corroborated the markedly differential labeling intensity found on flow analysis for these eight surface markers. The expression of CD10 correlated with sensitivity to androgens with mRNA expression only in the androgen sensitive cell line LNCaP, and not in the hormone refractory cell lines, DU145, PC-3, CL1, or CL2. Though LAPC-4 is an androgen sensitive cell line, it showed no CD10 expression by RT-PCR. This may be

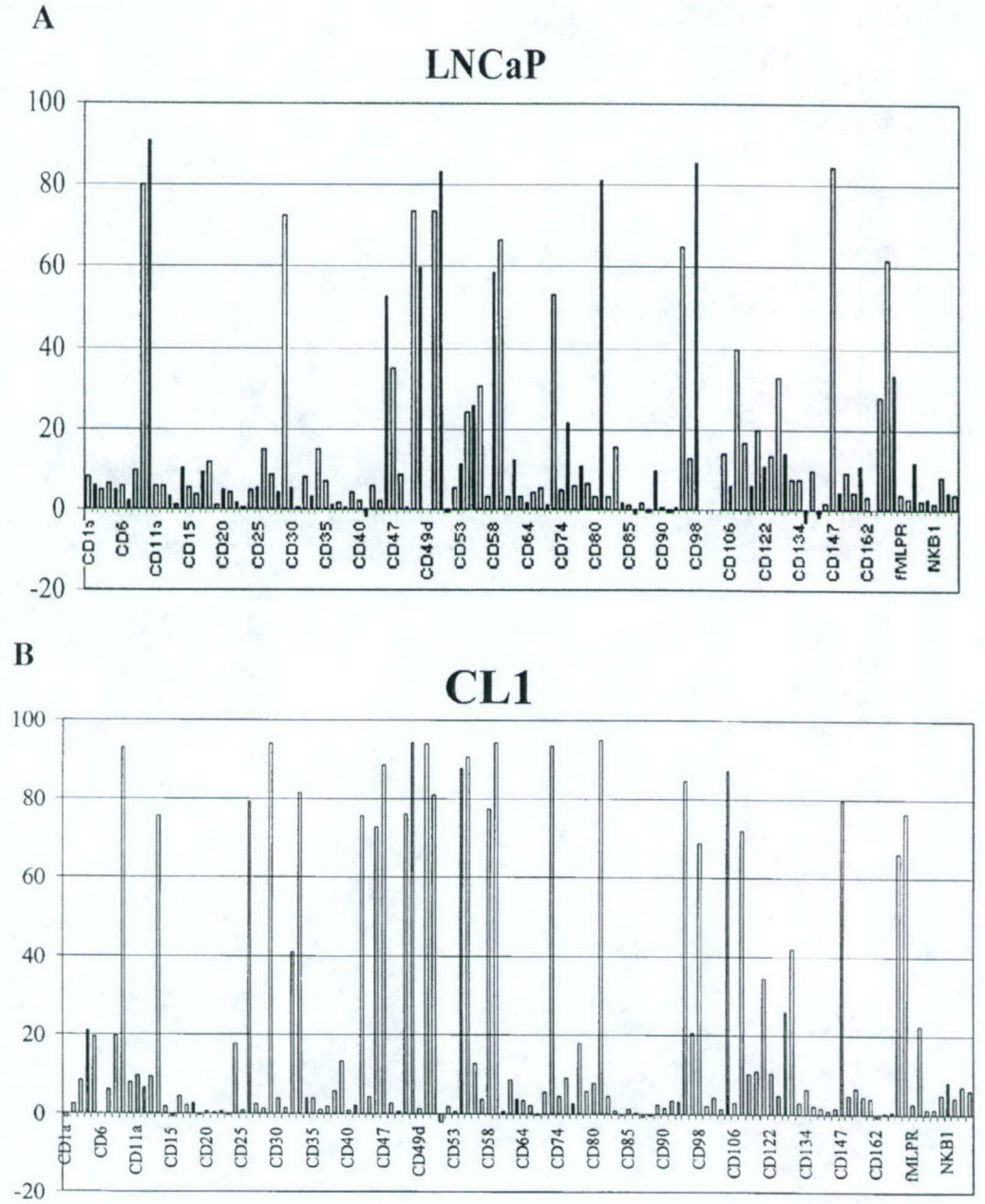

Fig. 2. CD profiles of (**A**) LNCaP and (**B**) CL1 cells. The percentages of positive events scored by flow cytometry are indicated on the Y-axis, and the specificities tested are listed on the X-axis. The specificities are arranged in the order of CD1a, CD2, CD3, CD4, CD5, CD6, CD7, CD8, CD9, CD10, CD11a, CD11b, CD11c, CD13, CD14, CD15, CD16, CDw17, CD18, CD19, CD20, CD21, CD22, CD23, CD24, CD25, CD26, CD27, CD28, CD29, CD30, CD31, CD32, CD33, CD34, CD35, CD36, CD37, CD38, CD39, CD40, CD43, CD44, CD45, CD46, CD47, CD48, CD49a, CD49b, CD49c, CD49d, CD49e, CD49f, CD50, CD51/61, CD53, CD54, CD55, CD56, CD57, CD58, CD59, CDw60, CD61, CD62P, CD64, CD66b, CD68, CD69, CD71, CD74, CDw75, CDw78, CD79a, CD79b, CD80, CD81, CD82, CD83, CD84, CD85, CD86, CD87, CD88, CD89, CD90, CDw92, CD94, CD95, CD97, CD98, CD99, CD100, CD101, CD104, CD106, CD107a, CD107b, CD116, CD117, CD122, CDw123, CDw128, CD130, CD132, CD134, CD135, CDw137, CD140b, CD141, CD147, CDw150, CD152, CD154, CD161, CD162, CD163, CD165, CD166, EGFR, fMLPR, IL8RB, IL10R, LAP, mannose receptor, NKB1, NGFR, perforin, T-cell receptor γδ.

TABLE I. Percentage Ranks of CD Positivities in LNCaP and CL1

LNCaP			CL1		
>50%		>20–50%	>50%		>20–50%
CD9	CD95	CD47	CD9	CD54	CD4
CD10	CD98	CD54	CD13	CD55	CD32
CD29	CD147	CD55	CD26	CD58	CD97
CD46	CD166	CD56	CD29	CD59	CD117
CD49b		CD107a	CD33	CD71	CDw128
CD49c		CD117	CD44	CD81	CD130
CD49e		CDw128	CD46	CD95	CD147
CD49f		CD165	CD47	CD98	IL8RB
CD58		EGFR	CD49b	CD104	
CD59			CD49c	CD107a	
CD71			CD49e	CD166	
CD81			CD49f	EFGR	

explained by the fact that LAPC-4 was derived from a patient with HRPC [5].

IHC staining for CD10, CD13, CD44, CD54, and CD104 Among Prostate Cancer Cell Lines Using a Cell Line Microarray

We sought to further support the RT-PCR results with IHC staining using the same prostate cancer cell lines. However, of the eight differentially expressed surface markers, only five had commercially available antibodies for formalin-fixed paraffin embedded tissue. Therefore, the expression of these five surface markers (CD10, CD13, CD44, CD54, and CD104) was determined using IHC staining of a cell line microarray constructed of formalin fixed, paraffin embedded cells derived from cell culture that contained the prostate cancer lines LAPC-4, LNCaP, DU145, PC-3, CL1, and CL2 (Table III). Staining of LNCaP and CL1 are depicted in Figure 4A. The expression patterns for CD10 and CD44 were similar to the results of the RT-PCR data. However, differences were found in the expression patterns of CD13, CD54, and CD104 among the IHC, flow cytometry, and RT-PCR results.

TABLE II. Differential Percentage Ranks of CD Positivities Between CL1 and LNCaP*

High (>60%)	Intermediate (>35–60%)	Low (20–35%)
CD10 (LNCaP)	CD47 (CL1)	CD29 (CL1)
CD13 (CL1)	CD71 (CL1)	CD32 (CL1)
CD26 (CL1)	EGFR (CL1)	CD49c (CL1)
CD33 (CL1)		CD49e (CL1)
CD44 (CL1)		CD59 (CL1)
CD54 (CL1)		CD107a (CL1)
CD55 (CL1)		CD130 (CL1)
CD104 (CL1)		CD165 (LNCaP)

*Cell line with the higher expression in parenthesis.

Tissue Microarray Expression of CD10

Once it was identified that decreased CD10 expression correlated with hormone refractory phenotype in our limited cell line sampling, we sought to determine the expression of CD10 among clinical prostate samples to examine the prevalence of loss of CD10 expression among hormone naïve patients with early stage prostate cancer. To accomplish this, a tissue microarray containing tissue spots from surgical specimens of 219 hormone naïve patients that underwent radical prostatectomy was examined for CD10 expression. CD10 expression was scored for the maximal intensity of staining (0–3) and the percent of cells that stained positive at any intensity (0–100%). Prostate cancer spots demonstrated significantly reduced intensity of CD10 expression relative to matched morphologically normal ($P < 0.0001$) and BPH samples ($P < 0.0001$). PIN specimens showed CD10 staining that was intermediate between the high expression of normal ($P = 0.033$) and the low expression of prostate cancer ($P = 0.0001$) (Fig. 5A). The median number of CD10 positive cells was 100% for BPH, 90% for normal prostate tissue and PIN, but only 30% for prostate cancer cases. Moreover, 34% of prostate cancer spots showed no CD10 expression relative to only 3% of normal or hyperplastic prostatic tissue, and 5% of PIN spots. In order to combine the information obtained from the maximum staining intensity and percent of cells staining positive, these two variables were multiplied to generate a new variable. This new variable was

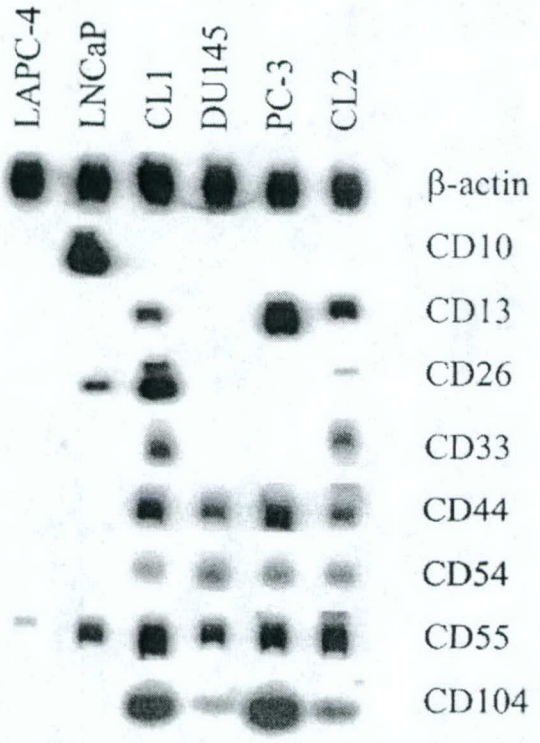

Fig. 3. RT-PCR analysis of gene expression of the eight markedly differentially expressed surface markers between CLI and LNCaP across various prostate cancer cell lines. The differences in band intensities correlated with the data from the flow analysis. Autoradiographs were exposed for differing lengths of time for each gene and thus gene expression cannot be compared between genes.

scored from 0 (0% cells staining at an intensity of 0) to 300 (100% of cells staining at an intensity of 3). A trend was found with BPH having the highest median score (300) followed by normal prostate tissue (200), with decreased expression found in PIN (120) and prostate cancer (30) (Fig. 5B). Among prostate cancer samples, 86% showed CD10 expression below the median expression of normal prostatic tissue and 68% showed expression below the 25% percentile of normal prostate tissue. While several clinical and pathological variables (Gleason sum, organ confinement, node status, seminal vesicle involvement, capsular invasion, and margin status) were significant predictors of biochemical recurrence and time to recurrence, no relationship was identified between any of the CD10 expression measures and pathological Gleason score, pathological stage, or biochemical recurrence in either univariate or multivariate analysis ($P > 0.1$ for all comparisons).

DISCUSSION

Liu et al. previously examined the expression of a panel of surface markers among the prostate cancer cell

TABLE III. Comparison of Gene Expression Across Prostate Cancer Cell Line Using Different Techniques*

	CD10			CD13			CD44			CD54			CD104		
	Flow[a]	RT-PCR[b]	IHC[a]	Flow	RT-PCR	IHC	Flow	RT-PCR	IHC	Flow	RT-PCR	IHC	Flow	RT-PCR	IHC
LNCaP	+++	+++	+++	–	–	–	–	–	–	+	–	–	+	–	–
LAPC-4	nt	–	–	nt	–	–	nt	–	–	nt	–	–	nt	–	–
CL1	–	–	–	+++	+	–	+++	+	+++	+++	+	+	+++	+	–
CL2	–	–	–	+++	+	–	+++	+	+++	+++	+	–	+++	+	+
DU145	nt	–	–	nt	–	–	nt	+	+++	nt	+	+++	nt	+	+
PC3	nt	–	–	nt	+	+++	nt	+	+++	nt	+	+	nt	+	+++

*Flow, flow cytometry; IHC, immunohistochemistry; nt, not tested.
[a]Flow and IHC data recorded as "–" for < 10% positive, "+" for 10–33% positive, "++" for 34–66% positive, "+++" for ≥ 67% positive.
[b]RT-PCR data recorded as "–" for absent and "+" for present.

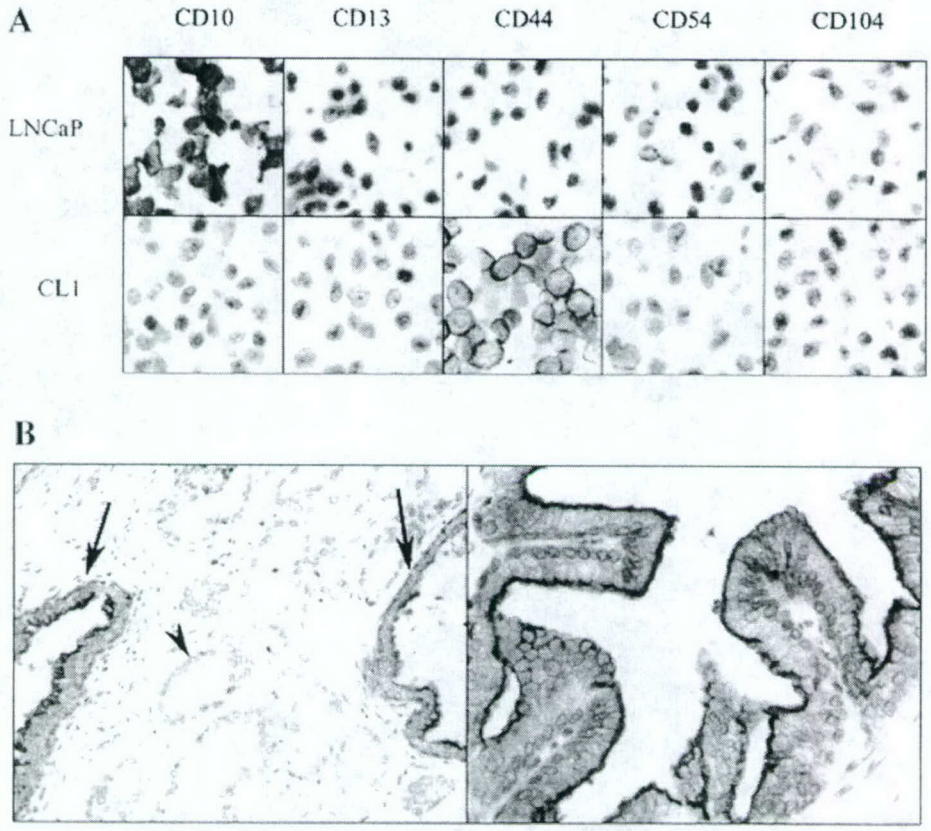

Fig. 4. IHC results on the cell line array and prostate tissue microarray. In (**A**), the spectrum of IHC staining of LNCaP and CL1 to anti-CD10, CD13, CD44, CD54, and CD104 are shown (400×). In (**B**) (**left**), prostate adenocarcinoma (arrowhead) is seen infiltrating between two normal glands (arrows), which are both stained by anti-CD10 in contrast to the unstained tumor (200×). In (B) (**right**), the typical apical staining distribution of CD10 is seen on benign luminal glandular epithelial cells (400×).

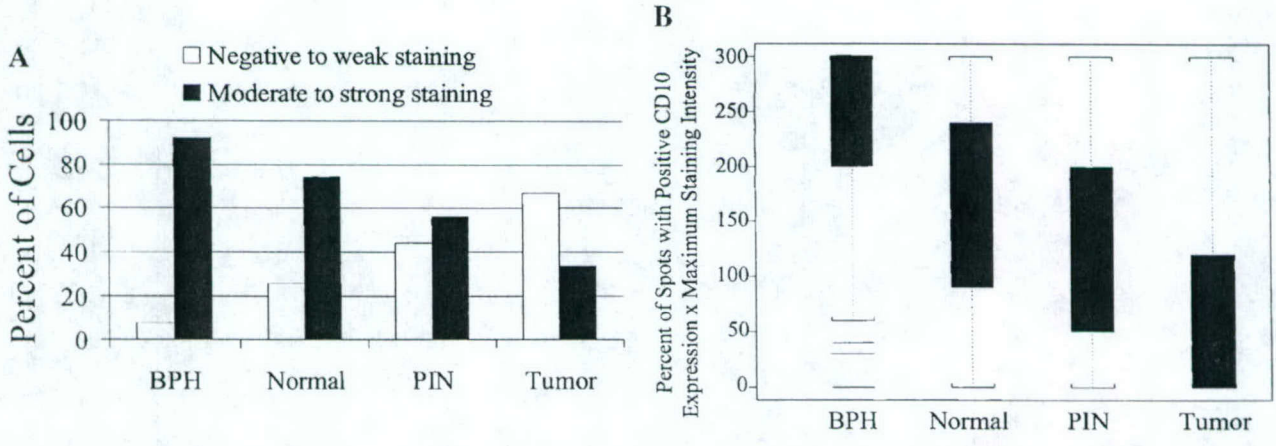

Fig. 5. CD10 staining results from the prostate tissue microarray. In (**A**), the percent of spots that stained negative to weak (0–1 on a 3 point scale) or moderate to strong (2–3 on a 3 point scale) for CD10 are segregated by histological type. In (**B**), box plots of the percent of spots that stained positive at any intensity multiplied by the maximum intensity of staining on a 0 to 3 scale. For box plots, the black box represents the 75th and 25th percentiles. The thin white box represents the median. The single black line with brackets containing the dots represents the 5th and 95th percentiles. The single black lines represent outliers beyond the 5th or 95th percentiles.

lines DU145, PC-3, and LNCaP [1]. In the current report, we extended this screening of surface markers to a new aggressive HRPC cell line, CL1, which was derived via in vitro androgen deprivation from the androgen sensitive, poorly tumorigenic cell line LNCaP. In the progression from LNCaP to CL1, several marked changes in CD expression occurred. There was loss of the luminal cell marker CD10 (neutral endopeptidase) and gain of the basal cell markers CD44 (hyaluronic acid receptor), CD55 (decay-accelerating factor), and CD104 (integrin-β4). There was also gain of the luminal cell markers CD13 (aminopeptidase N) and CD26 (dipeptidyl peptidase IV), the non-prostate epithelial marker CD54 (intracellular adhesion molecule 1), and the myeloid-associated antigen CD33 (sialic acid binding receptor). These changes support prior suggested models of prostate cancer progression in which cells acquire the expression of basal cell markers as the disease worsens [1,2]. The significance of the loss of one (CD10) and gain of two luminal cell markers (CD13 and CD26) during this progression is unclear.

In order to determine whether the differences in surface marker expression between CL1 and LNCaP typified differences between early and late stage prostate cancer, we sought to further examine the expression of the most differentially expressed surface markers among a panel of well-characterized hormone-sensitive (LNCaP, LAPC-4) and hormone-refractory (CL1, CL2, DU145, and PC-3) cell lines. Using RT-PCR and IHC (only five of the eight surface markers had commercially available antibodies for formalin-fixed paraffin embedded tissues), we found that the hormone refractory cell lines all expressed CD44 and none expressed CD10 (Table III). Both hormone sensitive cell lines demonstrated no CD44 expression. However, CD10 was expressed in the hormone sensitive cell line LNCaP, but not by LAPC-4. One possible explanation is that CD10 expression does not correlate with androgen sensitivity. Alternatively, the lack of CD10 expression by LAPC-4 may be due to LAPC-4's derivation. Though LAPC-4 demonstrates in vivo androgen sensitivity, it was derived from a patient who died of HRPC [5]. Therefore, it is difficult to determine a priori for any given gene, whether LAPC-4's expression profile would more closely resemble that of an androgen sensitive or resistant cell line. When taking into account the ability of LAPC-4 to be considered as either a hormone sensitive or hormone refractory cell line, loss of CD10 expression appeared to correlate with resistance to androgen deprivation.

There were discrepancies between the RT-PCR, IHC, and flow cytometry results for CD13, CD54, and CD104. The reasons for this are unclear. However, the RT-PCR results corroborated the flow cytometry data. A prior study, using flow-cytometry, found that both DU145 and PC-3 expressed CD104, in agreement with our flow cytometry and RT-PCR results [1]. Given that IHC, flow cytometry, and RT-PCR were performed on different cultures flasks at different times, perhaps differences in cell culture conditions, which are known to affect surface marker expression, may explain the discrepancy [8]. Other possibilities include differences in antibody targets or affinity, differences in cell fixation and processing, differences between RNA and protein content, and differences in sensitivity between various techniques especially given that flow cytometry showed equivalent or greater percentage of cells staining positive relative to IHC for all markers examined.

Of the two surface markers (CD10 and CD44) whose expression by all three techniques (RT-PCR, flow cytometry, and IHC) correlated with androgen sensitivity, CD10 was the most interesting given its biological function and the fact that CD10 has already been implicated in prostate cancer progression [9,10]. CD10 is a luminal cell marker that cleaves and inactivates bioactive neuropeptides that serve as growth factors for HRPC, including bombesin, endothelin-1, and neurotensin [11]. Expression of CD10 is under the control of androgens, with androgen withdrawal resulting in CD10 downregulation [9,12]. Moreover, no CD10 expression was detected in the hormone refractory cell lines CL1, CL2, DU145, PC-3, and TSU-Pr1 [9] and in LAPC-4, which was derived from a patient with HRPC. Downregulation of a growth factor inactivator by androgen independent cells may be one mechanism for the development of alternate growth pathways that become important in the absence of androgenic stimulation. CD10 is further implicated in prostate cancer progression by the fact that reintroduction of CD10 into hormone refractory cells resulted in significant growth inhibition [9,10]. The fact that the cells that resulted from the return of CL1 to androgen containing medium, CL2, demonstrated no CD10 expression, suggests that the loss of CD10 during prostate cancer progression may be an irreversible event. However, little has been examined regarding whether loss of CD10 is an early or late event in prostate cancer progression. When CD10expression was examined among 219 hormone naïve patients that underwent radical prostatectomy, 68% of tumor samples demonstrated CD10 expression that was below the 25th percentile of the matched, morphologically normal prostatic tissue. Eighty-six percent of prostate cancers had CD10 expression below the median expression of the normal prostate tissue and 34% of tumors showed no CD10 expression. Thus, the loss of CD10 expression is both a frequent and early event in human prostate cancer. Moreover, PIN

specimens showed an intermediate level of CD10 expression between prostate cancer and normal prostate tissue, suggesting that loss of CD10 might occur as early as the pre-malignant phase.

Among prostate cancer patients, CD10 expression did not correlate with pathological grade, stage, or biochemical recurrence following radical prostatectomy. Thus, a decrease or lack of CD10 expression did not portend a worse prognosis among patients undergoing radical prostatectomy. This is not surprising in that loss of CD10 has been implicated in resistance to androgen deprivation, not tumor aggressiveness. This is best exemplified by the lack of CD10 expression in prostate cancer cell line, LAPC-4, which was derived from a patient with HRPC and yet grows slowly both in vitro and in vivo [5]. Thus, lack of CD10 expression does not necessarily imply increased tumor aggressiveness. However, given that decreased CD10 expression did correlate with hormone refractory phenotype in our limited cell line sampling, lack of CD10 expression in a clinical tumor sample may predict decreased androgen sensitivity and a worse response to hormonal deprivation therapy. This raises the possibility that reintroduction of CD10 expression may be therapeutic not only for late stage HRPC [9], but also early stage prostate cancer when combined with hormonal withdrawal therapy.

CONCLUSION

CL1, an aggressive and well-characterized HRPC cell line, demonstrated a distinct surface marker expression profile based upon flow-cytometry, RT-PCR, and IHC relative to its parental slowly growing androgen sensitive prostate cancer cell line LNCaP. Of the most differentially expressed surface markers, CD10 expression appeared to possibly correlate with hormone sensitivity among a panel of well-characterized prostate cancer cell lines. Using a tissue microarray of 219 radical prostatectomy specimens from hormone naïve patients, we found that 68% of prostate cancers showed CD10 protein expression below the 25th percentile of matched, morphologically normal prostatic tissue. There was no correlation between CD10 expression and tumor grade, stage, or biochemical recurrence. This study implicates loss or decreased expression of CD10 as an early and frequent event in human prostate cancer progression and suggests that CD10 may be a useful therapeutic target for early stage disease.

ACKNOWLEDGMENTS

The authors thank Ms. Sheila Tze and Mr. Gregg Kanter for technical assistance.

REFERENCES

1. Liu AY. Differential expression of cell surface molecules in prostate cancer cells. Cancer Res 2000;60:3429–3434.
2. Liu AY, True LD, LaTray L, Ellis WJ, Vessella RL, Lange PH, Higano CS, Hood L, van den Engh G. Analysis and sorting of prostate cancer cell types by flow cytometry. Prostate 1999; 40:192–199.
3. Tso CL, McBride WH, Sun J, Patel B, Tsui KH, Paik SH, Gitlitz B, Caliliw R, van Ophoven A, Wu L, deKernion J, Belldegrun A. Androgen deprivation induces selective outgrowth of aggressive hormone-refractory prostate cancer clones expressing distinct cellular and molecular properties not present in parental androgen-dependent cancer cells. Cancer J Sci Am 2000;6:220–233.
4. Patel BJ, Pantuck AJ, Zisman A, Tsui KH, Paik SH, Caliliw R, Sheriff S, Wu L, deKernion JB, Tso CL, Belldegrun AS. CL1-GFP: An androgen independent metastatic tumor model for prostate cancer. J Urol 2000;164:1420–1425.
5. Klein KA, Reiter RE, Redula J, Moradi H, Zhu XL, Brothman AR, Lamb DJ, Marcelli M, Belldegrun A, Witte ON, Sawyers CL. Progression of metastatic human prostate cancer to androgen independence in immunodeficient SCID mice. Nat Med 1997; 3:402–408.
6. Kononen J, Bubendorf L, Kallioniemi A, Barlund M, Schraml P, Leighton S, Torhorst J, Mihatsch MJ, Sauter G, Kallioniemi OP. Tissue microarrays for high-throughput molecular profiling of tumor specimens. Nat Med 1998;4:844–847.
7. Gleason DF. Classification of prostatic carcinomas. Cancer Chemother Rep 1966;50:125–128.
8. Liu AY, LaTray L, van Den Engh G. Changes in cell surface molecules associated with in vitro culture of prostatic stromal cells. Prostate 2000;44:303–312.
9. Papandreou CN, Usmani B, Geng Y, Bogenrieder T, Freeman R, Wilk S, Finstad CL, Reuter VE, Powell CT, Scheinberg D, Magill C, Scher HI, Albino AP, Nanus DM. Neutral endopeptidase 24.11 loss in metastatic human prostate cancer contributes to androgen-independent progression. Nat Med 1998;4:50–57.
10. Dai J, Shen R, Sumitomo M, Goldberg JS, Geng Y, Navarro D, Xu S, Koutcher JA, Garzotto M, Powell CT, Nanus DM. Tumor-suppressive effects of neutral endopeptidase in androgen-independent prostate cancer cells. Clin Cancer Res 2001;7: 1370–1377.
11. Nelson JB, Carducci MA. Small bioactive peptides and cell surface peptidases in androgen-independent prostate cancer. Cancer Invest 2000;18:87–96.
12. Shen R, Sumitomo M, Dai J, Hardy DO, Navarro D, Usmani B, Papandreou CN, Hersh LB, Shipp MA, Freedman LP, Nanus DM. Identification and characterization of two androgen response regions in the human neutral endopeptidase gene. Mol Cell Endocrinol 2000;170:131–142.